A PROCESSING TECHNIQUE FOR OFDM-MODULATED WIDEBAND RADAR SIGNALS

A PROCESSING TECHNIQUE FOR OFDM-MODULATED WIDEBAND RADAR SIGNALS

Proefschrift

ter verkrijging van de graad van doctor
aan de Technische Universiteit Delft,
op gezag van de Rector Magnificus Prof. ir. K. C. A. M. Luyben,
voorzitter van het College voor Promoties,
in het openbaar te verdedigen op
donderdag 4 november 2010 om 10.00 uur

door

Recep Fırat TİĞREK

Master of Science in Electrical and Electronics Engineering
Middle East Technical University, Turkije
geboren te Antalya, Turkije

Dit proefschrift is goedgekeurd door de promotoren:
Prof. ir. P. van Genderen
Prof. dr. ir. L. P. Ligthart

Samenstelling promotiecommissie:

Rector Magnificus,	voorzitter
Prof. ir. P. van Genderen,	Technische Universiteit Delft, promotor
Prof. dr. ir. L. P. Ligthart,	Technische Universiteit Delft, promotor
Prof. dr. ing. J. Detlefsen,	Technische Universität München
Prof. ing. F. Le Chevalier,	Technische Universiteit Delft
Prof. dr. ir. A. J. van der Veen,	Technische Universiteit Delft
Prof. DSc. O. Yarovyi,	Technische Universiteit Delft
Prof. ir. P. Hoogeboom,	Technische Universiteit Delft, reservelid

A Processing Technique for OFDM-Modulated Wideband Radar Signals

Recep Fırat Tiğrek.

Thesis Delft University of Technology.
With references and with summary in Dutch.

ISBN 978-94-6113-022-8

Subject headings: OFDM, radar signal processing, spread spectrum radar, range migration, PAPR, Golay codes, radar communication.

Printed in The Netherlands

Part of the work presented in this thesis has received research funding from the Early Stage Training action in the context of the European Community's Sixth Framework Programme.

This work has contributed to the PARSAX project of the Technology Foundation STW, applied science division of the Dutch Organization for Scientific Research NWO.

to my family &
our future baby

Contents

Chapter 1

Introduction

Since its emergence a hundred years ago, the radar has found use in security and science applications, thanks to the wide range of information it provides in many different and usually adverse conditions where other information gathering tools fail. The information gathered from the radar system can be enhanced further by combining the radar with other types of sensors as well as introducing multiple radars situated at diverse locations. The position diversity is especially essential for observing natural phenomena that occur over a large area; also, monitoring vulnerable locations for security and disaster management purposes requires data coming from radar stations at different locations to provide the optimal coverage.

Regarding the security and disaster management assignments the prime objective of the radar system is to detect and track the movements of individuals and groups of people along with vehicles and, depending on the setting, animals. The scene may include thick vegetation or urban features, further complicating the detection and classification of targets. Under such adverse conditions a single monostatic radar may not provide satisfactory performance due to poor coverage in certain areas and clutter masking the weak targets. Multiple monostatic radars with position diversity, where the acquired data is combined with data fusion techniques, may provide significant improvement in the radar performance. Targets can be tracked, despite gaps in the coverage of individual radars, through the fusion of data at plot level or track level [62]. Moreover, methods are proposed for fusion of raw video data for target classification [12].

This concept of combining the information from multiple monostatic radars requires establishing a network that connects the radar stations. A network of radars requires communication links between the radars and

possibly to a centralized fusion and control center. These links can be very susceptible to interference and disruptions if based on commercially available communication infrastructure. Integrating the communication capability in the radar system is considered as a robust solution that avoids almost all the vulnerabilities of a commercial communication infrastructure. The integration is not only in the hardware level; the radar signal has double functionality as communications signal, which reduces the footprint of the combined system on the already congested spectrum.

It must be noted that tracking small and slow-moving targets such as people, requires much higher range and velocity resolution. The higher range resolution translates into wider frequency bandwidth and the velocity resolution is determined by the time duration the radar beam dwells on the particular target; this combined increase in the signal bandwidth and dwell-time leaves a very tight time-frequency budget for the combined radar and communication operation.

The development of a wide-band radar signal with the dual-use as the communication signal and the design of the associated radar signal processing technique is the main focus of this thesis.

1.1 Motivation for the Multi-Carrier Radar Signal

As mentioned before, integrating the communication capability in the radar system is considered as a robust solution that avoids almost all the vulnerabilities of a commercial communication infrastructure. Two approaches prevail in the literature regarding the fusion of the communication and radar functions in the same signal. One approach, which is essentially adopted in passive bistatic radar applications, considers the use of a purely communication oriented signal for the radar [48, 52]. Such passive radars use illuminators of opportunity like radio and television broadcasting signals and mobile communication signals, relinquishing the control over the transmitted signal for the sake of the stealthy operation. Not having any control on the signal illuminating the target results in unreliable radar performance that depends on the content of the broadcast. The other approach is based on embedding an auxiliary communication signal in the radar signal, usually resulting in a more complicated radar receiver structure and the degradation in radar performance [4, 61]. Moreover, the signal in reality has no double functionality, which results in either increasing the spectrum occupancy of the signal or reducing the radar signal's share of the available resources.

When considering the option of sharing the spectrum between distinct

signals that fulfill the radar and communication functions, the presence of multiple radars in the same region has to be taken into account. The network of radars is meant to provide undisrupted coverage in a complex area, and fusion of data from radars at different locations can improve target classification performance. However, care must be taken to prevent interference between radars. As coding techniques can only provide limited isolation between different radars [36], the alternative is to make sure that those radars in the vicinity of one another are assigned non-overlapping segments of the available spectrum. Under such condition, it is vital to reduce the footprint of each radar over the spectrum, which is already quite wide in order to provide the required high range resolution. The high Doppler resolution necessitates long dwell times, which makes partitioning the transmit time between the radar and communication functions an unfavorable option.

Concerns as outlined above call for utilizing a purely communication oriented signal that has double functionality as radar signal; this is in order to avoid a bottleneck in the time-frequency budget. Different from the passive radars, the co-located illuminator and receiver translates into having in the receiver the complete information on the transmitted signal. The communication signal does not have to comply with any of the existing standards; while there is inherently little control on the contents of the communication signal, other parameters such as the bandwidth and the center frequency can be selected for optimal radar operation.

The orthogonal frequency division multiplexing (OFDM) is a multi-carrier spread-spectrum technique which finds wide-spread use in communications [49]. Amplitudes and phases of carriers constituting the OFDM signal carry the communication message. As each carrier can have an amplitude and phase independent of other carriers, there is unprecedented control over the spectrum of the signal. Moreover, the carriers can be turned on and off individually. Such flexible allocation of carriers and carrier contents is the prime motivation for choosing OFDM as a candidate for the multi-carrier radar signal. However, the flexibility of the OFDM signal comes with the computational cost of the digital signal processing. The de-ramping techniques available for the linear frequency modulated (LFM) radar signals cannot be utilized for OFDM radar signals [73]. Hence, much higher sampling frequencies are needed for the OFDM signal, which translates into much higher data processing burden. The same computational burden is present also for other spread-spectrum signals such as code-division multiple access (CDMA) signals and random noise signals [3], which do not offer the same level of control on the spectral properties of the signal as OFDM. As the computational power increases with reasonable prices for processing units, the computational burden of the OFDM signal can be justified.

Another motivation point for the multi-carrier radar signal is the Doppler sensitivity its unique structure creates. OFDM multi-carrier structure can guarantee the independence and orthogonality of the spectrum components, while such relation between the spectrum components cannot be guaranteed for many other waveforms, and definitely is not present in the linear frequency modulated radar signals. The Doppler sensitivity in the conventional pulse compression radars requires the implementation of Doppler-matched filter banks, which is considered to be a disadvantage in surveillance radars. However, the multicarrier structure of the OFDM signal allows compensating for the Doppler effect in the digital domain in a computationally efficient manner, because the spectrum components of the signal can be modified independent of one another.

The Doppler sensitivity can be exploited in the radar signal processing to solve the Doppler ambiguity, which arises in the conventional pulse-Doppler processing where the target velocity is measured through phase change in the signal echo from one pulse compression output to the next. The multi-carrier structure provides extra information on the target velocity, which can be used to solve the Doppler ambiguity. Such information is not always available or reliable in other pulse compression techniques, where there is no means of direct retrieval and management of the spectrum components.

1.2 Waveform Structure and Performance Analysis Methodology

The design of OFDM radar signal involves understanding first the evolution of the echo signal, which starts with determining the signal parameters. While the waveform design is inherently bounded by the conventional OFDM modulation-demodulation technique, which utilizes the discrete Fourier transform (DFT) and the inverse discrete Fourier transform (IDFT), the flexibility posed by the multi-carrier structure allows determining waveform parameters, such as the bandwidth, carrier spacing and the number of carriers, as required to achieve the needed radar performance. Moreover, symbol sets that permit communication between distinct radars have to be adopted for the OFDM modulation; in other words the symbols modulating the OFDM carriers must be chosen from the standard communication symbols. It must also be noted that the communication signal essentially consists of random symbols, which can be compared to noise waveforms from the radar perspective. Thus, the waveform design can be regarded as adapting the already existing communication-oriented features

of the OFDM signal for the radar purposes.

The investigation on the evolution of the echo signal is aimed at constructing the mathematical model of the echo signal, which involves the multi-carrier structure of the OFDM along with the parameters of the signal and the target from which the radar signal echo is originating. Such modeling is fundamental to the development of the radar signal processing method that exploits the multi-carrier structure of the OFDM to solve the Doppler ambiguity.

When designing radar waveforms the performance of the proposed signals has to be evaluated while making certain assumptions on the radar system. It can be asserted that the fundamental processing method for radar signals is the matched filtering, which corresponds to calculating the correlation of the received echo with the transmitted radar signal in an effort to minimize the additive white Gaussian noise [26]. The ambiguity function introduced in [78], which is the standard first step for evaluating the performance of a radar signal, is based on the matched filtering technique. The ambiguity function of the OFDM radar signal is adopted as the principal method for demonstrating the performance of the radar signal, and the derivation of the ambiguity function constitutes the first step of the performance analysis. The mathematical model for the received echo is used extensively at this step.

As the OFDM signal is modulated by the random symbols constituting the communication messages, the ambiguity function is expected to have random features as well. Thus, the second step for the performance analysis focuses on the statistical properties of the ambiguity function, namely the probability density function, the expected value and the variance. Finding the analytical formulations for the statistical properties is the ultimate goal of this step.

The third step of the performance analysis is the validation of the analytical derivations through Monte Carlo simulations, which are aimed also at demonstrating the statistical properties of the ambiguity function to validate the analytical formulations. Such demonstration technique is especially valuable when the more complicated modulation symbols render the analytical formulations intractable. Thus, establishing the agreement between the analytical derivations and the Monte Carlo simulations is essential for tackling OFDM signals with more complicated or advanced modulation symbols.

Since both analytical formulations and Monte Carlo simulations are based on the same mathematical model of the radar signal echo, the errors in the mathematical model may not be evident even when there is perfect

agreement between the two. Thus, the final step of the performance analysis is the validation of the mathematical models, the analytical formulations and the simulations through experiments where the radar transmitter and receiver are implemented using commercially available equipment. With the experiments confirming the results of the analytical derivations and the Monte Carlo simulations, the mathematical model can be considered as concrete.

The methodology for the performance analysis, as described above, not only demonstrates the performance of the OFDM radar signal but also validates the mathematical model and the simulation platform for OFDM radar signals for the investigation of different modulation symbols. Thus, this methodology is applied first for the quadrature phase shift keying (QPSK) symbols and later the investigation is extended over the other modulation symbols such as the quadrature amplitude modulation (QAM). The QPSK symbols are chosen for the initial investigation due to the tractability of the analytical derivations that consider only the random phase modulation on the carriers.

A second aspect of the performance analysis is the move from the pulse compression of the single OFDM segment, which is called an *OFDM symbol*, or alternatively an *OFDM chip*, in the communication literature, to the coherent integration of a train of compressed OFDM chips. The statistical properties investigated using the above mentioned methodology may not be enough to understand the performance of the coherent integration stage. Monte Carlo simulations that explore sets of waveform and target parameters are conducted to assess the accuracy with which the target parameters are measured after the signal processing.

1.3 Overview of the State of the Art

1.3.1 Pulse Compression Waveforms

The spread-spectrum techniques are used in radar systems to increase the time-bandwidth product of the signal. Such signals are called *the pulse compression waveforms*, as the matched filtering technique compresses the energy spread over a longer duration into a pulse of the shortest duration that the signal bandwidth can accommodate. Any other signal component in the echo such as thermal noise and interference is not compressed, which translates into *pulse compression gain* over such interfering signals. Such pulse compression gain allows for transmitting the signal with lower peak power while the total transmitted energy is high enough to satisfy the signal

to noise ratio (SNR) requirements of the radar, due to the long signal duration. Moreover, the range and Doppler sidelobes of the pulse compression signals can be controlled better, compared to pulsed systems, and in some cases multiple radars can occupy the same band in the spectrum thanks to the low cross correlation between different pulse compression waveforms.

The most common pulse compression waveform is *the linear frequency modulation* (LFM), where the frequency increases or decreases linearly for the duration of the pulse. Such waveforms are utilized in many different radar systems, however embedding communications on such waveforms is possible only by means of sharing the spectrum band or the time that would otherwise be allocated to the execution of the radar tasks [4].

Another pulse compression waveform that can be considered as similar to the multi-carrier OFDM due to the utilization of distinct frequency bands is *Costas frequency hop codes*, where one frequency is transmitted at a time to compose a pulse train such that each subpulse has a different frequency [7]. The order of the frequencies is determined such that they follow a permutation matrix, limiting the sidelobes in the delay and Doppler. *Hyperbolic frequency hop codes* are also proposed, where the permutation matrix is generated according to a particular pattern that also reduces the cross-correlation between the multiple stations using the same family of codes [36]. Such frequency hop codes cannot carry communication messages as long as the permutation matrix is determined purely for optimal radar performance.

Phase coding over the single carrier, similar to the communication signals in the *code division multiple access* method, has been studied extensively in the literature. An overview of such phase coded pulse compression waveforms can be found in many sources [27]. Their comparison with OFDM signals for radar applications, however, leads to the conclusion that the bandwidth efficiency of the OFDM signal is much better compared to the phase coded signals [29]. Moreover, pulse compression codes such as Barker codes are fixed sequences of symbols, which cannot accomodate the communication symbols that are essentially random.

1.3.2 OFDM Radar Signals

The OFDM radar signals were first introduced in [29], where complementary phase codes are transmitted over each carrier. The investigation is extended over trains of such pulses with various windowing methods to improve the performance [31]. This line of investigation does not investigate the effect of features commonly found in the OFDM communication signals such as the guard interval and synchronization symbols over the radar performance.

Moreover, the use of complementary codes precludes embedding the communication messages into the radar signal.

The flexibility of the OFDM modulation is based on the modulation technique granting control of phases and amplitudes for the individual spectrum components. Such flexibility gives rise to a wide variety of techniques aimed at improving the various aspects of the radar performance [50, 55, 56]. However, in all such proposals the focus is on the performance of the single radar station, and embedding communication messages or incorporating the indispensable features of the OFDM communication signals such as the guard interval has not been considered.

Use of broadcasted communication signals for radar applications is usually considered in the context of passive bistatic radar development; OFDM based digital broadcasting signals were considered upon the widespread use of such broadcast format [48]. Recently in a study parallel to this thesis, use of OFDM communication waveforms in radars that are constituents of a netted radar system is suggested [44]. The utilization of OFDM signal in systems that combine the synthetic aperture radar and communication functions is also considered [16].

The concept of a network of radars that establish communication links through their directive beams has been proposed in [17], which can be considered as seminal since it suggests OFDM as the modulation of choice for the communication signal. A continuation of that effort takes into account the directional antenna pattern [25], and a more rigorous modeling of the time-varying channel [13]. However, it is noted that the synchronization symbols and forward error correction coding are an integral part of the contents of the communication signal, and there must be an upper limit for the bit error rate (BER) to ensure a reliable communication link. In addition to this, the antenna sidelobe level and the distance between the transmitter and the receiver have to be considered when calculating the channel capacity [70]. Hence, with all these system aspects, a channel capacity comparable to ethernet or fast ethernet is deemed achievable, depending on the precise conditions. Such contributions mostly focused on the OFDM as the communication signal, while the use of OFDM communication signal as the radar signal was not elaborated upon until now in the context described here.

1.3.3 Solving the Doppler Ambiguity

The principal method for solving the Doppler ambiguity is to compare the measurements from multiple trains of pulses with different pulse repetition frequency (PRF) or carrier frequency. As the Doppler ambiguity depends

on those parameters, the comparison of the ambiguous measurements using the Chinese Remainder Theorem solves the Doppler ambiguity [28]. Other solutions to the Doppler ambiguity in pulse Doppler radar measurements have been proposed in the literature, where the fundamental concept behind the proposed solutions is the introduction of a diverse source of Doppler information.

In a networked radar system angular diversity is achievable, which can solve the Doppler ambiguity by exploiting the fact that the target velocity vector has a different projection over the radial direction for each of the radars [20]. Frequency diversity is possible with multi-carrier signals, where the Doppler is measured by determining the frequency-dependent phase change from pulse to pulse in a bi-pulsed Doppler radar scheme [9]. It must be noted that the proposed scheme has Doppler resolution limited by the time duration of two pulses. Moreover, coding of the OFDM carriers or the coherent integration to improve the Doppler resolution are not considered in [9]. The actual shift in the carrier frequency can be measured using intermediate-frequency phase-locked loop and spectrum peak search, which can be considered as introducing the frequency diversity [79]. However, each proposed method is aimed at a very specific application.

1.4 Novelties and Main Results

The two fundamental aspects of the OFDM communication signal, namely the cyclic prefix guard interval and the random message content, are incorporated in the OFDM radar signal and the signal processing technique is developed to make use of these features rather than avoid them. Different from the other techniques proposed in the literature there is no resource sharing and therefore no associated degradation of the radar performance. The monostatic operation translates into perfect knowledge of the transmitted signal, a feature that passive radar systems lack.

Such use of the OFDM communication signal for the radar applications with the aim of establishing a network of radars is novel, with similar proposals appearing in the literature only recently [44, 60]. Moreover, transmitting communication signals through the directive radar antenna that rotates periodically is demonstrated to be a viable method [25], by demonstrating that high data rates can be achieved in such scenario, where the transmitting antenna is directive and rotating while the receiving antenna is omnidirectional.

The Doppler ambiguity solving capability of the OFDM signal with

phase coding on the carriers is demonstrated, where the coherent integration of the pulse compression output for a train of OFDM chips yields the high resolution Doppler measurement. With the conventional processing methods, multiple trains of OFDM chips with different PRF and/or RF carrier frequency would be necessary to solve the Doppler ambiguity associated with the coherent integration. Through the innovative pulse compression method presented in this thesis, the Doppler ambiguity is solved by exploiting the Doppler sensitivity of the random phase modulated OFDM signal.

The Doppler frequency shift manifests itself as a shift of the carrier locations in the spectrum, which is compensated by the cyclic shift of the spectrum components before the pulse compression. The signal processing technique is simplified further, as the pulse compression is accomplished in frequency domain thanks to the cyclic repetitiveness of the OFDM signal. In other pulse compression techniques the Doppler effect is considered to cause loss in the pulse compression, and filter banks matched to different Doppler shifts is proposed as a remedy. The Doppler compensation in the digital domain is a simpler solution with higher precision. Moreover, the additional information on Doppler, which the pulse compression method provides, helps solve the Doppler ambiguity associated with the coherent integration and Doppler processing of compressed pulses.

Another novelty presented in the thesis is the modeling of the OFDM signal echo using matrix formulations, where each transformation that the transmitted OFDM chip undergoes is formulated as a matrix operation. In a similar approach, the steps of the signal processing chain are also developed based on the matrix operations, and the level of clarity and modularity reached through this modeling is indispensable when the novel processing method is extended over different implementations of the OFDM modulation.

Besides the derivation and validation of the OFDM pulse compression method for the conventional case of PSK and QAM coding on the OFDM carriers, the newly proposed single-carrier-OFDM (SC-OFDM) is investigated to assess its performance for radar applications. The SC-OFDM is proposed in the literature as a method to limit, or even eliminate, the varying time envelope of the OFDM. The validity of the mathematical modeling and the simulation method, which is guaranteed by the methodology outlined in Section 1.2, ensures that this investigation, the first in the literature, reflects accurately the performance that can be expected of the SC-OFDM signal.

The Doppler frequency shift, which is an approximation of the actual Doppler effect, is accurate only when the narrowband assumption is satisfied.

The easily accessible matrix formulations reveal two mechanisms of failure for the narrowband assumption. First, the target may migrate between range cells throughout the coherent Doppler integration duration. This range migration may occur even at relatively moderate velocities when the dwell time is kept long to obtain high Doppler resolution. The second failure of the narrowband assumption occurs when the target is fast enough, which, coupled with long pulse compression signal duration and large bandwidth, may lead to the actual Doppler effect revealing itself as the scaling of the signal. Both of these effects are isolated in the matrix formulation of the OFDM signal echo, which provides a unique wideband radar signal echo model. By exploiting the Doppler sensitive nature of the OFDM radar signal, a novel range migration compensation operation is developed for the coherent Doppler integration that corrects the phases of each OFDM chip in parallel with the Doppler compensation. The Doppler scaling is also isolated in the OFDM pulse compression stage, and another novel method to generate a reference signal for the pulse compression is proposed.

1.5 Outline of the Thesis

The signal description is formulated in Chapter 2 with emphasis on its use as a radar signal. Thus, the priority is to reflect the multicarrier structure and the modulation symbols. The modulation technique utilizes the IDFT, implemented through IFFT, and the signal is demodulated by the DFT operation, implemented through FFT. The cyclic prefix guard interval, which is an important feature of the OFDM communication signal, is introduced by demonstrating its effect on the receiver side. Also the time and frequency synchronization of the receiver is investigated, for the delay and Doppler effect in the radar echo has similar behavior.

In Chapter 3 the mathematical model of the radar signal echo as reflected by a point target is developed in line with the methodology adopted throughout the thesis. The model is constructed starting with only a delay limitation to preserve the cyclic repetitiveness of the OFDM signal. Later the narrow band assumption is introduced and a matrix structure is adopted to clearly show the delay and Doppler effects on the echo. The matrix structure also provides a framework in which the signal processing steps such as the demodulation and pulse compression are integrated. The Doppler ambiguity solving property of the multi-carrier signal is demonstrated while considering the random nature of the OFDM signal content. The chapter is concluded with an evaluation of the computational complexity of the signal processing encompassing the pulse compression and the coherent integration

of multiple OFDM sections.

Chapter 4 provides a deeper investigation of the statistical properties of the signal and their reflection on the pulse compression output, which is shown to be equivalent to the ambiguity function. The noise-like features of the signal are considered, and parallels are drawn with the treatment of other noise radar waveforms. The contribution of the thermal noise, which is assumed to be additive white Gaussian noise, is modeled as well. The results of the analytical formulas are verified through Monte Carlo simulations and experiments, demonstrating some unique features of the OFDM radar signal described in this thesis. The accuracy of the delay and Doppler measurements for the complete radar processing chain is also investigated through Monte Carlo simulations; effects of the different waveform parameters as well as the noise and target conditions over the measurement accuracy are explored.

The OFDM radar signal investigated in the previous chapters has only the phase modulation over its carriers to keep the analytical formulations tractable. Upon proving the rigour of the novel signal processing technique with the simplest OFDM signal configuration, the concept is generalized over more complicated configurations in Chapter 5. After the investigation of the OFDM signal with quadrature amplitude modulation on its carriers, the focus is shifted to the peak power reduction schemes that use Golay codes or DFT spreading matrices. At the end of the Chapter 5, the possibility of substituting the train of OFDM chips with a single OFDM chip is discussed, and the trade-off's involved in such an arrangement are evaluated.

Chapter 6 presents the final step in generalizing the signal processing method by exploring the conditions under which the fundamental assumptions regarding the limits of delay and Doppler are violated. The violation of the narrowband assumption for the coherent Doppler integration manifests as the range migration due to high target velocity and high range resolution of th radar. For the pulse compression of the individual OFDM chips, the Doppler scaling effect becomes significant for high target velocities. Compensation techniques are developed for both the range migration and the Doppler scaling. The OFDM pulse compression method is further modified to take into account the violation of the delay limit.

Chapter 2

Orthogonal Frequency Division Multiplexing (OFDM) Signal

OFDM is a spread-spectrum transmission technique where the signal is comprised of multiple carriers. The technique is based on the carriers constituting the signal being mathematically orthogonal, as a result of the uniform frequency spacing in between the carriers. Apart from this arrangement in the spectrum of the signal, the orthogonal carrier structure also requires the signal duration to be the inverse of the carrier spacing.

It must be noted that this chapter does not give the complete treatment of the OFDM signal as used in the communications; the sole aim of this chapter is to familiarize the reader with the fundamentals of the OFDM modulation technique. A great volume of literature that provides in-depth treatment is available and referred in the beginning of the Section 2.1.

Thereafter the chapter progresses by giving the mathematical definition the OFDM signal under the ideal conditions, where there are no channel and receiver effects. The actual OFDM signal as used in communication systems, use of which as radar signal is proposed in this dissertation, is gradually presented by introducing the effects of the communication channel and the transmitter-receiver imperfections in Section 2.2.

The OFDM signal is the sum of harmonics with different starting phases and amplitudes, and as a result has a variable envelope. The effect of the varying envelope is explained in the Section 2.3, and the definition of the metric that quantizes the envelope fluctuations is given.

2.1 OFDM Signal Definition

The original implementation of the OFDM is based on the generation of the multiple carriers via a bank of shaping filters which provide the orthogonality between the carriers [81]. The orthogonal carriers generated in this way can be recovered by a matched filter bank with each filter matched to one channel, where the matched filter eliminates all the carriers except the one that the filter is matched to. Such orthogonality relation enables the carriers to overlap in frequency, eliminating the need for the guard bands between the channels.

While the first conception of the OFDM was based on the filter banks and multiple oscillators that generate the carriers, the arrays of coherent oscillators in the transmitter and the receiver are not practical for the implementation of the OFDM with large number of carriers. The bank of filters and oscillators are later replaced with the fast Fourier transform algorithms, where the digital implementation provides much better precision with lower cost [77]. Although today there is a parallel branch of research that again focuses on generating the OFDM through implementation of digital multirate filter banks, the focus of this thesis is on the OFDM generated and demodulated through IFFT and FFT respectively.

According to the convention set above, the orthogonality of the carriers constituting the OFDM chip is provided by the specific relationship between the timing of the receiving frame and the frequency spacing between the carriers. The OFDM signal can be considered as constituted of individual segments of duration

$$T = \frac{1}{\Delta f}, \tag{2.1}$$

where Δf is the carrier spacing. In other words, one OFDM segment has to have a duration that is the inverse of the carrier spacing for the carriers to be orthogonal. Each such segment will henceforth be called an OFDM chip[1].

In literature the OFDM signal is formulated to encompass blocks of multiple OFDM chips in order to reflect the data package structures associated with the communication protocols. In other words, the emphasis is on groups of OFDM chips rather than the single chip. However, the focus here is on the single OFDM chip for the radar applications, where trains

[1] In literature, the term *OFDM symbol* finds more common usage for the description of such segments.

of such chips are transmitted, which in turn are integrated coherently after the pulse compression to obtain high resolution Doppler information. Thus, different from the definitions used in publications related to communication applications, the mathematical definition of the complex baseband OFDM signal is given here for a single OFDM chip as

$$p(t) = \text{rect}(t) \sum_{m=0}^{M-1} A_m \exp\{j\phi_m\} \exp\{j2\pi m \Delta f t\}. \tag{2.2}$$

where

$$\text{rect}(t) = \begin{cases} 1, & 0 \leq t < T \\ 0, & elsewhere \end{cases} \tag{2.3}$$

and the A_m and ϕ_m are respectively the amplitude and the starting phase of the carrier denoted by the index m, and M is the number of the carriers constituting the OFDM signal. The modulation parameters for each carrier can be determined independently; consequently, the communication messages are transmitted using phase shift keying (PSK) or quadrature amplitude modulation (QAM) on each carrier.

2.1.1 The Modulation and Demodulation Technique

As explained above, the orthogonality of the carriers in the DFT-generated OFDM is provided by the particular relation between the carrier spacing and the chip duration. The OFDM chip definition is important, as the chip duration also defines the duration during which the receiver should be receiving and sampling the OFDM chip. The timing relation is already satisfied in the transmitter when the modulation is generated via the IDFT. The communication symbols, which can be PSK or QAM, are fed into the IDFT as the complex numbers representing the amplitudes and the phases of the spectrum components. The output of the IDFT then has a specific number of samples N which is determined by the number of spectrum components M, and the sampling rate is in turn determined by the carrier spacing, meaning $M = N$. Such equality can be interpreted as generating the baseband OFDM signal with critical sampling according to the Nyquist sampling criterion. It must be noted that by choosing the number of samples N as an integer multiple of M, it is possible to achieve over-sampling. For the rest of the text the critical sampling is adopted unless stated otherwise.

For demodulation, the samples are processed via DFT to acquire the

magnitudes and phases of the spectrum components, on which the communication content was mapped in the transmitter. For the demodulation to successfully recover the modulation parameters, all the samples generated by the IDFT have to be present at the input of the DFT. Thus, the DFT input has to cover the whole time frame of duration T during which the signal is present. In other words, the DFT frame has to be precisely aligned with the OFDM chip.

Equation 2.2 is meant to explain the composition of the OFDM signal; the actual modulation is implemented digitally and has to be formulated accordingly as

$$p(n) = \sum_{m=0}^{N-1} A_m \exp\{j\phi_m\} \exp\{j2\pi m \frac{n}{N}\},\ n = \{0,\ 1,\ 2,\ ...,\ N-1\}, \quad (2.4)$$

where the variable for the time in Eq. 2.2 is replaced by the sampling period,

$$t = n\frac{T}{N} = \frac{n}{N\Delta f}. \quad (2.5)$$

The signal is demodulated via DFT, which yields

$$q(k) = \sum_{n=0}^{N-1} p[n] \exp\left\{-j2\pi k \frac{n}{N}\right\},\ k = \{0,\ 1,\ 2,\ ...,\ N-1\}. \quad (2.6)$$

The orthogonality of the carriers is visible once Eq. 2.4 is inserted in Eq. 2.6,

$$q(k) = \sum_{n=0}^{N-1} \sum_{m=0}^{N-1} A_m \exp\{j\phi_m\} \exp\left\{-j2\pi(m-k)\frac{n}{N}\right\} \quad (2.7)$$

The expression above yields zero when $m \neq k$, because the exponential term has an integer number of cycles within the DFT frame; each DFT output contains only the modulation parameters of the carrier that it corresponds to.

2.1.2 The Cyclic Prefix Guard Interval

In communications the guard interval is introduced to the OFDM signal to remedy the effects of the multipath reflection of the signal. The channel

through which a signal propagates contains non-uniformities that interact with the signal. The interaction usually takes the form of scattering and reflection, and it can be modeled as a filter modifying the signal. As any filter, the channel has a certain duration and can be modeled by time taps with corresponding coefficients. With the channel explained as such, the received signal is comprised of multiple copies of the transmitted signal with different delays, amplitudes and phases corresponding to different filter coefficients.

In order to gain insight on the effects of the channel we analyze analytically the simplest case of line-of-sight path between the transmitter and the receiver where there is one point scatterer. The signal at the receiver, which consists of the sum of the direct signal and the slightly delayed scattered signal, is

$$r(t) = p(t) + p(t-\tau) = \sum_{m=0}^{N-1}\Big[A_m \exp\{j\phi_m\}\exp\{j2\pi m\Delta f t\} \big(\mathrm{rect}(t) + \mathrm{rect}(t-\tau)\exp\{-j2\pi m\Delta f\tau\}\big)\Big]. \tag{2.8}$$

The above expression holds when only one OFDM chip is transmitted and there are no preceding or following chips, which is not realistic in communication applications but adopted here to simplify the treatment of the signal without any loss of the validity. It must also be noted that the scattered signal undergoes an amplitude and a phase change, possibly frequency-dependent, which is omitted again to focus solely on the effect of the guard interval. This signal can be reorganized such that the behavior of the summation at different time intervals is more transparent,

$$r(t) = \begin{cases} \sum_{m=0}^{N-1} A_m \exp\{j\phi_m\}\exp\{j2\pi m\Delta f t\}, & 0 \le t < \tau \\ \sum_{m=0}^{N-1} \Big[A_m \exp\{j\phi_m\}\exp\{j2\pi m\Delta f t\} \big(1+\exp\{-j2\pi m\Delta f\tau\}\big)\Big], & \tau \le t < T \\ \sum_{m=0}^{N-1} \Big[A_m \exp\{j\phi_m\}\exp\{j2\pi m\Delta f t\} \exp\{-j2\pi m\Delta f\tau\}\Big], & T \le t < T+\tau \end{cases} \tag{2.9}$$

The expression above shows that none of the intervals spans the time duration T that is required to keep the carriers orthogonal. Thus, there will be a change of the modulation parameters within the time frame T during which the signal is digitized and fed into the DFT due to the interference

between the consecutive OFDM chips, which is also called inter-symbol interference (ISI). The remedy to this problem is extending the signal duration by modifying the rect(t) function such that

$$\text{rect}(t) = \begin{cases} 1, & -\tau \leq t < T \\ 0, & elsewhere \end{cases}, \tag{2.10}$$

which will modify the duration of the middle row in Eq. 2.9 to span a time frame of length T. In this case the modulation parameters are modified by the time taps that represent the channel, and the carriers are still orthogonal when demodulated by the DFT.

This modification of the rect(t) function is achieved by appending a patch of the OFDM chip from the end with duration τ to the beginning of the OFDM chip. The OFDM waveform, consisting of carriers with an integer number of periods within the time frame T, is cyclically repetitive; the appending operation as described here is equivalent to the extension of the signal duration as shown in Eq. 2.10.

When this modification of the signal is carried out for a train of OFDM chips, the result is a guard interval between two consecutive OFDM chips that consists of a cyclic repetition of the end portion of the following OFDM chip; hence, this specific guard interval technique is called the cyclic prefix. The simple example provided above demonstrates that the duration of the cyclic prefix must encompass the longest delay that is expected to be present in the channel. Moreover, the cyclic repetitiveness of the OFDM enables the treatment of the multipath channel response as a cyclic convolution, which is equivalent to point-wise multiplication in frequency domain [11]. The effect of the multipath channel can be compensated for in frequency domain by multiplication with the inverse of the coefficients describing the channel response.

Functions of the cyclic prefix as explained in the previous paragraph from a communications perspective have their counterparts in the radar domain. The longest delay in the so called *radar channel* corresponds to the round trip radio path for the maximum range of interest. The cyclic prefix in radar context can be regarded as the equivalent of the *delayed sampling* in the frequency modulated continuous wave (FMCW) radar system, which means the radar receiver is turned off at the beginning of each new frequency sweep. The duration has to be greater than the round trip time for the maximum range of interest to prevent the interference from the preceding sweep. The cyclic convolution property that the cyclic prefix guard interval accommodates, translates into the matched filter implementation in the frequency

domain. The utility of the cyclic prefix will manifest in the implementation of the OFDM pulse compression in Chapter 3.

2.2 Synchronization of the OFDM Communication Systems

Taking into account the communication channel between the transmitter and the receiver in Section 2.1.2 was the first step towards understanding the physical reality in which the OFDM modulation has to function. The next step is to consider the time and frequency synchronization between the separately located transmitter and the receiver; the modulation symbols are recoverable only when there is an agreement on the signal parameters such as the carrier frequency and the time reference of the transmitted signal on both sides.

The OFDM signal, while it is quite robust against the multipath reflection along the propagation path, presents an important challenge in this respect due to its sensitivity to the frequency and frame offset between the transmitter and the receiver. This section does not focus on any specific synchronization technique; the emphasis is on the formulation of the effects of the frequency and frame offset. Both aspects will be demonstrated in this section to have a clearer understanding of the effects of delay and Doppler on the OFDM radar signal.

2.2.1 The Time Synchronization

The precise alignment of the DFT window of the receiver with the received OFDM chip is vital for the proper recovery of the modulation symbols. When the DFT window encompasses the transition between the two consecutive OFDM chips due to a random offset τ, the received signal can be written as

$$\begin{aligned} r(t) = \quad & p_1(t+T+2T_g-\tau)\mathrm{rect}_r(t) + p_2(t+T_g-\tau)\mathrm{rect}_r(t) \\ r(t) = \quad & \mathrm{rect}_r(t)\mathrm{rect}(t+T-\tau)\sum_{m=0}^{N-1} A_{1,m}\exp\{j\phi_{1,m}\}\exp\{j2\pi m\Delta f t\} \\ & + \mathrm{rect}_r(t)\mathrm{rect}(t-\tau)\sum_{m=0}^{N-1} A_{2,m}\exp\{j\phi_{2,m}\}\exp\{j2\pi m\Delta f t\} \end{aligned} \quad (2.11)$$

where the $p_1(.)$ and $p_2(.)$ are the preceding and the current OFDM chips, T_g

is the guard interval duration and $rect_r(t)$ function is the window function imposed by the receiver. When $\tau \leq T_g$, the DFT window and the preceding OFDM chip do not intersect, resulting in the elimination of the *inter-symbol interference* (ISI). The ISI is also present for radar signals that have full duty cycle, in other words, continuous transmission. One such radar signal is the FMCW, where the ISI is prevented through delayed sampling.

It must be noted, however, that the primary function of the guard interval is not the relaxing of the time synchronization requirements. When there is an offset between the DFT window and the OFDM chip that is smaller than the guard interval, the phases of the OFDM carriers are modified by the random delay τ,

$$p(t-\tau) = \text{rect}(t-\tau) \sum_{m=0}^{N-1} A_m \exp\{j\phi_m\} \exp\{j2\pi m\Delta f\} \exp\{-j2\pi m\Delta f\tau\}. \tag{2.12}$$

Thus, the communication symbols cannot be recovered correctly when the delay is unaccounted for. However, the delay on the received signal can be measured from the phases of the carriers when the transmitted signal is known. Pilot OFDM chips, which are standardized OFDM chips that the receiver seeks for the time synchronization, are transmitted for this purpose. The timing synchronization of the communication systems is widely covered in literature, with different techniques proposed for the detection of the start of an OFDM chip [5, 38, 39, 40].

A similar technique can be utilized in a monostatic radar, where the perfect knowledge of the transmitted OFDM chip is available at the co-located receiver, for the target delay measurement. In other words, the random communication content is no obstacle for the measurement of the target delay in radar applications, as the information is available on phases of the carriers constituting the transmitted OFDM chip.

2.2.2 The Frequency Synchronization

The OFDM modulation and demodulation takes place in the digital domain, where the IDFT and DFT are implemented as the efficient IFFT and FFT algorithms. The frequency synchronization is needed to solve two distinct types of frequency offset between the transmitter and the receiver: The mismatch between the oscillators in the homodyne or heterodyne upconversion and downconversion steps, in the transmitter and the receiver respectively, is called the carrier frequency offset. The mismatch of the digital clocks

governing the functioning of the digital circuitry in the transmitter and the receiver is called the sampling frequency offset.

Carrier Frequency Offset

The effect of the carrier frequency offset between the transmitter and the receiver, which may be the case in a communication link, has the effect of displacing the locations of the OFDM carriers such that the whole spectrum of the recovered OFDM signal is shifted in the frequency. As a result, the orthogonality relation between the carriers as described in Eq. (2.7) fails. The random frequency offset can be inserted into Eq. (2.7) as

$$q(k) = \sum_{n=0}^{N-1} \sum_{m=0}^{N-1} A_m \exp\{j\phi_m\} \exp\left\{-j2\pi(m-k+\epsilon)\frac{n}{N}\right\} \tag{2.13}$$

where the ϵ term is the frequency offset normalized by the carrier spacing Δf. When ϵ is an integer the carriers are still orthogonal, as the exponential term will sum up to yield zero for $m-k+\epsilon = 0$. However, the communication symbols are displaced by ϵ. On the other hand, the ϵ term will not be an integer in general, and the exponential term will not sum up to zero anymore for any value of m and k. In other words, inter-carrier interference (ICI) will disrupt the communications as a result of the carrier frequency offset. Methods based on the presence of pilot carriers and/or pilot symbols are present in the literature [6, 23, 24].

The carrier frequency offset as described above is apparently not relevant to the monostatic radar with the co-located transmitter and receiver which share the same frequency source. The round trip time of the radar signal from any practically possible range of interest is not long enough for the local oscillators to drift substantially. However, the frequency shift in Eq. (2.13) occurs also due to the Doppler shift that is associated with the radial velocity of targets.

Sampling Frequency Offset

The sampling period, as given in Eq. (2.5), is modified due to the sampling frequency offset as

$$t = n\frac{T}{N} = \frac{n(1+\alpha)}{N\Delta f}. \tag{2.14}$$

where α is the scaling factor. The modified sampling period can be inserted in Eq. (2.7) to yield

$$q(k) = \sum_{n=0}^{N-1} \sum_{m=0}^{N-1} A_m \exp\{j\phi_m\} \exp\left\{-j2\pi(m-k)\frac{n}{N}\right\} \exp\left\{-j2\pi\frac{mn\alpha}{N}\right\}. \tag{2.15}$$

It can immediately be noticed that the orthogonality between the carriers is again lost as the scaling factor α is never an integer, and the exponential term will not sum up to zero. Hence, the ICI will again disrupt the communications. Detection and correction methods for the sampling frequency offset are proposed in the literature, which are based on the transmission of pilot OFDM chips followed by the maximum likelihood estimation of the sampling frequency offset [58, 59].

2.3 Peak to Average Power Ratio (PAPR)

The synthesis of signals through the manipulation of the spectrum components gives rise to a possibly high peak power compared to the average power in one OFDM chip. The peak to average power ratio (PAPR) of the OFDM signal is defined as

$$\text{PAPR} = \frac{\max\left(|p_c(t)|^2\right)}{\frac{1}{T}\int\limits_{n=0}^{T} |p_c(t)|^2 \, dt}, \tag{2.16}$$

where

$$p_c(t) = p(t)\cos\{2\pi f_c t\} \tag{2.17}$$

is the pass-band OFDM signal, that is, the OFDM signal which is up-converted by an RF frequency f_c, with the continuous time variable t. The continuous time variable is adopted here to avoid any inconsistency with regards to the Nyquist sampling criterion when considering the passband signal. It is also very common to assess the envelope fluctuations of the OFDM signal by considering the complex baseband signal expression. The peak-to-mean envelope power ratio (PMEPR) is defined as

$$\text{PMEPR} = \frac{\max\left(|p(t)|^2\right)}{\frac{1}{T}\int\limits_{n=0}^{T} |p(n)|^2\, dt}, \tag{2.18}$$

where the PAPR $\leq$ PMEPR. The reason for separate definitions for the baseband and passband cases is the convenience of calculating the PMEPR that is independent of the RF carrier frequency, while the PAPR is the actual factor that affects the high-frequency hardware in the transmitter. Thus, the terms PAPR and PMEPR can be used alternatively in the context of the qualitative and empirical discussions. It is also noted that, when calculating the PMEPR of an OFDM signal there is a discrepancy between the PMEPR of the critically sampled and the continuous versions of the same signal. This discrepancy is alleviated, although not completely eliminated, when the PMEPR is calculated after over-sampling the discrete signal [74].

The OFDM signal, except in very special cases, has a fluctuating envelope. There are statistical approaches to determine the cumulative distribution function (CDF) of the PMEPR for random modulation content given the waveform parameters and the modulation technique, an example of which is plotted in Figure 2.1 showing that the probability of having a very high (or very low) PAPR is minuscule [75].

With the varying envelope level of the OFDM, the amplifiers must be linear to prevent the distortion of the signal, which would preclude the use of class C amplifiers in compression and result in low amplifier efficiency [57]. To keep the amplifiers working in the linear mode the peak signal power has to be limited, necessitating a certain amount of back-off power and preventing the use of the amplifier at its maximum power level. Referring again to the distribution of the PMEPR for random signal content given in Figure 2.1, the back-off level must be determined such that the amplifier stays in the linear mode of operation with a probability high enough to satisfy the specified bit-error rate requirements of a communication system.

This challenge of high PAPR that is presented by the nature of the signal synthesis was noticed very early in the development of the multi-carrier data transmission technique. Solutions based on special arrangements of the spectrum components, which made the multi-carrier signal resemble a frequency-modulated waveform, were offered to remedy the high peak factor [53]. However the constraints on the modulation of the individual carriers to achieve such frequency modulation resemblance of the OFDM signal severely limit the degree of freedom of the signal, which translates into very small number of bits that can be conveyed by an OFDM chip.

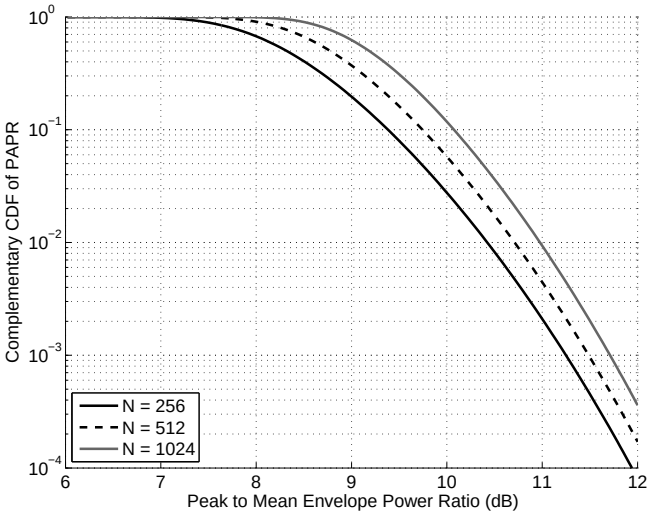

Figure 2.1: The complementary cumulative distribution function of the PMEPR for three different numbers of carriers N=256, 512 and 1024.

The prominence of the challenge the fluctuating OFDM spectrum creates is evident in the volume of literature and the variety of methods developed to remedy it. Novel methods are proposed to lower the peak factor, such as mapping the OFDM envelope on the phase of a single carrier [64] and inserting a DFT spreading matrix (which can be compared to other spreading matrices such as Walsh-Hadamard [54]) before the IFFT in the transmitter to make the OFDM resemble a single-carrier phase coded signal [22, 51]. A comprehensive overview that introduces various other techniques is provided in [19].

2.4 Conclusion

The OFDM communication signal is introduced with the goal of exploring the relevance of its prominent features for the radar application.

The orthogonality of the carriers is an important feature of the OFDM, which requires precise synchronization, between the transmitter and the receiver, of the reference time and frequency. While such synchronization does not appear to be relevant for the monostatic radar application, it has been observed that the synchronization errors in time and frequency, in telecommunication applications, have a similar effect as delay and Doppler frequency shift on the radar echo, respectively.

Thus, in a communication system the aim is to identify the delay and the frequency mismatch between the transmitter and the receiver, so that the communication symbols that are the phases and amplitudes of the OFDM carriers can be recovered in the receiver. On the other hand, in a radar system the goal is to measure the delay and the Doppler effect on the radar signal echo, whereas the communication symbols (i.e. the coding) on the received echo are perfectly known in the receiver.

Chapter 3

OFDM Radar Signal and the Processing Scheme

The description of OFDM in Chapter 2 focused on the aspects of the communication signal, namely the guard interval, the synchronization and the peak to average power ratio (PAPR), and their relevance to the radar application. As combining the radar and communication functions for a network of monostatic radars in one signal is a strong motivation for choosing the OFDM signal, the same OFDM communication signal is the focus of investigation when developing the OFDM radar signal processing chain in this chapter.

The radar operation can be described as the retrieval of target parameters from the received echo signal; the most fundamental parameters are the range and the radial velocity of a target. The OFDM signal as echoed from a point target is modeled in this section, where the effect of the target range and radial velocity is described. The modeling of the echo progresses such that the boundaries of the target and waveform parameters are introduced one at a time, culminating with the introduction of the matrix formulations where the effects of the target parameters and the modulation symbols are explicit.

The fundamental assumption is that the modulation symbols conveying the communication messages are random with uniform distribution over the available states. The novel pulse compression for the OFDM chip, which is constructed over the matrix formulations, exploits the multi-carrier structure of the OFDM in combination with the random modulation symbols to measure the Doppler shift of the received OFDM signal echo. By compensating for the displacement of the OFDM carriers due to the Doppler effect,

the pulse compression recovers echoes from targets with matched Doppler while the other target responses are spread in the background. The OFDM pulse compression method does not require prior information on the target velocity; the compensation method is applied for an interval of velocities of interest to detect all targets with different velocities, effectively implementing a Doppler filter bank in the digital domain. The novel pulse compression method was first reported in [65, 67].

The actual Doppler measurement based on the coherent integration of the compressed OFDM chips, like is done in classical pulse-Doppler radar, exhibits the Doppler ambiguity, where the Doppler effect on the signal is mapped over a limited interval determined by the pulse repetition frequency (PRF). The additional information coming from the OFDM pulse compression method helps solve the Doppler ambiguity, which would otherwise necessitate transmitting multiple trains of OFDM chips with different PRF and/or RF carrier frequency. In other words, the ability to solve the Doppler ambiguity through the additional Doppler information provided by the multicarrier structure of the OFDM signal is presented as another novelty.

The transformation that the echo signal undergoes, due to the effect of the target, is modeled through matrix operations, where the transmitted modulation symbols on the OFDM carriers, as well as the delay and the Doppler parameters, are explicit. The signal modeling method provides the foundation over which the various steps of the pulse compression method are developed. Such explicit presentation of transmitted spectrum components and effects of target parameters in a matrix setting is a new approach.

3.1 OFDM Communication Signal as the Radar Signal

As explained previously, one of the aims of using the multi-carrier OFDM modulation technique is to embed communications in the radar signal, and different from the previous applications where the resources are divided between the two functions, the goal is to utilize a completely communication oriented signal as the radar signal. Thus, the OFDM communication signal as defined in Section 2.1 is used for the purpose of radio detection and ranging of the targets. The baseband OFDM signal in Section 2.1 is modified to include the RF carrier frequency,

$$p_c(t) = \text{rect}(t) \sum_{m=0}^{N-1} A_m \exp\{j\phi_m\} \exp\{j2\pi(m\Delta f + f_c)t\}. \tag{3.1}$$

It must be noted that the radar cross section of a target is a complex quantity, introducing extra amplitude and phase terms associated with the target properties. These amplitudes and phases may vary with frequency and from pulse to pulse for distributed targets that can be modeled as multiple point scatterers. The reflections from such multiple scatterers can interfere constructively or destructively depending on the signal frequency and the phases of the RCS for the individual scatterers. The complex reflection coefficient can be considered as a source of degradation of the pulse compression output, or alternatively it can be utilized for target recognition. However, the treatment of the OFDM signal echo in this thesis will ignore such effects, so that the workings of the pulse compression technique can be demonstrated in a concise manner.

3.1.1 The Wideband Echo Signal

The OFDM communication signal, when echoed from a target, undergoes a certain delay and is modified further by the radial velocity of the target. In literature the effect of the radial velocity is considered as the shift in the frequency of the signal which is called the Doppler shift. The Doppler shift, however, is an approximation of the actual Doppler effect which is the scaling of the signal. The validity of the approximation depends on the time-bandwidth product of the target and the maximum target velocity of interest. While most narrowband radar signals satisfy the assumptions underlying the Doppler shift approximation, we adopt a rigorous approach to ensure the validity of our modeling of the OFDM signal echo and consider the wideband echo signal which is scaled due to the Doppler effect. Thus, the OFDM signal reflected from a point target at range R with radial velocity v is

$$\begin{aligned} p_c(t) = \quad & \text{rect}\left(t\varrho - \tau\right) \sum_{m=0}^{N-1} \Big[A_m \exp\{j\phi_m\} \\ & \exp\{j2\pi(m\Delta f + f_c)\left(t\varrho - \tau\right)\} \Big], \end{aligned} \tag{3.2}$$

where $\tau = 2R/c$ and the scaling factor is

$$\varrho = \frac{c - v}{(c + v)} \tag{3.3}$$

which can be simplified through a Taylor expansion as

$$\varrho = 1 - \frac{2v}{c} \tag{3.4}$$

by assuming $v \ll c$. Substituting Eq. (3.4) in Eq. (3.2), and grouping the complex exponentials according to their frequencies the wideband echo signal becomes

$$\begin{aligned} p_c(t) = \quad & \text{rect}\left(t\left(\left(1 - \tfrac{2v}{c}\right) - \tau\right)\right) \sum_{m=0}^{N-1} \Big[A_m \exp\{j\phi_m\} \\ & \exp\left\{j2\pi m\Delta f t\left(1 - \tfrac{2v}{c}\right)\right\} \exp\left\{j2\pi f_c t\left(1 - \tfrac{2v}{c}\right)\right\} \\ & \exp\left\{-j2\pi m\Delta f \tfrac{2R}{c}\right\} \exp\left\{-j2\pi f_c \tfrac{2R}{c}\right\} \Big]. \end{aligned} \tag{3.5}$$

At this stage the signal is downconverted to obtain the complex baseband signal

$$\begin{aligned} s(t) = \quad & \text{rect}\left(t\left(\left(1 - \tfrac{2v}{c}\right) - \tau\right)\right) \sum_{m=0}^{N-1} \Big[A_m \exp\{j\phi_m\} \\ & \exp\left\{j2\pi m\Delta f t\left(1 - \tfrac{2v}{c}\right)\right\} \exp\left\{-j2\pi f_c t \tfrac{2v}{c}\right\} \\ & \exp\left\{-j2\pi m\Delta f \tfrac{2R}{c}\right\} \exp\left\{-j2\pi f_c \tfrac{2R}{c}\right\} \Big]. \end{aligned} \tag{3.6}$$

It must be noted that assuming $v \ll c$, which leads to Eq. (3.4), does not result in the elimination of the velocity term in the scaling factor. Due to the multiplication of the scaling factor in Eq. (3.6) by $N\Delta f$ and $f_c t$, which can have large values, the effect of the scaling factor on the exponential terms can be profound. The relative magnitudes of the target velocity v, the bandwidth of the signal $m\Delta f$ and the total signal duration T have to be considered to determine if the scaling factor can be ignored in the equation.

The downconverted signal is to be processed in the digital domain; hence, the discrete form of the downconverted signal is obtained by equating the time variable t to

$$t = \frac{nT}{N} = \frac{n}{N\Delta f} \tag{3.7}$$

where n is the sample number, N is both the number of carriers and the total number of samples for critically sampled (i.e. according to Nyquist sampling criterion) complex baseband OFDM, T is the total duration of the OFDM chip and Δf is the carrier spacing.

Substituting the time variables in Eq. (3.6) by Eq. (3.7), the discrete form of the complex baseband OFDM signal echo is obtained as

$$\begin{aligned} s\left(\frac{n}{N\Delta f}\right) = \quad & \operatorname{rect}\left(\tfrac{n}{N\Delta f}\left(\left(1-\tfrac{2v}{c}\right)-\tau\right)\right)\sum_{m=0}^{N-1}\Big[A_m \exp\{j\phi_m\} \\ & \exp\left\{j2\pi m\Delta f \tfrac{n}{N\Delta f}\left(1-\tfrac{2v}{c}\right)\right\}\exp\left\{-j2\pi f_c \tfrac{n}{N\Delta f}\tfrac{2v}{c}\right\} \\ & \exp\left\{-j2\pi m\Delta f \tfrac{2R}{c}\right\}\exp\left\{-j2\pi f_c \tfrac{2R}{c}\right\}\Big]. \end{aligned} \tag{3.8}$$

For the rest of the text, the shorthand notation $s(n)$ is used to designate the discrete form of the complex baseband OFDM signal echo.

3.1.2 The Range Limit for the OFDM Radar Signal

As explained in Paragraph 2.2.1, to keep the carriers orthogonal and prevent interference from the neighboring OFDM chips, the time frame during which the receiver is active must fall in the time interval covering the delayed OFDM chip and its cyclic prefix. In other words, during the time frame of reception the echoes returning from the different targets must not include any portion of the preceding or the following OFDM chips; this condition is imperative for the mapping of target delays on the phases of the carriers. The timing relation between the transmission of the OFDM communication signal and the active period of the radar receiver that provides the isolation between the different OFDM chips is depicted in Fig. 3.1. It can immediately be noticed that the particular timing relation is the same as the delayed sampling in the FMCW radar signals.

To keep the echoes for the consecutive OFDM chips isolated, the guard interval duration has to satisfy the relation

$$T\alpha \geq \frac{2R_{max}}{c} \tag{3.9}$$

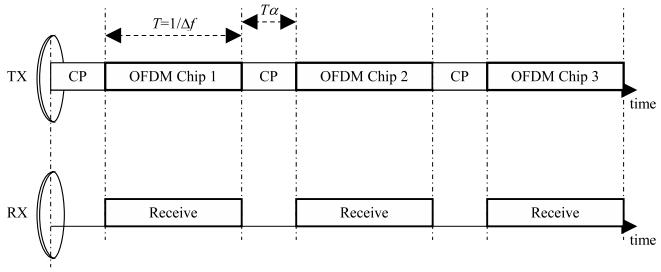

Figure 3.1: The timing relation between the transmitted OFDM chips and the active periods of the receiver provides the isolation between the consecutive OFDM chips.

where $T\alpha$ is the duration of the cyclic prefix. Such relation guarantees that the echo from the farthest target will include the whole cyclic prefix besides a portion of the actual OFDM signal itself. With this condition in mind, the rect(.) function will be omitted in the future references to the OFDM echo.

It must be noted that the violation of this condition does not lead to an immediate loss of the detection capability; the performance of the radar suffers a gradual degradation associated with the increasing interference between the consecutive OFDM chips. The performance of the OFDM radar signal under the violation of the above mentioned condition will be investigated in Chapter 6.

3.1.3 The Matrix Representation of the Echo Signal

The next step is to express the signal and the processing steps in terms of matrix operations on discrete samples of the critically sampled echo signal. The matrix representation is adopted since the processing steps are much more visible in matrix form, and the ultimate goal is to obtain an expression where the amplitude and the phase of the individual carriers are also visible.

The received echo is arranged as a column vector $\mathbf{s}$ where each element corresponds to a discrete sample. The index term n for the sample number designates the row number in this case. For the single element of the vector $\mathbf{s}$, we can organize the summation term on the right hand side of Eq. (3.8) into a vector multiplication such that

$$s(n) = \psi\gamma^n \boldsymbol{\beta}_{\mathbf{n}}(\mathbf{a} \otimes \boldsymbol{\phi}), \tag{3.10}$$

where $\otimes$ represents the Hadamard multiplication, which is the point-wise

multiplication of two vectors or matrices of the same size. The components constituting the complex baseband sample $s(n)$ are

$$\psi = \exp\left\{-j2\pi f_c \frac{2R}{c}\right\}, \tag{3.11}$$

$$\gamma = \exp\left\{-j2\pi f_c \frac{2v}{c}\frac{1}{N\Delta f}\right\}, \tag{3.12}$$

$$\boldsymbol{\beta_n} = \left[\ 1\ \beta^n\ \beta^{2n}\ ...\ \beta^{(N-1)n}\ \right], \tag{3.13}$$

$$\beta = \exp\left\{j2\pi\left(1 - \frac{2v}{c}\right)\frac{1}{N}\right\}, \tag{3.14}$$

$$\mathbf{a^T} = \left[\ 1\ a\ a^2\ ...\ a^{N-1}\ \right], \tag{3.15}$$

$$a = \exp\left\{-j2\pi\Delta f \frac{2R}{c}\right\}, \tag{3.16}$$

$$\boldsymbol{\phi^T} = \left[\ A_0\exp\{j\phi_0\}\ A_1\exp\{j\phi_1\}\ ...\ A_{N-1}\exp\{j\phi_{N-1}\}\right]. \tag{3.17}$$

To combine the $s(n)$ into a column vector $\mathbf{s}$, we have to stack the vectors $\boldsymbol{\beta_n}$ to form a matrix $\boldsymbol{\beta}$ where each row of the matrix is the row vector $\boldsymbol{\beta_n}$. Each row of $\mathbf{s}$ has its specific γ^n as well, which can be arranged by stacking the γ^n in a diagonal matrix $\boldsymbol{\Gamma}$ that is multiplied by the rest of the expression from the left side. Consequently, the received echo is expressed as

$$\mathbf{s} = \psi\boldsymbol{\Gamma}\boldsymbol{\beta}(\mathbf{a}\otimes\boldsymbol{\phi}), \tag{3.18}$$

where $\mathbf{s}$ is the column vector containing the samples of the received echo, and for critical sampling

$$\boldsymbol{\Gamma} = diag\left\{\ 1\ \gamma\ \gamma^2\ ...\ \gamma^{N-1}\right\}, \tag{3.19}$$

$$\boldsymbol{\beta} = \begin{bmatrix} 1 & 1 & 1 & ... & 1 \\ 1 & \beta & \beta^2 & & \beta^{N-1} \\ 1 & \beta^2 & \beta^4 & & \beta^{2(N-1)} \\ & \vdots & & \ddots & \vdots \\ 1 & \beta^{N-1} & \beta^{2(N-1)} & \dots & \beta^{(N-1)^2} \end{bmatrix}. \tag{3.20}$$

The matrix equations are convenient for clearly showing the structure and order of the different operations that take place in the signal processing. The target parameters that are of interest are embedded in the $\boldsymbol{\Gamma}$ matrix, the $\mathbf{a}$ vector and in the scalar ψ term. The target velocity parameter in the $\boldsymbol{\beta}$ term will be eliminated through the narrowband assumption in the following paragraph.

3.1.4 The Narrowband Assumption

In the matrix expression of Eq. (3.18) the only matrix that includes the scaling factor is $\boldsymbol{\beta}$, which is the IDFT matrix whose coefficients are scaled due to the wideband Doppler effect. Our aim is to assess the validity of the narrowband assumption which can simplify the $\boldsymbol{\beta}$ matrix into the IDFT matrix.

So far the derivations of the echo signal are only based on the simple assumption that the target velocity is much smaller than the speed of light, which leads to scaling of the time variable by the scaling factor in Eq. (3.4). As discussed earlier in Section 3.1.1, the condition that $v \ll c$ does not lead to the elimination of the scaling factor, due to the multiplication of the scaling factor in Eq. (3.6) by $m\Delta f$ and $f_c t$, which can have large values. The narrowband assumption relates the signal time-bandwidth product with the velocity of the target such that the scaling of the signal within the duration of the measurement is not significant. As a first condition, the amount of scaling that the OFDM chip undergoes should be less than the critical sampling period, according to the Nyquist sampling criterion, in the digital processing, which yields

$$T\frac{2v}{c} < \frac{1}{N\Delta f}. \tag{3.21}$$

As the signal duration is the inverse of the carrier spacing, the expression simplifies into

$$\frac{2v}{c} < \frac{1}{N}. \tag{3.22}$$

By requiring that the difference in the phase of the matrix element in the lower right corner is less than 2π, another condition can be inferred from the $\boldsymbol{\beta}$ matrix directly,

$$\frac{2v}{c}\frac{(N-1)^2}{N} < 1, \tag{3.23}$$

which yields approximately the same result as in Eq. (3.22) for large N. This condition points out the significance of the scaling effect when the OFDM signal has several tens, or hundreds, of thousands of carriers. It is interesting to note, again, that the carrier spacing does not appear in these expressions due to its cancellation by the signal duration in the formulations.

With the conditions in Eq. (3.22) satisfied, the β term in Eq. (3.20) can be simplified to omit the radial velocity term, resulting in the replacement of the $\boldsymbol{\beta}$ matrix by the IDFT matrix. Thus, the received echo becomes

$$\mathbf{s} = \psi \boldsymbol{\Gamma} \mathbf{F}^{-1}(\mathbf{a} \otimes \boldsymbol{\phi}), \tag{3.24}$$

where $\mathbf{F}^{-1}$ is the IDFT matrix. The results of the violation of the narrowband assumption will be investigated in Chapter 6.

3.2 OFDM Radar Signal Processing

The OFDM communication signal consists of OFDM chips that are separated by cyclic prefix guard intervals. While the transmission is continuous, the reception of the echoes organized as individual frames separated by the guard interval durations can also be considered as a train of OFDM chips as depicted in Fig. 3.1, where the timing relation between the transmitted signal and the receiving frame resembles the delayed sampling in the FMCW radar. Hence, the signal processing method adopted for the OFDM radar signal is pulse compression for the individual OFDM chips followed by the coherent integration of the compressed chips. The multi-carrier structure of the OFDM signal, which is explicit in the matrix formulation developed earlier, is exploited when developing the pulse compression technique to measure the Doppler effect on the individual OFDM chips. The Doppler effect, which is considered as a cause of pulse compression loss for pulse compression

waveforms, is compensated for in the frequency domain. The additional information on the Doppler effect helps solve the Doppler ambiguity occurring in the coherent Doppler integration stage.

3.2.1 The Pulse Compression to Generate the Range Profiles

For the sake of clarity in demonstrating the steps of the pulse compression, we focus first on the echo signal from a stationary target. This assumption simplifies the $\mathbf{\Gamma}$ matrix into the identity matrix; as a result the IDFT matrix $\mathbf{F}^{-1}$ becomes the leftmost matrix operation. The pulse compression starts with the multiplication of the digitized echo signal in Eq. (3.24) by the DFT matrix, and we obtain

$$\mathbf{Fs} = \psi \mathbf{F}\mathbf{F}^{-\mathbf{1}}(\mathbf{a} \otimes \boldsymbol{\phi}) = \psi(\mathbf{a} \otimes \boldsymbol{\phi}), \tag{3.25}$$

where $\mathbf{F}\mathbf{F}^{-1}$ yields again the identity matrix. The multiplication by the DFT matrix to extract the spectrum components of the received echo is actually the same demodulation technique described in Section 2.1.1 that the communication systems utilize.

While in communications the spectrum components are the modulation symbols that carry the content, for the radar signal echo they also contain the velocity and range information. The communication content can be eliminated from the received echo, to leave only the effect of target velocity and range over the OFDM carriers, by Hadamard multiplication of the received spectrum components with the inverse of the transmitted spectrum components [60]. For PSK, where $A_m = 1$ in Eq. (3.17), the inverse of the transmitted modulation parameter is its complex conjugate, while for QAM or other modulation symbols that utilize the carrier magnitudes the inverse of the modulation parameters are $(1/A_m)\exp\{j\phi_m\}$. For purposes of implementing the matched filtering in the frequency domain, however, multiplication with the complex conjugates is adopted and the *compensation vector* composed as such is

$$\mathbf{P}^{\mathrm{T}} = [\ A_0 \exp\{-j\phi_0\}\ A_1 \exp\{-j\phi_1\}\ ...\ A_{N-1} \exp\{-j\phi_{N-1}\}]\,. \tag{3.26}$$

From now on in this chapter the focus will be on the PSK, eliminating the magnitude terms from the modulation symbols; the use of different modulation techniques will be considered in Chapter 5.

Since the Hadamard multiplication between the vectors is commutative we can switch the positions of the $\mathbf{a}$ and $\mathbf{P}$ vectors. The Hadamard multiplication between $\boldsymbol{\phi}$ and $\mathbf{P}$ results in the cancellation of the starting phases, leaving only the $\mathbf{a}$ vector whose elements are determined by the target range. The structure of the $\mathbf{a}$ vector in Eq. (3.15) clearly shows the effect of delay in the received echo signal; a similar structure was demonstrated in Section 2.2.1 for the case when there is a delay in the communication signal.

If the conventional pulse compression scheme is to be followed, the next step is to obtain the range profile by operating the IDFT on the compensated spectrum,

$$\boldsymbol{\chi} = \mathbf{F}^{-\mathbf{1}} \left(\mathbf{P} \otimes (\mathbf{F}\mathbf{s}) \right), \tag{3.27}$$

which gives us the correlation of the echo with the transmitted signal. The structure of the OFDM signal, which is cyclically repetitive, makes the inverse Fourier transform of the multiplication of the frequency domain coefficients equivalent to the cyclic convolution of the received echo with the transmitted signal. This same property is the basis of the frequency domain equalization in the communication systems that eliminates the effects of the multipath reflections in the communication channel, and the pulse compression as described above is nothing but matched filtering.

3.2.2 Doppler Compensation for OFDM Pulse Compression

The Doppler effect on matched filtering manifests itself as a loss in the pulse compression gain, which is also true for the OFDM radar signal [14]. The pulse compression in the previous section was developed considering a stationary target for the sake of achieving a clearer understanding. To see the influence of the Doppler effect on the pulse compression, which is approximated as a shift in the signal frequency due to the narrowband assumption described in Section 3.1.4, we now introduce back the matrix $\boldsymbol{\Gamma}$ into the pulse compression formulation:

$$\mathbf{P} \otimes (\mathbf{F}\mathbf{s}) = \psi \mathbf{P} \otimes (\mathbf{F}\boldsymbol{\Gamma}\mathbf{F}^{-\mathbf{1}}(\mathbf{a} \otimes \boldsymbol{\phi})). \tag{3.28}$$

The structure in Eq. (3.28) presents a challenge to the developed pulse compression technique, as the IDFT and DFT matrices are separated by the $\boldsymbol{\Gamma}$ matrix and they can no longer be eliminated from the expression in a straightforward manner. To find a solution, we need to consider the multiplication between the $\boldsymbol{\Gamma}$ matrix and the DFT matrix $\mathbf{F}$. As the $\boldsymbol{\Gamma}$ matrix

is diagonal, each diagonal element is multiplied by the corresponding column of the **F** matrix, which yields

$$\mathbf{F\Gamma} = \begin{bmatrix} 1 & \gamma & \gamma^2 & ... & \gamma^{(N-1)} \\ 1 & \gamma W & \gamma^2 W^2 & & \gamma^{(N-1)} W^{N-1} \\ 1 & \gamma W^2 & \gamma^2 W^4 & & \gamma^{(N-1)} W^{2(N-1)} \\ & \vdots & & \ddots & \vdots \\ 1 & \gamma W^{N-1} & \gamma^2 W^{2(N-1)} & \dots & \gamma^{(N-1)} W^{(N-1)^2} \end{bmatrix}, \tag{3.29}$$

where

$$W = \exp\left\{-j2\pi\frac{1}{N}\right\}. \tag{3.30}$$

It is visible from the structure of the matrix in Eq. (3.29) that when $\gamma W = 1$, the resulting matrix is again a DFT matrix with rows cyclically shifted downwards. We can generalize this cyclic shift behavior by considering the case where $\gamma(W)^k = 1$, which is possible when the Doppler shift is equal to an integer multiple of the carrier spacing, i.e.

$$\frac{2v}{c} f_c = \epsilon \Delta f. \tag{3.31}$$

In other words, when the complex exponential term γ is equal to the complex conjugate of the $(W)^k$ term, the corresponding powers of the complex exponentials are related as

$$-j2\pi\frac{1}{N}\frac{2vf_c}{c\Delta f} = j2\pi\frac{1}{N}k. \tag{3.32}$$

When the ϵ term defined in Eq. (3.31) equals k, the equality described in Eq. (3.32) holds, and the effect of Doppler corresponds to cyclic shifting of the rows of the DFT matrix downward by the integer number ϵ.

This cyclic shift of the rows of the **F** matrix can be compensated for, before the Hadamard multiplication by the compensation vector **P** in Eq. (3.28) takes place. The *Doppler compensation* operation is a matrix multiplication with another matrix $\mathbf{C}_\epsilon^{-1}$, which is the identity matrix that is cyclically shifted by ϵ in the opposite direction. Thus, the final result of all operations is the range profile for the cyclic shift ϵ:

$$\boldsymbol{\chi}_{\epsilon} = \mathbf{F}^{-\mathbf{1}} \left[\mathbf{P} \otimes \left(\mathbf{C}_{\epsilon}^{-1} \mathbf{F} \mathbf{s} \right) \right]. \tag{3.33}$$

The range profile for the ϵ that is needed to correctly compensate for the Doppler effect on the echo will have the pulse compression gain that the matched filter normally yields for stationary targets. This approach is also valid when the Doppler frequency shift is not an integer multiple of the carrier spacing Δf. In that case the cyclic shift that compensates for the Doppler frequency the best will yield the higher pulse compression gain. From this point onwards, the *OFDM pulse compression* will refer to the Doppler compensating pulse compression operation as described in Eq. (3.33).

3.2.3 Equivalence of the OFDM Pulse Compression to the Ambiguity Function

As explained in Paragraph 3.2.1, the pulse compression method without Doppler compensation is equivalent to matched filtering, the performance of which can be understood by generating the ambiguity function for the signal under consideration. It can also be demonstrated that the OFDM pulse compression technique itself generates the same results as the periodic ambiguity function (PAF), which is devised as a means of investigating the waveforms consisting of coherent identical pulses [15]. Obviously the pulse burst consisting of OFDM chips with random phases does not fulfill the conditions under which the use of the PAF is valid. However, the guard interval being implemented as cyclic prefix allows the use of PAF with the condition that the delay under consideration is less than the guard interval duration; hence, the PAF can be used justifiably for the OFDM pulses. The PAF expression that suits the OFDM radar signal the best is

$$\chi(\tau, f_d) = \frac{1}{T} \int_0^T p(t) p^*(t+\tau) \exp\{j 2\pi f_d t\} dt \tag{3.34}$$

where $p(t)$ is the single period transmitted signal, τ is the delay and f_d is the Doppler frequency shift. It has to be noted that the actual ambiguity function is defined as the squared modulus of the function in Eq. (3.34), which is $|\chi(\tau, f_d)|^2$. As the OFDM pulse compression is implemented digitally, the periodic ambiguity function also has to be converted into the discrete form by replacing the time variable t with the discrete time variable given in Eq. (3.7). Thus, the discrete form of the periodic ambiguity function equals

$$\chi(\tau, f_d) = \frac{1}{N} \sum_{n=0}^{N-1} p\left(\frac{n}{N\Delta f}\right) p^*\left(\frac{n}{N\Delta f} + \tau\right) \exp\left\{j2\pi f_d \frac{n}{N\Delta f}\right\}. \quad (3.35)$$

When the transmitted signal $p(t)$ in Eq. (3.35) is replaced by the discrete form of the transmitted OFDM signal expression in Eq. (3.1), the PAF for the OFDM chip is obtained as

$$\begin{aligned} |\chi(\tau, f_d)| = \Bigg| \sum_{n=0}^{N-1} \Bigg[\sum_{k=0}^{N-1} \left[A_k \exp\{j\phi_k\} \exp\left\{j2\pi \left(k\Delta f + f_c\right) \tfrac{n}{N\Delta f}\right\}\right] \\ \sum_{m=0}^{N-1} \left[A_m \exp\{-j\phi_m\} \exp\left\{-j2\pi(m\Delta f + f_c)\left(\tfrac{n}{N\Delta f} + \tau\right)\right\}\right] \\ \exp\left\{j2\pi f_d \tfrac{n}{N\Delta f}\right\} \Bigg] \Bigg|. \end{aligned} \quad (3.36)$$

The sum terms and the exponentials can be grouped to obtain a simplified expression such that

$$\begin{aligned} |\chi(\tau, f_d)| = \Bigg| \sum_{n=0}^{N-1} \sum_{k=0}^{N-1} \sum_{m=0}^{N-1} \Bigg[A_k A_m \exp\{j(\phi_k - \phi_m)\} \exp\left\{j2\pi(k-m)\tfrac{n}{N}\right\} \\ \exp\left\{-j2\pi m\Delta f\tau\right\} \\ \exp\left\{j2\pi f_d \tfrac{n}{N\Delta f}\right\} \Bigg] \Bigg|, \end{aligned} \quad (3.37)$$

where f_c is eliminated from the equation as it is not multiplied by any of the summation indexes. In other words, the effect of the $f_c\tau$ term is a constant phase which will be significant only when a train of OFDM chips are coherently integrated. The coherent integration extracts the high-resolution Doppler information by measuring the change of this phase term from chip to chip.

For comparison we need to translate the matrix formulation of the pulse compression in Eq. (3.33) into the sum formulation under the assumption that the OFDM pulse compression operates on the echo from a stationary target at zero range, which is also the condition when generating the ambiguity function. The cyclic shift of the carriers nevertheless takes place to search for targets with different velocities, hence, the cyclic shift matrix

$\mathbf{C}_\epsilon^{-1}$ is still present in the formulation while the $\mathbf{\Gamma}$ matrix is eliminated due to the stationary target assumption. The zero range assumption similarly eliminates the $\mathbf{a}$ vector.

It is possible in this setting to transfer the $\mathbf{C}_\epsilon^{-1}$ matrix to the right side of the $\mathbf{F}$ matrix to yield the same cyclic shift of the DFT matrix. The next matrix has the same structure as the $\mathbf{\Gamma}$ matrix, but represented by $\mathbf{\Gamma}_\epsilon$ since it has diagonal elements determined by the amount of the cyclic shift ϵ. The final form of the pulse compression becomes

$$\boldsymbol{\chi}_\epsilon = \mathbf{F^{-1}} \left[\mathbf{P} \otimes \left(\mathbf{F} \mathbf{\Gamma}_\epsilon \mathbf{F}^{-1} \boldsymbol{\phi} \right) \right]. \tag{3.38}$$

Starting from the right hand side, the IDFT of the phase vector $\boldsymbol{\phi}$ is

$$\mathbf{F}^{-1}\boldsymbol{\phi} = \sum_{k=0}^{N-1} \exp\{j\phi_k\} \exp\left\{ j2\pi \frac{kn}{N} \right\}, \tag{3.39}$$

which is multiplied by the $\mathbf{\Gamma}_\epsilon$ matrix to yield

$$\mathbf{\Gamma}_\epsilon \mathbf{F}^{-1}\boldsymbol{\phi} = \sum_{k=0}^{N-1} \exp\{j\phi_k\} \exp\left\{ j2\pi \frac{kn}{N} \right\} \exp\left\{ j2\pi \frac{\epsilon n}{N} \right\}. \tag{3.40}$$

The DFT adds another summation term to the formula

$$\mathbf{F}\mathbf{\Gamma}_\epsilon \mathbf{F}^{-1}\boldsymbol{\phi} = \sum_{n=0}^{N-1} \sum_{k=0}^{N-1} \exp\{j\phi_k\} \exp\left\{ j2\pi \frac{(k-m+\epsilon)n}{N} \right\}. \tag{3.41}$$

The spectrum coefficients recovered through the last DFT operation have to be Hadamard multiplied by the compensation vector $\mathbf{P}$, with one coefficient for each spectrum component that is indexed by the variable m:

$$\mathbf{P} \otimes (\mathbf{F}\mathbf{\Gamma}_\epsilon \mathbf{F}^{-1}\boldsymbol{\phi}) = \sum_{n=0}^{N-1} \sum_{k=0}^{N-1} \exp\{j(\phi_k - \phi_m)\} \exp\left\{ j2\pi \frac{(k-m+\epsilon)n}{N} \right\}. \tag{3.42}$$

The final step is the IDFT to generate the range profiles, which adds the third summation term as

$$\mathbf{F}^{-1}\left[\mathbf{P}\otimes(\mathbf{F}\boldsymbol{\Gamma}_{\epsilon}\mathbf{F}^{-1}\boldsymbol{\phi})\right] = \sum_{m=0}^{N-1}\sum_{n=0}^{N-1}\sum_{k=0}^{N-1}\exp\left\{j2\pi\frac{m\theta}{N}\right\}\exp\{j(\phi_k-\phi_m)\}\exp\left\{j2\pi\frac{(k-m+\epsilon)n}{N}\right\}, \tag{3.43}$$

where θ is the index for the final discrete time variable. We can equate the delay τ in Eq. (3.37) to the discrete time variable θ as

$$\frac{\theta}{N} = -\tau\Delta f. \tag{3.44}$$

The Doppler frequency shift is related to the cyclic shift ϵ through the relation defined in Eq. (3.31), which can be made more explicit as

$$\epsilon = \frac{f_d}{\Delta f}. \tag{3.45}$$

In the end, the same expression as that in Eq. (3.37) is obtained.

The importance of this derivation is due to its validation of the OFDM pulse compression as the equivalent of matched filtering. Moreover, the PAF expression can now be used to demonstrate in the following section the important property of solving the Doppler ambiguity.

3.2.4 Coherent Integration of the Train of OFDM Chips and Solving the Doppler Ambiguity

The final step in the OFDM radar signal processing is the coherent integration of the compressed pulses. The coherent integration is applied over the same range cell of the consecutive compressed pulses, however coherent integration between the compressed pulses with different amounts of Doppler compensation is not possible. Thus, for each cyclic shift step and range cell the results of the pulse compression for a specific number of OFDM chips are integrated coherently by another DFT operation,

$$\Lambda(\theta,\epsilon,v) = \sum_{p=0}^{K-1}\boldsymbol{\chi}_p(\theta,\epsilon)\exp\left\{-j2\pi\frac{p\nu}{K}\right\}, \tag{3.46}$$

where Λ denotes the outcome of the coherent integration, K is the number of the OFDM chips that are coherently integrated, $\nu = 0, 1, ..., K-1$ is the

corresponding Doppler bin of the Doppler DFT output and $\boldsymbol{\chi}_p(\theta, \epsilon)$ is the entry corresponding to the range bin θ of the pulse compression vector $\boldsymbol{\chi}_\epsilon$, as given in Eq. (3.33), for the OFDM chip indexed as p.

The coherent integration actually measures the change in the scalar phase term ψ in the matrix formulations from one compressed pulse to the next throughout a train of such compressed pulses. Thus, this final operation is the same as that applied in the conventional pulse-Doppler radar to extract the Doppler information. The complete processing scheme is depicted in Fig. 3.2.

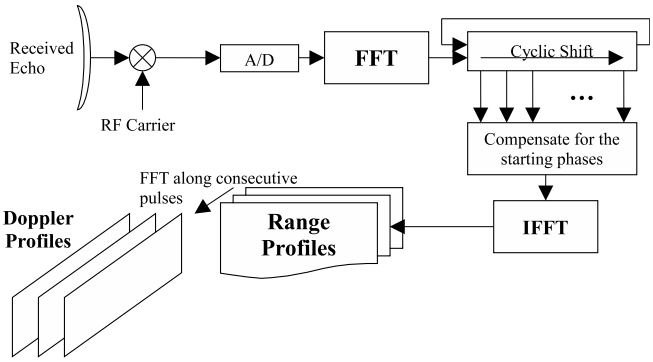

Figure 3.2: The complete processing scheme coherently integrates the OFDM pulse compression output.

The Doppler ambiguity is an important issue for pulse-Doppler radar, where the pulse repetition frequency (PRF) determines both the Doppler ambiguity and the range ambiguity. The principal method for solving the Doppler ambiguity is to transmit multiple trains of pulses with different PRF or carrier frequency, which has different Doppler ambiguity. By comparing the measurements from these different pulse trains, the Doppler ambiguity can be solved. The drawback of this method is the need to transmit multiple pulse bursts, which multiplies the dwell time necessary to obtain the required Doppler resolution.

The novel pulse compression technique, which was described in the preceding paragraphs, offers a new solution to the ambiguity in the Doppler measurements from the pulse Doppler processing by exploiting the muti-carrier signal structure. As explained in Paragraph 3.2.2, use of random phases with uniform distribution creates a sensitivity in pulse compression gain against the Doppler shift. The processing can be regarded as combining the result of pulse-Doppler processing with the Doppler sensitive response of pulse compression. The whole process can be understood better when

the PAF for the pulse burst is considered. The PAF for the train of OFDM chips is

$$|\chi_{PAF}(\theta,\epsilon)| = |\chi(\theta,\epsilon)| \left| \frac{\sin(K\pi\epsilon\Delta fT(1+\alpha))}{K\sin(\pi\epsilon\Delta fT(1+\alpha))} \right|, \tag{3.47}$$

where $|\chi(\theta,\epsilon)|$ is the single-period PAF, the ambiguity function for the single OFDM chip. In Section 3.2.3 the equivalence of the OFDM pulse compression to the ambiguity function of the single OFDM chip is demonstrated.

The second part of Eq. (3.47) is the ambiguity function for the pulse-Doppler waveform with unmodulated pulses, which is independent of the range and repetitive in Doppler frequency by $1/T(1+\alpha)$. Thus, the Doppler response of the single OFDM chip determines the performance of the OFDM radar signal also when a train of compressed OFDM chips are coherently integrated.

Since we consider the OFDM communication signal as radar signal, the phase codes modulating the OFDM chips are essentially random with uniform distribution, and such random distribution requires considering the statistical properties of the ambiguity function when determining the performance of the OFDM radar signal. In Eq. (3.47) the ambiguity function for the single OFDM chip is derived, where the phase terms are the only random components. The randomly determined phase coding is assumed to have a uniform distribution over the available phases, the expected value of the phase terms being

$$E\left[\exp\{j(\phi_m - \phi_k)\}\right] = \begin{cases} 0 & m \neq k \\ 1 & m = k \end{cases} \tag{3.48}$$

and leading to the expected value

$$|E[\chi(\theta,\epsilon)]| = \left| \frac{1}{N^2} \sum_{k=0}^{N-1} \sum_{n=0}^{N-1} \exp\left\{ j2\pi k \frac{\theta}{N} \right\} \exp\left\{ -j2\pi \frac{\epsilon n}{N} \right\} \right| \tag{3.49}$$

for the ambiguity function. The Doppler response of the ambiguity function is obtained by equating the delay variable to zero,

$$|E[\chi(0,\epsilon)]| = \left| \frac{1}{N} \sum_{n=0}^{N-1} \exp\left\{ -j2\pi \frac{\epsilon n}{N} \right\} \right|. \tag{3.50}$$

Eq. (3.50) can be simplified further to

$$|E[\chi(0,\epsilon)]| = |\mathrm{sinc}(\pi\epsilon)|\,. \tag{3.51}$$

Figure 3.3 shows the function in Eq. (3.51) superimposed with the PAF for the unmodulated pulse train and the PAF for the OFDM pulse train, which is obtained by substituting Eq. (3.51) in Eq. (3.47). The Doppler sensitivity arising from the use of the random phases with uniform distribution is clearly visible in the pulse compression result for the single OFDM chip, and the way this sensitivity is used to solve the Doppler ambiguity is demonstrated in the PAF for the OFDM pulse train.

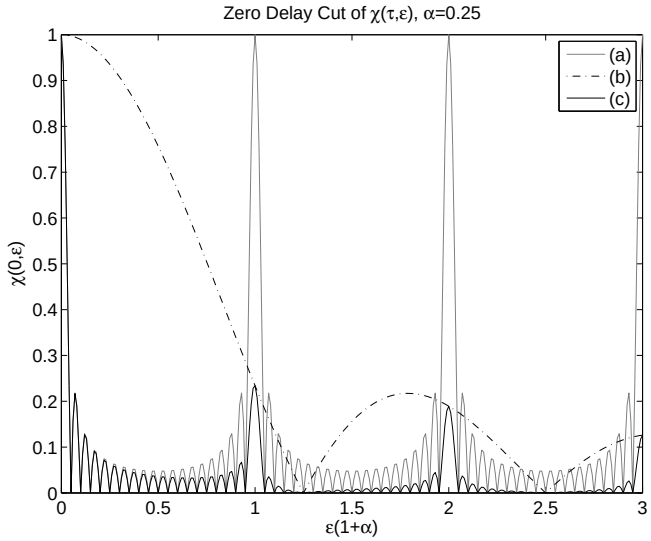

Figure 3.3: The zero-delay Doppler cut is generated through the OFDM pulse compression method; where the responses for the unmodulated pulse train (a), the single OFDM chip (b) and the multiplication of the two, which is the response for the train of OFDM chips (c), are superimposed.

It must be noted that the Doppler ambiguity cannot be fully suppressed due to the discrepancy between the pulse repetition interval (PRI) and the OFDM chip duration, which is the inverse of the carrier spacing. The Doppler ambiguity in the pulsed Doppler processing is the inverse of the PRI,

$$f_{d,amb} = \frac{k}{T(1+\alpha)}, \tag{3.52}$$

where k is an integer. The ambiguous Doppler frequency translates into the cyclic shift as

$$k = \epsilon_{amb}(1 + \alpha), \tag{3.53}$$

which establishes the locations of the peaks for the PAF for the unmodulated pulse train as those points that satisfy the Eq. (3.53). The nulls of the PAF for the single OFDM chip, on the other hand, is related to the Doppler resolution of the OFDM pulse compression, which corresponds to $\epsilon = 1$. Hence, the discrepancy between the PRI and the OFDM chip length, which is the result of the guard interval, reduces the efficiency with which the Doppler ambiguity is suppressed.

It is possible to derive the levels of the Doppler ambiguities as determined by the relative guard interval duration α, by calculating the value of the OFDM pulse compression response at the ambiguous Doppler frequency values. By substituting the ambiguous Doppler frequency expression of Eq. (3.52) in the Eq. (3.51) with the help of Eq. (3.33), the normalized level of the ambiguity sidelobes for the zero delay Doppler cut is

$$A_q = \left| \operatorname{sinc}\left(\frac{q\pi}{1+\alpha}\right) \right|, \tag{3.54}$$

where q is a positive integer and A_q is the amplitude of the ambiguity at

$$\epsilon = \frac{q+1}{1+\alpha}. \tag{3.55}$$

The consequence of the discrepancy between the PRI and the OFDM chip duration, which can be interpreted as less than 100% duty cycle for the pulse train, is the increasing magnitude of the Doppler-ambiguous responses with increasing relative guard interval duration as depicted in Fig. 3.4.

Eq. (3.54) learns that while the lower limit for the guard interval duration is determined by the maximum range of interest, the upper limit for the relative duration of the guard interval must be chosen so as to minimize the magnitude of the ambiguous responses. Consequently, the duration of the OFDM chip has to be kept long to satisfy both conditions; this result establishes a rule of thumb for a possible trade-off between the carrier spacing, maximum range of interest and the ambiguity solving performance.

To summarize, the single OFDM chip can only provide the Doppler resolution that corresponds to the chip duration, and the coherent integration of the OFDM chips can be considered as a method to increase the

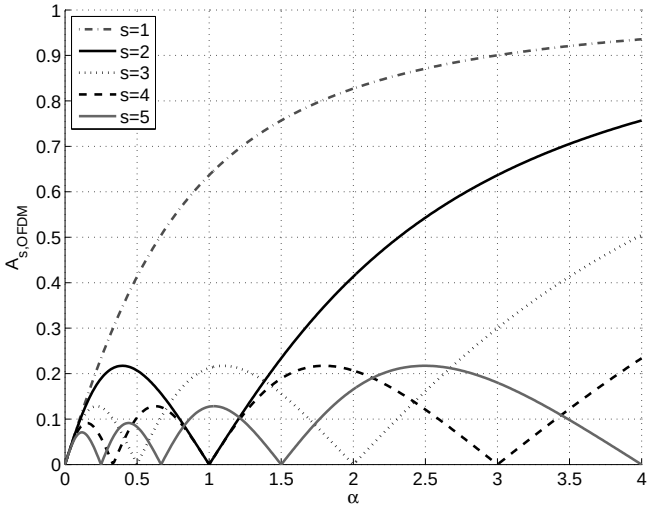

Figure 3.4: The relative magnitudes of the Doppler ambiguity peaks, as observed in Fig. 3.3, vs. the guard interval duration. s indexes the peaks starting from the peak closest to the actual target Doppler.

measurement duration in an effort to increase the Doppler resolution. However, the coherent integration yields Doppler measurements with ambiguity associated with the PRF and RF carrier frequency. The extra information on the Doppler that is obtained through the OFDM pulse compression, obtained through the novel carrier shifting method, helps to solve the Doppler ambiguity.

A valid point to discuss at this stage is the feasibility of substituting the train of OFDM chips with a single OFDM chip that has the same time duration as the whole train of OFDM chips. Following this approach, it can be argued that the Doppler resolution obtained from the OFDM pulse compression will eliminate the need for the coherent integration.

However, it is noted that to occupy the same bandwidth in an effort to achieve the same range resolution as the train of OFDM chips, the number of carriers havs to be multiplied by the same factor with which the the duration of the OFDM chip is multiplied. In other words, the narrower carrier spacing associated with the longer chip duration compels the increase in the number of carriers if the same range resolution is to be preserved.

One consequence of such an arrangement is the possible violation of the narrowband condition, which is described in Eq. (3.22), and given here again for convenience:

$$\frac{2v}{c} < \frac{1}{N}. \tag{3.56}$$

A more detailed analysis of the consequences of this scheme is provided in Chapter 5.

3.3 Computational Complexity

The processing chain that incorporates the OFDM pulse compression with the Doppler compensation introduces greater computational complexity as a result of the need for the cyclic shifts to cover the target velocities of interest. In other words, each cyclic shift of the received echo has to be compressed and recorded for the later coherent integration of the train of such OFDM chips.

If the signal processing is assumed to accept as input the sampled complex baseband signal, then for each received OFDM chip the OFDM pulse compression starts with an N point complex FFT. Afterwards, there are M cyclic shifts to be compressed, each of which starts with an N point complex multiplication followed by an N point IFFT. At this stage the outcome of the pulse compression is recorded into the memory for later access by the coherent integration stage.

The number of floating point operations for the N point complex FFT, when the number of points is a power of 2, equals

$$5N\log_2(N). \tag{3.57}$$

Moreover, each complex multiplication requires six floating point operations. The total number of floating point operations per OFDM chip can be calculated as

$$5N\log_2(N) + M \times (6N) + M \times (5N\log_2(N)). \tag{3.58}$$

For real time operation, the number of operations calculated in Eq. (3.58) has to be completed within the duration of one OFDM chip plus the guard interval duration during which the receiver is turned off; as the chip duration is the inverse of the carrier spacing, the number of floating point operations per second (FLOPS) becomes [1]

[1]The required number of floating point operations for processing a train of OFDM

$$[5N\log_2(N) + M \times (6N) + M \times (5N\log_2(N))] \times \frac{\Delta f}{1+\alpha}. \tag{3.59}$$

It must be kept in mind that the data generated through the OFDM pulse compression has to be written into memory for coherent integration over the train of OFDM chips, which corresponds to a data rate of

$$(M \times N) \times \frac{\Delta f}{1+\alpha} \tag{3.60}$$

complex floating point numbers per second.

The coherent integration is implemented as an FFT operation over the same range bin and the same cyclic shift Doppler bin of the train of OFDM chips. There are $N \times \alpha$ range bins of interest for each OFDM chip, which gives the total number of operations for the coherent integration alone as

$$(N \times \alpha) \times M \times (5K\log_2(K)), \tag{3.61}$$

again assuming that K is a power of 2. It should be noted that the total number of operations for the coherent integration is not significant when compared to that of the OFDM pulse compression in Eq. (3.58).

3.4 Summary and Novelties

A method of pulse compression, which exploits the multi-carrier structure of the OFDM communication signal for solving the Doppler ambiguity in the coherent integration of the train of compressed pulses, has been developed. A novel matrix representation of the OFDM signal echo that encompasses the carrier amplitudes and phases and the effects of the target range and velocity proves to be a vital tool in developing the OFDM pulse compression method and understanding the workings of each processing step in a solid mathematical framework. Such understanding will be necessary for the analysis of the OFDM pulse compression performance in Chapter 4 and

chips with $2^{18} = 262144$ carriers, $\Delta f = 1$KHz carrier spacing and $f_c = 10$GHz RF carrier frequency is 1.2×10^9 operations per chip for the target velocity of interest bounded by the propagation speed of the sound waves in the atmosphere under standard conditions. The real time processing, with the guard interval duration $\alpha = 0.1$ requires 1.1 TFLOPS. At the time of publication of this thesis, graphical processing units (GPU) with the capability of achieving such operation speeds are commercially available.

the generalization of the pulse compression technique over different OFDM implementations in Chapter 5. The rigorous approach of introducing each component of the signal model successively such as the limitations on the target and signal parameters helps explore the limits of the pulse compression technique. Violation of the range and velocity limits is the subject of investigation in Chapter 6.

Solving the Doppler ambiguity by exploiting the multi-carrier structure of the OFDM signal translates into a reducing of the dwell time required by the classical method. The time on target determines the Doppler resolution of the radar, however in the conventional pulse-Doppler radars the ambiguity in the Doppler measurements necessitates the repetition of the measurement with different PRF or RF carrier frequency. For the OFDM signal, the Doppler ambiguity is solved simply with the Doppler information supplemented by the OFDM pulse compression. The coherent integration in this method can be regarded as a means of increasing the SNR as well as the Doppler resolution, when compared to the single OFDM chip.

The prospect of utilizing communication signals for radar applications, or embedding communications in the radar signal from a swapped point of view, enables the implementation of a network of monostatic radars that does not depend on the availability of the commercial wireless communication infrastructure. The novelty of the approach adopted in this thesis lies in the utilization of an OFDM signal as the radar signal, facilitating not only the double use of the hardware for both communication and radar functions but also allowing such double use in the signal level.

Chapter 4

Performance Analysis for the OFDM Radar Signal Processing

The OFDM pulse compression method introduced in Chapter 3 puts forth a novel method of pulse compression that also measures the Doppler effect on the received OFDM signal echoes before the coherent integration of the compressed pulses takes place. The OFDM pulse compression method is intended to operate over the OFDM communication signals, which inherently involves random modulation symbols that carry the digital communication messages. The random OFDM signal translates into random OFDM pulse compression output, which has to be analyzed through the investigation of its statistical properties.

The complete processing chain as described in Chapter 3 consists of the pulse compression and the coherent integration stages; the investigation of the OFDM radar signal processing performance starts from the OFDM pulse compression stage and progresses to the coherent integration. The analysis of the OFDM radar signal processing performance was also covered in [72].

The performance of the OFDM signal and the processing technique are evaluated for three distinct regions of the delay-Doppler plane. The Doppler cut focuses on the Doppler response for the delay bin where the target is present, while the delay cut focuses on the delay response of the target for the Doppler bin where the target is present, which is also called the range profile. The third region is called the far-off sidelobes, which designates those points that are displaced from the delay and Doppler cuts by at least one bin.

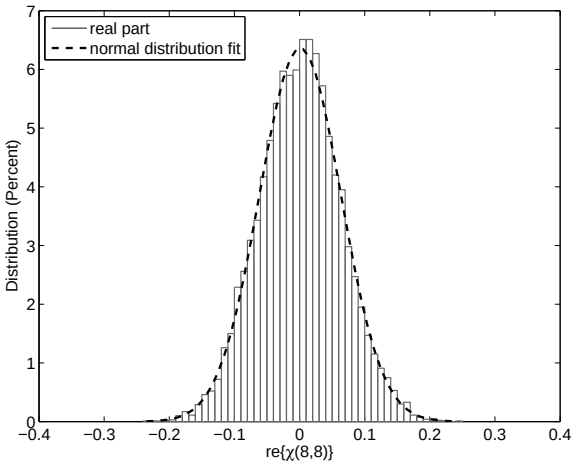

a

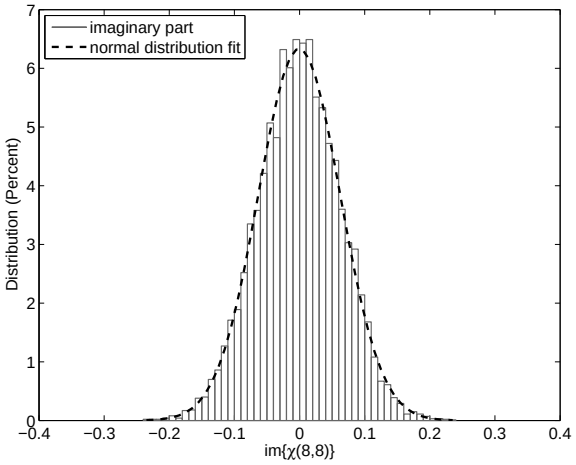

b

Figure 4.1: The PDF for (a) the real part and (b) the imaginary part of a single point in the delay-Doppler plane are calculated from the Monte Carlo simulation results and fitted with the normal distribution curve. The point in the delay-Doppler plane is designated as the 8^{th} range bin and the 8^{th} Doppler bin, and the OFDM signal is with $N = 128$ carriers.

4.1 Statistical Properties of the OFDM Pulse Compression

As a consequence of the random starting phases, the analysis of the pulse compression has to focus on the statistical properties of the ambiguity function, namely the expected value and the variance of the pulse compression output as well as the probability density function (PDF). The expected value and the variance are analytically derived and the derivations are compared to the Monte Carlo simulation results. Both derivations and simulations are validated through experiments where the radar transmitter and receiver are implemented using commercially available equipment. However, for the expected value and the variance to be meaningful, the PDF for the pulse compression output has to be determined, which is accomplished through Monte Carlo simulations.

While the matrix operations are concise, it is hard to evaluate the expected value and the variance of the pulse compression output easily in that form where amplitudes and phases of the carriers are isolated from the compensation matrices, both of which involve the random coefficients that determine the statistical properties of the OFDM pulse compression output. Thus, the pulse compression is given in the summation form as

$$\chi(\theta,\epsilon) = \frac{1}{N^2}\sum_{k=0}^{N-1}\sum_{n=0}^{N-1}\sum_{m=0}^{N-1}\Big[\exp\left\{j2\pi k\left(\frac{\theta}{N}-\frac{2R\Delta f}{c}\right)\right\}\exp\left\{-j2\pi f_c\frac{2v}{c}\frac{n}{N\Delta f}\right\} \exp\left\{j2\pi\frac{(m-k-\epsilon)n}{N}\right\}\exp\{j(\phi_m-\phi_k)\}\Big], \tag{4.1}$$

which is actually the ambiguity function as derived in Section 3.2.3. In this particular form the random phase terms are grouped together and explicit, which helps in the evaluation of the expected value as the only random components in the pulse compression output are easily isolated.

4.1.1 The Probability Density Function of the Pulse Compression Sidelobes

It can be argued that the PDF of the pulse compression output, as given in Eq. (4.1), will converge to the normal distribution as the number of carriers increases. The Central Limit Theorem, the basis of this argument, indicates that the sum of a large number of variables having the same PDF, which is uniform distribution in our specific case where OFDM carriers are

PSK-coded, will attain the normal distribution. However, the sum term in Eq. (4.1) does not consist only of the straightforward sum of random variables due to the presence of the phase terms the pulse compression steps introduce. Hence, bearing this initial argument in mind, Monte Carlo simulations are conducted to determine the PDF of the pulse compression output for OFDM whose carriers are coded with uniformly distributed random PSK. In the Monte Carlo simulations, the histogram of a single point on the delay-Doppler plane is recorded for randomly generated OFDM signal, and the PDF is extracted from the recorded histogram.

The PDF's for the real and the imaginary parts of the pulse compression output for the 8^{th} range bin and the 8^{th} Doppler bin of the delay-Doppler plane, which designates a point corresponding to the far-off sidelobes of the delay-Doppler plane, are calculated. The OFDM signal used in the simulations is with 128 carriers and the target is with zero range and velocity; the results are plotted in Fig. 4.1, where the distributions obtained from the Monte Carlo simulations are fitted with normal distributions. For the distributions in Fig. 4.1 the χ^2 goodness of fit test yielded $\chi^2 = 47.15$ for the real part and $\chi^2 = 56.35$ for the imaginary part. For the significance level of 0.05 and number of degrees of freedom equal to 50, the upper limit that indicates a good fit is $\chi^2 = 67.5$ [63] [1]; in other words the normal distribution exhibits a good enough fit over the Monte Carlo simulation results. Similar goodness of fit results are observed also for the other points in the far-off sidelobes. This agreement between the normal distribution fit and the data obtained from the Monte Carlo simulations suggests that the expected value and the variance calculated in the next section are by themselves sufficient to define the statistical properties of the pulse compression output for the far-off sidelobes of the delay-Doppler plane. The PDF of the pulse compression output for the range cut at zero-Doppler, however, deviates from the normal distribution.

4.1.2 Expected Value and Variance

After the PDF for the pulse compression output is found out to attain the normal distribution at the outlying sections of the delay-Doppler plane, the expected value and the variance are enough to parametrize the general behavior of the OFDM pulse compression. The expected value of the Eq. (4.1) is

[1] The symbol χ^2 is used in the literature to designate the particular distribution that is utilized in the goodness of fit test [63]. However, in the radar literature the χ symbol corresponds to the radar ambiguity function, which is also adopted throughout the text, except in Paragraph 4.1.1.

$$E[\chi(\theta,\epsilon)] = \frac{1}{N^2}\sum_{k=0}^{N-1}\sum_{n=0}^{N-1}\sum_{m=0}^{N-1}\Big[\exp\left\{j2\pi k\left(\frac{\theta}{N}-\frac{2R\Delta f}{c}\right)\right\} \exp\left\{-j2\pi f_c\frac{2v}{c}\frac{n}{N\Delta f}\right\} \exp\left\{j2\pi\frac{(m-k-\epsilon)n}{N}\right\} E\left[\exp\{j(\phi_m-\phi_k)\}\right]\Big]. \quad (4.2)$$

The exponential terms that do not contain any random variables are regarded as deterministic coefficients, and since the expected value operation is linear, those deterministic coefficients are taken outside the expected value.

Evaluating the expected value for the random phase terms requires that a certain probability distribution function is assumed; for a phase code that conveys communication messages it can be assumed that the phases constituting the PSK constellation are equally likely to occur. As these phases are distributed symmetrically over the unit circle on the complex plain, the expected value for them is zero. However, we are dealing with the multiplication of the complex phase terms, which amounts to subtracting the phase values as seen in Eq. (4.2). The subtraction yields zero phase when the indices of the phase variables are the same, which means the outcome is not random anymore but is real and of unity magnitude. However when the indices are different, the outcome of the subtraction is itself random and uniformly distributed, again yielding zero as the expected value. Consequently, the expected value for the exponential phase term is

$$E\left[\exp\{j(\phi_m-\phi_k)\}\right] = \begin{cases} 0 & m \neq k \\ 1 & m = k \end{cases} \quad (4.3)$$

and the expected value for the OFDM pulse compression output is

$$E[\chi(\theta,\epsilon)] = \frac{1}{N^2}\sum_{k=0}^{N-1}\sum_{n=0}^{N-1}\Big[\exp\left\{j2\pi k\left(\frac{\theta}{N}-\frac{2R\Delta f}{c}\right)\right\}\exp\left\{-j2\pi f_c\frac{2v}{c}\frac{n}{N\Delta f}\right\} \exp\left\{-j2\pi\frac{\epsilon n}{N}\right\}\Big]. \quad (4.4)$$

The modulus of the expected value expression in Eq. (4.4) is revealed to be equal to the modulus of the Sinc function, which was also described in Chapter 3 [14].

While the expected value satisfies the range and Doppler resolution the signal bandwidth and duration should provide, and the sidelobes follow

the typical Sinc function profile, the randomness of the pulse compression output is not evident there. The variance is a useful means of demonstrating how much the output of the pulse compression deviates from its expected value and showing whether there will be frequently occurring random high sidelobes that may render the pulse compression method ineffective.

The variance is defined as

$$\sigma_\chi^2 = E\left[\left(\chi - E[\chi]\right)^2\right], \tag{4.5}$$

which can be simplified into

$$\sigma_\chi^2 = E\left[|\chi|^2\right] - |E\left[\chi\right]|^2. \tag{4.6}$$

Finding an analytical expression for the variance involves the derivation of the second moment of the OFDM pulse compression output. The square of the pulse compression output, since it is complex, is obtained through multiplying the Eq. (4.1) by its complex conjugate. The square of the expected value of the pulse compression is similarly obtained through multiplying the Eq. (4.4) by its complex conjugate. Both expressions are provided in Appendix A for the sake of brevity. During these operations it is important to differentiate the summation indexes of the original expressions and their complex conjugates; in Appendix A the indexes for the complex conjugates are distinguished by the overlined mark.

In the second moment expression in Eq. (A.2), which is the expected value of the square of the pulse compression output in Eq. (4.1), the random terms are again grouped in the final exponential and the rest of the exponential terms can be taken outside the expected value operation in the same manner as previously done in Eq. (4.2). In this particular case there are 4 summation indexes that interact with each other, and there are two specific cases that lead to the mutual cancellation of the phase terms, yielding

$$E\left[\exp\{j(\phi_m - \phi_k - \phi_{\overline{m}} + \phi_{\overline{k}})\}\right] = \begin{cases} 1 & m = k, \overline{m} = \overline{k} \\ 1 & m = \overline{m}, k = \overline{k} \\ 0 & m,\ otherwise \end{cases}. \tag{4.7}$$

The final variance expression is

$$\sigma^2_{\chi(\theta,\epsilon)} = \frac{1}{N^4} \sum_{k=0}^{N-1} \sum_{n=0}^{N-1} \sum_{m=0}^{N-1} \sum_{\overline{n}=0}^{N-1} \left[\exp\left\{ j2\pi \frac{(m-k-\epsilon)(n-\overline{n})}{N} \right\} \right.$$
$$\left. \exp\left\{ -j2\pi f_c \frac{2v}{c} \frac{n-\overline{n}}{N\Delta f} \right\} \right]. \tag{4.8}$$

The analytical formulation of the variance in Eq. (4.8) starts with the normalization coefficient, $\frac{1}{N^4}$, which corresponds to normalizing the energy of the OFDM signal to unity.

Monte Carlo simulations are carried out to validate the analytical derivations, the mean value of which is depicted in Fig. 4.2 for 128 carriers. The Sinc $(\sin(x)/x)$ profiles along the delay and Doppler frequency axes are clearly visible, which matches the absolute value of the expected value expression in Eq. (4.4). The same Sinc shape along the delay and the Doppler axes is also derived in [14].

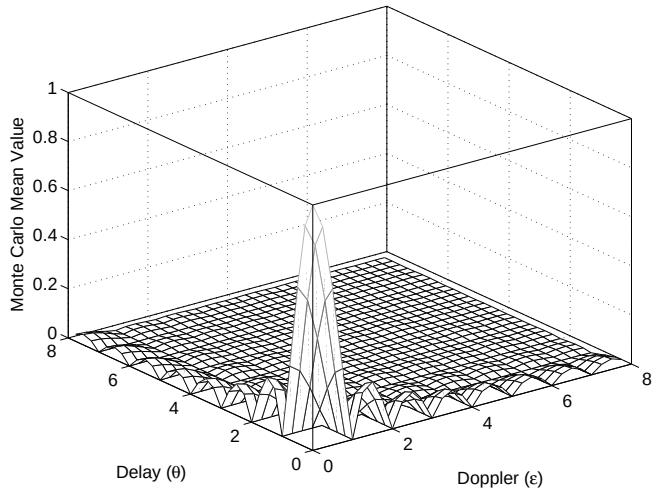

Figure 4.2: The mean value of the pulse compression output for an OFDM signal with $N = 128$ carriers is calculated from the Monte Carlo simulation results.

The variance is also calculated from the Monte Carlo simulations, and plotted in Fig. 4.3, which resembles the behavior of the pulse compression for noise waveforms. An investigation of the statistical properties for the autocorrelation of the noise waveforms in [3] shows that the random time domain samples give rise to random sidelobes of the autocorrelation function. The noise-like effect of the random components in the transmitted signal is described as *the correlation noise*. The variance expression in Eq. (4.8)

matches very well with the variance obtained from the Monte Carlo simulations; this result consolidates our confidence in the model of the OFDM signal echo utilized in the simulations and the derivations.

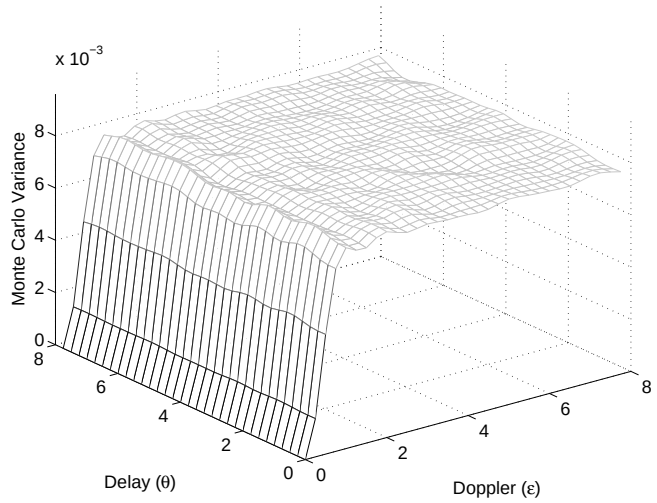

Figure 4.3: The variance of the pulse compression output for an OFDM signal with $N = 128$ carriers is calculated from the Monte Carlo simulation results.

A particular feature of the OFDM pulse compression for the random phase coded OFDM signal is the zero variance along the zero-Doppler range cut of the ambiguity function. This feature is due to the flat power spectrum of the OFDM when the carriers are m-PSK modulated. The zero-Doppler range cut of the ambiguity function is determined purely by the Fourier transform of the power spectrum of the signal, which is deterministic and flat for OFDM with m-PSK modulated carriers. The lack of correlation noise in the autocorrelation function may provide an advantage in the detection of slowly moving ground targets by reducing the interference from stationary ground clutter, as the pulse compression response for such slow moving targets can be located in the *trench* of low variance by arranging the carrier spacing according to the particular scenario.

Both the Monte Carlo simulations and the analytical expression in Eq. (4.8) show that the variance of the sidelobes converges to a certain value with the Doppler shift further away from the compensated value. This convergence value for the variance is plotted with respect to the number of carriers, as calculated from the analytical formula in Eq. (4.8) and from the Monte Carlo simulations, in Fig. 4.4. There is an excellent matching of the values derived from both methods, and the relation between the value to

which the variance converges and the number of carriers N is revealed to be

$$\sigma^2_{\chi(\epsilon)} = \frac{1}{N}. \tag{4.9}$$

It must be noted that this variance level is considered for the ambiguity function with unity peak, which can be translated as the signal having unity energy. The analytical expressions in Eq. (4.4) and Eq. (4.8), with the normalization factors $1/N^2$ and $1/N^4$ respectively, also satisfy this condition of unity signal energy.

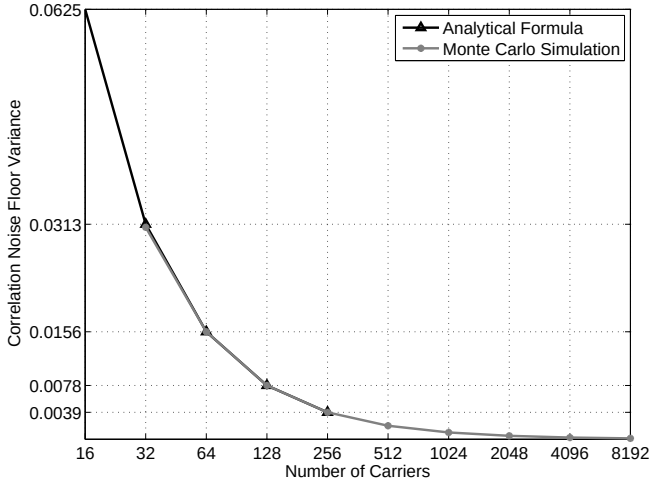

Figure 4.4: The variance of the pulse compression output is inversely proportional to the number of carriers according to both the Monte Carlo simulation results and the analytical formulation of the variance.

4.1.3 The Contribution of the Additive White Gaussian Noise

Besides the random starting phases of the carriers, the additive white Gaussian noise (AWGN) also has an effect on the pulse compression, which can be included in the derivations of the expected value and the variance easily through two assumptions:

Assumption 1: The expected value for the noise alone is zero. This assumption is useful as the pulse compression operation is linear; the output of the pulse compression for the AWGN is eliminated when considering the expected value of the pulse compression.

Assumption 2: The AWGN and the signal are orthogonal. When considering

the variance of the pulse compression output, the correlation of the noise and received echo appears in the expected value of the squared processing output. This assumption eliminates the covariance terms, leaving the final expression for the variance as

$$\sigma^2 = \sigma^2_{\chi(\epsilon)} + \sigma^2_{AWG}. \tag{4.10}$$

The variance of the AWGN can be related to the more familiar signal-to-noise ratio (SNR) metric. For a signal of 1 Watt average power, which is our reference normalization level, the noise variance is equal to $1/SNR$. The *correlation noise* variance in Eq. (4.8), however, is calculated for unity OFDM signal energy. The SNR expression can also be written in terms of signal energy, such that

$$\frac{E}{W_0} = \frac{ST}{\frac{W}{N\Delta f}} = N\frac{S}{W} = N \times SNR, \tag{4.11}$$

where E is the signal energy, W_0 is the noise power density, S is the signal average power, W is the noise average power, T is the OFDM chip duration, N is the number of carriers and Δf is the carrier spacing. Thus, to write the σ^2_{AWG} for the energy-normalized case, we need to multiply the SNR by the number of carriers N, which gives the resulting variance as

$$\sigma^2 = \frac{1 + \frac{1}{SNR}}{N}. \tag{4.12}$$

The SNR under consideration in Eq. (4.12) is for the received signal before pulse compression; the correlation noise is calculated for the output of the pulse compression, and for a meaningful comparison the SNR after pulse compression has to be considered. The pulse compression gain is determined by the time-bandwidth product, which is equal to the number of carriers N for the OFDM signal as the OFDM chip duration is equal to the inverse of the carrier spacing Δf. Hence, the variance term in Eq. (4.12) can be reorganized to include the SNR after the pulse compression as

$$\sigma^2 = \frac{1}{N} + \frac{1}{SNR_{PC}}. \tag{4.13}$$

where $SNR_{PC} = N \times SNR$.

The equation (4.13) provides important insight on the interaction of the random phase coded OFDM signal with noise. We can immediately

note that as the SNR increases the correlation noise becomes dominant, and with decreasing SNR the noise variance is the greatest contributor to the variance of the ambiguity function sidelobes. The important difference between the two noise types is the correlation noise floor's being determined by the strongest echo received from the reflecting agents when there are multiple reflecting objects such as other targets and clutter. In other words, in the presence of strong clutter the noise floor is dominated by the correlation noise rather than the AWGN, and weak targets may be concealed by the correlation noise from the strong clutter. It must be noted, however, that the stationary clutter will not interfere with the stationary targets through the correlation noise, due to the presence of the *trench* that was described in Paragraph 4.1.2 and that is also visible in Fig. 4.3. This is also true for two targets that have the same velocity; for the range cut at the Doppler value that is matched to the target velocity the variance is zero, which means that the two targets with the same velocity will not mask each other through the correlation noise.

4.1.4 The Experimental Validation of the Statistical Properties

The analytical derivations and the Monte Carlo simulations reveal several important and interesting features of the OFDM radar signal, such as the correlation noise floor, the Sinc-shaped expected value for the range and the Doppler cuts, and the lack of correlation noise on the zero-Doppler range cut. The mathematical model for the OFDM radar signal echo was implemented in MATLAB to conduct Monte Carlo simulations, and the statistical properties of the simulation results are in perfect agreement with the analytical formulations. However, as the Monte Carlo simulations themselves are based on the same mathematical models that are the basis of the analytical derivations, a set of experiments is conducted to provide a final verification of those mathematical models. The experiment setup, where the radar transmitter and receiver stages are implemented using commercially available equipment, is described in detail in Appendix B.

The system description in Chapter 1, which provides the framework for the radar waveform design approach in this thesis, places emphasis on high range and Doppler resolution along with the communication capabilities to enable the radar network operation. In the light of these aspects, the waveform parameters provided in Table 4.1 are adopted for the set of experiments explained here, where the signal bandwidth provides 0.5 meters of range resolution and increased Doppler resolution can be achieved through the coherent integration of the compressed OFDM chips.

Table 4.1: Waveform parameters for the experiments.

Parameter Name	**Parameter Value**
Carrier Spacing	1 kHz
Number of Carriers	300000
RF carrier frequency	9.8 GHz
IF carrier frequency	250 MHz
Range resolution	0.5 m

The delay-Doppler plane in Fig. 4.5 is generated by applying the OFDM pulse compression method to the OFDM signal echo, which has uniformly distributed random QPSK phase coding on its carriers. The optical delay line, the length of the cables in the system and the distance between the transmit and the receive antennas introduces the 60.4 μs delay observed. When zoomed further over the range bins where the target is present in Fig. 4.6, multiple reflections in the anechoic chamber due to the presence of the transmitter and transponder equipment within the chamber are also visible on the delay-Doppler plane.

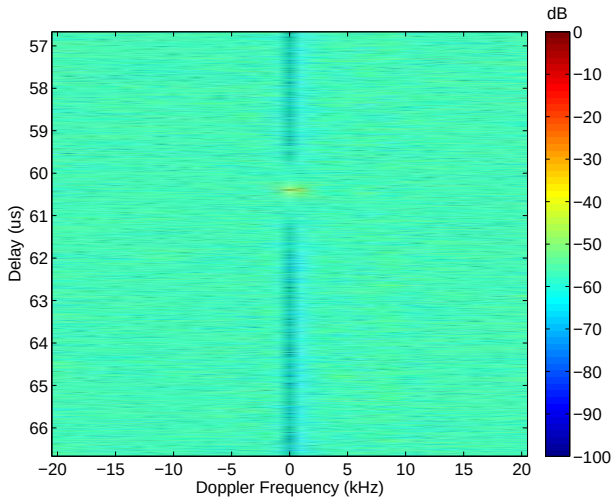

Figure 4.5: The delay-Doppler plane is generated through the OFDM pulse compression method.

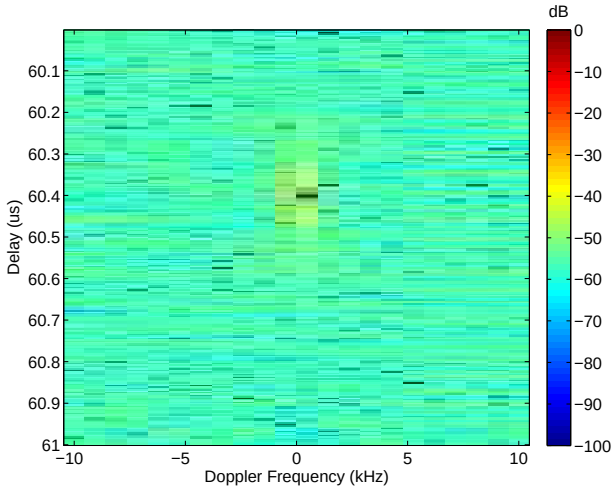

Figure 4.6: The delay-Doppler plane is generated through the OFDM pulse compression method.

The range profile in Fig. 4.7 is generated from the same ambiguity function by over-sampling to clearly demonstrate the close-in sidelobes, which is in excellent agreement with the mean value of the Monte Carlo simulations depicted in Fig. 4.2. The level of the first sidelobes are very close to -13dB, a common value for such profiles following the Sinc-shape function. The width of the mainlobe corresponds to 0.5 meters, which is the resolution the 300MHz signal bandwidth yields. As there is no correlation noise along the zero Doppler range cut, the sidelobes are visible until the thermal noise floor is reached.

The *trench* in the noise floor along the zero-Doppler range cut is clearly visible in the delay-Doppler plane depicted in Fig. 4.5, which can be compared to the variance of the pulse compression output that is calculated from the Monte Carlo simulations and plotted in Fig. 4.3. The non-zero level along the *trench* is due to the thermal noise in the transmitter and the receiver and in the optical delay line which is a part of the transponder. The power spectrum of the signal after down-conversion and decimation is plotted in Fig. 4.8, where the noise level is visible. Since the OFDM spectrum is rectangular the SNR can be deduced quantitatively from the difference between the noise floor level and the OFDM spectrum; Fig. 4.8 shows that the noise floor is 9 dB below the OFDM spectrum. It must be noted that the pulse compression takes place in the frequency domain, where only the spectrum components within the OFDM signal band are taken. Thus, the noise bandwidth is equal to the signal bandwidth.

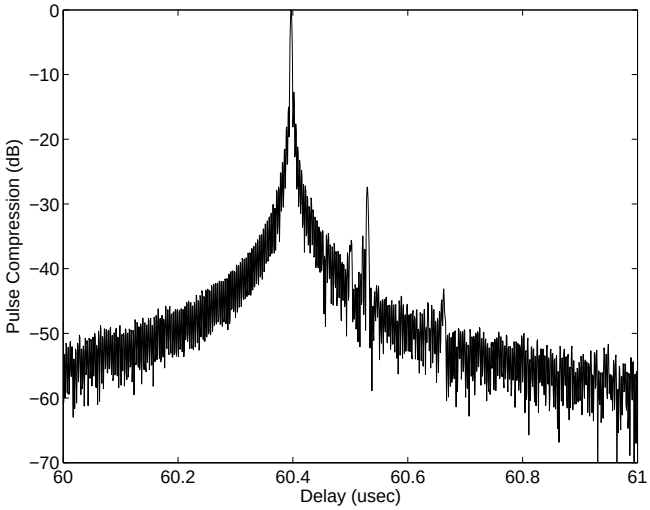

Figure 4.7: The range profile obtained from the experiments follows the Sinc function shape.

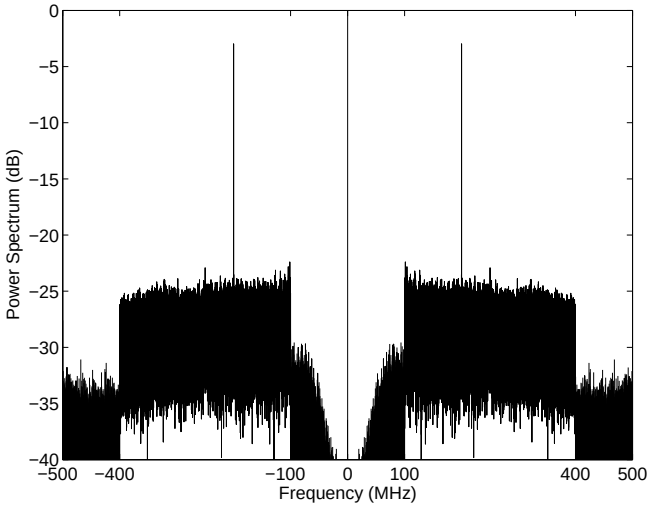

Figure 4.8: The noise level is visible in the spectrum of the received OFDM signal echo at IF stage.

It must also be noted that the high peak in Fig. 4.8 occurring at 200 MHz is a spurious carrier coming from the down-conversion chain. Another such spurious carrier, although less visible in the figure, is at 250 MHz. Although the peak appears very high, the percentage of the energy coming from the spurious carrier is relatively low due to the presence of many carriers

in the OFDM signal. The peak in Fig. 4.8 is approximately 25 dB above the OFDM spectrum level; however, the total number of carriers, which is $N = 300000$, translates into a gain of 54.8 dB after the pulse compression. Moreover, the energy in the spurious carrier will be spread over the pulse compression output, which consists of 300000 samples with critical sampling according to Nyquist sampling criterion. The combined effect of the pulse compression gain on the OFDM signal and the spreading of the spurious frequency component will reduce the effect of the spurious energy to -84 dB per sample, normalized with respect to the pulse compression peak. This value is already much lower than the correlation noise floor and the thermal noise floor, and the insignificance of the effect of spurious frequency assures the validity of the conclusions derived from the experiments. The spurious frequency components can also be eliminated during the digital signal processing, further limiting their effect on the pulse compression output; this is considered as an advantage of the multi-carrier signal structure.

For a more detailed investigation on the properties of the noise floor, the variance is calculated along the different range cuts for a section of the processing output that excludes the target. This way, the close-in sidelobes that follow the Sinc-shape function are excluded from the variance calculation. The variance along the Doppler trench is calculated as 2×10^{-7}, which agrees with the value $SNR \approx -9dB$ observed in the power spectrum of the IF signal in Fig. 4.8. The calculated variance of 3.73×10^{-6} agrees with Eq. (4.13), which yields 3.75×10^{-6} for the combined correlation noise and AWGN.

The experiment results as explained above validate the properties of the OFDM pulse compression that were revealed and explored through analytical derivations and simulations. The performance of the pulse compression under the realistic effect of the receiver chain on the received echo, such as the thermal noise and the spurious carriers, demonstrates the feasibility of the pulse compression technique. At the same time, the obtained measurement results give the opportunity to make comparisons with the simulations thanks to the reliable performance of the carefully designed receiver chain. Such careful receiver design ensures that the spurious effects and noise level are accounted for.

4.2 Accuracy of the Target Delay and Doppler Measurements

As explained in the previous section, modulating the carriers using uniformly distributed random phase codes is essential for alleviating the ambiguity in the Doppler measurements. The randomness of the modulation components imposes the use of the statistical properties of the processing output for assessing the performance of the waveform; hence, the expected value of the ambiguity function is used when demonstrating the approach for alleviating the Doppler ambiguity in Section 3.2.4.

The random phase codes modulating the carriers of the OFDM signal also introduce random fluctuations to the ambiguity function, which establish a noise floor that limits the accuracy of the target parameter measurements. While the variance of the ambiguity function due to the random phase codes and the thermal noise is derived in Eq. (4.13), the effect of this variance on the accuracy of the target parameter measurements has to be demonstrated as well to validate the use of the OFDM communication signal as the radar signal along with the the proposed coherent integration technique. The methodology adopted for determining the accuracy of the target parameter measurements is to repeat the Monte Carlo simulations of Section 4.1.2 with random target parameters which are, in turn, measured from the radar signal echo and compared with the actual parameters.

4.2.1 The Interpolation Technique to Measure the Target Parameters

Assessing the accuracy with which the radar measures the target parameters requires the adoption of an estimation technique. The discrete range and Doppler bins usually do not coincide with the actual target parameters, resulting in the straddling loss in the pulse compression and preventing the accurate measurement of the target parameters. Oversampling and various estimation and interpolation techniques can be adopted to prevent the straddling loss. While assessing different interpolation and estimation techniques for the novel pulse compression technique is of great interest, the volume of research needed for this assessment alone compels us to leave such research out of the scope of this thesis.

Instead of developing an interpolation technique which is based on linear regression or least squared error curve fitting techniques, we adopt the Sinc interpolation and numerically determine the peak location for simulated targets. The Sinc interpolation reconstructs a signal from its samples by

summing the sample-weighted Sinc functions such as

$$f(t) = \sum_{n=-\infty}^{\infty} x_n \text{sinc}(\pi(t - nT_s)) \tag{4.14}$$

where x_n are the discrete samples, T_s is the interval between the successive samples and $f(t)$ is the signal in the continuous-time form after interpolation.

Instead of the continuous time variable t, a discrete time variable with sampling period much shorter than T_s is substituted into the Eq. (4.14) such that the sampling rate is increased significantly to reduce the error arising from the straddling. The sample with the greatest amplitude and the two adjacent samples on each side are taken into account for the interpolation, for the curve fitting techniques described in the literature are also based on the few samples around the maximum [76, 37]. The interpolation is considered separately for the delay and the Doppler outputs for a specific cyclic shift, and the Doppler ambiguity is solved afterwards by again applying the same interpolation technique along the cyclic shift results. Thus, the interpolation is conducted in one dimension (1-D) at a time; techniques using 2-D functions for interpolation can be considered as well.

4.2.2 The Accuracy of the Measurements with Additive White Gaussian Noise

To verify the relation between the Doppler ambiguity and the guard interval duration, three different waveform parameters are determined for which Monte Carlo simulations are performed. The primary constraint when determining the waveform parameters is keeping the range and Doppler resolution the same for each parameter set while obtaining an integer number of samples for the guard interval and the number of pulses. Such constraint yields a very limited parameter set, which is given in Table 4.2 and Table 4.3. It must be noted that the guard interval duration $\alpha = 0.44$ is not realistic for communication systems, nor is it realistic for radar systems. However, it is included in the simulations to clearly demonstrate the relation between α and the rate of ambiguity solving success.

Other parameters that are crucial in obtaining meaningful Monte Carlo results are the range and velocity of the simulated point target, which are randomly determined for each run. For the range, the outcome of the signal processing is repetitive for each range cell. Thus, range is randomly determined such that it is uniformly distributed between the last half of one range cell and the next half of the following, covering all the range bin straddling

Table 4.2: Waveform parameters for the Monte Carlo simulations.

Parameter Name	**Parameter Value**
Carrier Spacing	1 kHz
Number of Carriers	1000
RF carrier frequency	10 GHz
Coherent integration time	21.6 ms
Range resolution	150 m
Velocity Resolution	0.69444 m/s

Table 4.3: Waveform and target parameters for evaluating the guard interval effect.

Parameter Name	**Simulation I**	**Simulation II**	**Simulation III**
Number of pulses	15	18	20
Guard interval relative duration	0.44	0.20	0.08
Target range interval (m)	$375 \leq R \leq 525$	$375 \leq R \leq 525$	$375 \leq R \leq 525$
Target velocity interval (m/s)	$0 \leq v \leq 375$	$0 \leq v \leq 375$	$0 \leq v \leq 375$

cases possible for one range bin.

Determining the velocity is more complicated, for there are two separate processing steps that have repetitive results with different periods. The result of the Doppler FFT is repetitive after the Doppler ambiguity is reached, and the aim is to make sure that an integer number of Doppler ambiguity repetitions and cyclic shifts are covered by the chosen velocity range of interest. The least common multiple (LCM) of the repetition periods is determined for each parameter set in Table 4.3, and the velocity is randomly chosen to obtain a uniform distribution between zero and the LCM velocity, which is 375m/s for the Simulation I and III, and 75m/s for

the Simulation II. It must be noted, however, that an upper velocity limit of 375m/s is adopted also for the Simulation II, for the sake of keeping the velocity interval the same for all three cases.

To see the effect of correlation noise and AWGN on the accuracy of the processing and interpolation techniques, Monte Carlo simulations are performed for different SNR levels. The number of unambiguous velocity estimations for sufficiently high (above 15dB) SNR_I (the SNR after coherent Doppler integration) is plotted in Fig. 4.9 for the three guard interval durations. The SNR_I is connected with the SNR_{PC}, which is defined in the context of Eq. (4.13), through the relation $SNR_I = K \times SNR_{PC}$ in the linear scale, where K is the number of OFDM chips that are coherently integrated. The Doppler ambiguity is solved by forming a list of ambiguous velocities that correspond to the Doppler FFT bin in which the target is present, and choosing among this list the velocity which is the closest to the velocity that corresponds to the cyclic shift which yields the highest pulse compression gain. Both the FFT bin and the cyclic shift corresponding to the target velocity are determined by a peak search in the pulse compression response. More advanced estimation methods, while they may possibly yield better results, are outside the scope of this thesis. The greatly increased percentage of ambiguous velocity estimations for longer guard interval durations verifies the assessment of [67], that the Doppler ambiguity is solved better when the relative duration of the guard interval is smaller. Fig. 4.9 also shows that oversampling the cyclic shift results by a factor of 2 corrects the ambiguous estimations, which is thanks to more accurate determination of the peak position for the pulse compression gain with respect to the amount of cyclic shift. It is observed that further increase in the over-sampling does not give further improvement.

When measured velocities are plotted against the actual target velocities, in Fig. 4.10, it is observed that ambiguous measurements are grouped at regular velocity intervals. The periodicity of the ambiguous measurements with respect to the target velocity reveals the nature of the ambiguous measurements: Those velocities that lie in between the center velocities for two consecutive cyclic shift values are solved ambiguously. Those velocities that lie at the lower end of one cyclic shift Doppler bin are folded to the upper end, the reverse occurs for those velocities at the upper end. This ambiguity is eliminated when the cyclic shift is oversampled by a factor of 2.

An important feature observed in Fig. 4.9 is the relatively rapid decrease in the percentage of correct solutions when SNR_I is reduced below 15dB. The reduction is dominated by erroneous measurements of the velocity rather than the Doppler ambiguity. Such behavior is expected due to the

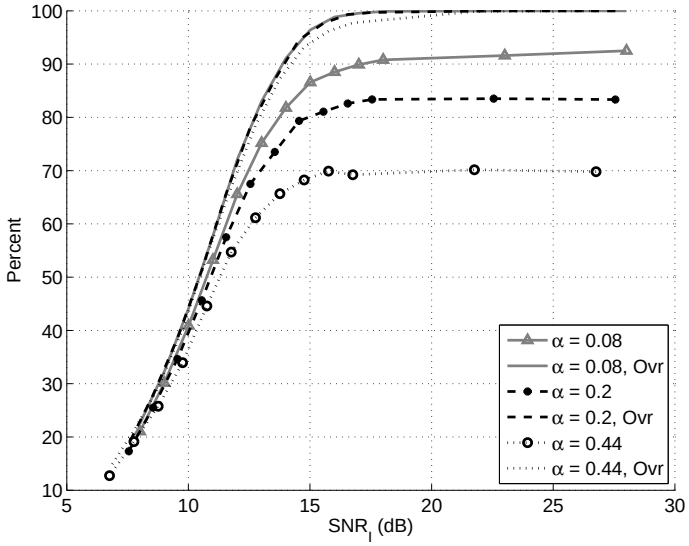

Figure 4.9: From the Monte Carlo simulations, the percentage of the unambiguous velocity measurements vs. SNR_I for different guard interval durations are determined. The plots designated by Ovr are with oversampling by a factor of 2, while the other plots are with critical sampling.

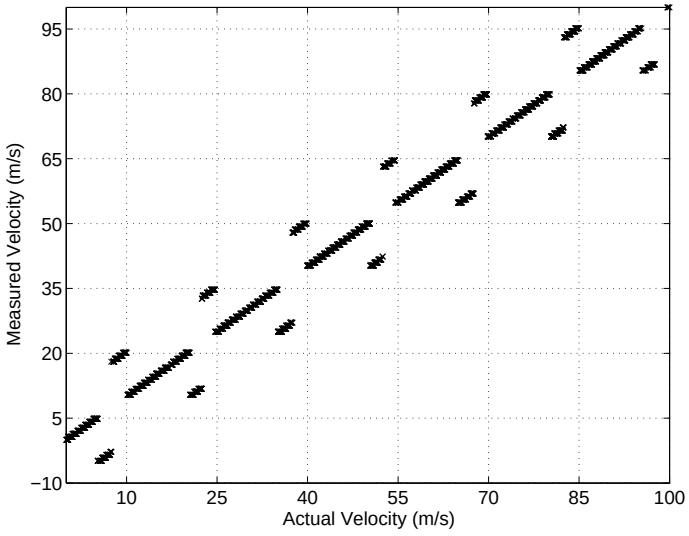

Figure 4.10: The measured velocities for 15 pulses, guard interval $\alpha = 0.44$, show ambiguous measurements occurring regularly with respect to actual target velocities, when there is no oversampling.

utilization of the peak search for finding the target velocity. Below a certain SNR_I value a spurious peak due to the noise comes up with an amplitude higher than the target response, and coupled with the size of the data set that is the output of the signal processing, peak search method yields erroneous measurement as the SNR decreases below a threshold determined by the size of the data set.

Accuracies of the range and ambiguous velocity measurements are assessed by focusing on the cyclic shift that yields the highest pulse compression gain; in other words, the one that corresponds to the actual target velocity. The error distributions for the range and velocity measurements are depicted in Fig. 4.11 and Fig. 4.12 respectively, which feature the combination of estimation errors coming from the interpolation technique and the correlation noise and AWGN.

The distribution of errors for the low-noise case resembles a uniform distribution, while the features of the error distribution increasingly resemble that of the normal distribution as the SNR_I decreases. A numerical experiment evaluating the distribution of the sum of two random variables, one with uniform distribution and other with normal distribution, yields similar features. Thus, this peculiar feature of the error distribution is due to the separate errors arising from the interpolation technique and the AWGN.

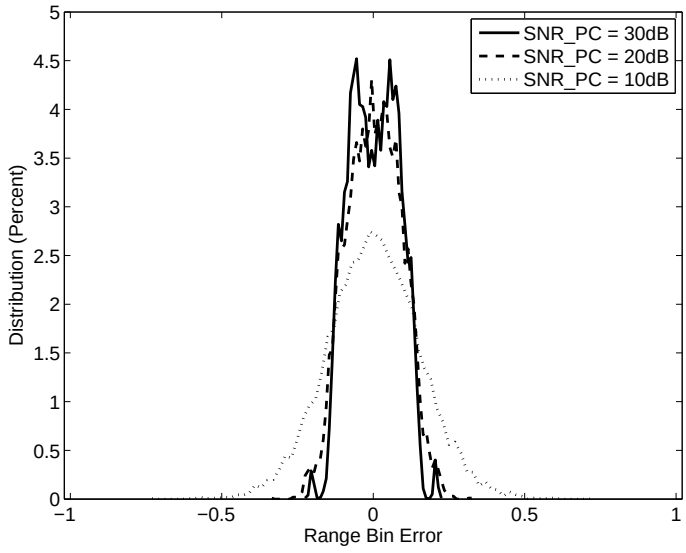

Figure 4.11: From the Simulation II, where $\alpha = 0.2$, the error distribution for the range estimations for different AWGN levels calculated after the pulse compression.

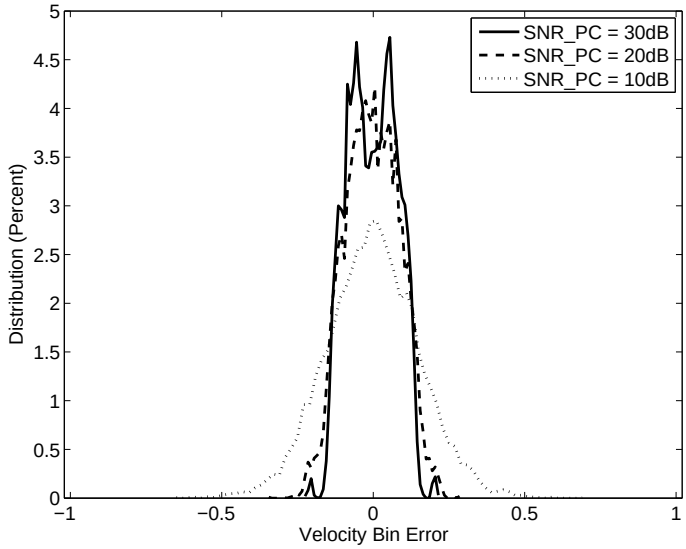

Figure 4.12: From the Simulation II, where $\alpha = 0.2$, the error distribution for the velocity estimations for different AWGN levels calculated after the pulse compression.

4.2.3 The Accuracy of the Measurements with Multiple Targets

The presence of the correlation noise in the delay-Doppler plane necessitates the investigation of its effects on the measurement accuracy using the same methodology as in the previous paragraph. The PDF of the correlation noise, for the far-off sidelobes, is Gaussian with variance determined by the Eq. (4.9). The distribution of the estimation error and the number of ambiguous velocity estimations are obtained from Monte Carlo simulations involving two targets, where the close-in target is stationary and acting as the clutter while the second target is moving. Thus, instead of SNR_I, the signal to clutter ratio parameter after the coherent integration (SCR_I) is explored and its effect on the measurement accuracy is assessed through Monte Carlo simulations. To isolate the effect of the correlation noise, the simulations are run with no AWGN added to the received echoes. In addition, the target range is increased to make sure that the separation between the two targets is enough to eliminate the effect of the range sidelobes that appear in the expected value of the ambiguity function. It must be noted that the SCR_I is calculated in the same manner as SNR_I, considering the ratio of the received echo power from the target to the received echo power from the clutter.

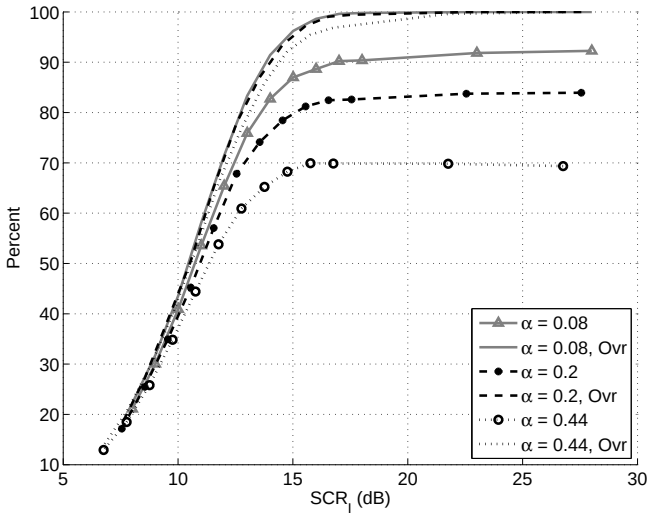

Figure 4.13: From the Monte Carlo simulations, the percentage of the unambiguous velocity measurements vs. SCR_I for different guard interval durations are determined. The plots designated by Ovr are with oversampling by a factor of 2, while the other plots are with critical sampling.

The number of unambiguous velocity estimations for sufficiently high (above 15dB) SCR_I (the SCR after coherent Doppler integration) and the three guard interval durations is plotted in Fig. 4.13. The agreement of the ambiguity rates in the velocity estimation with that of the AWGN case in Fig. 4.9 confirms that the correlation noise at the far-off sidelobes of the delay-Doppler plane has indeed the same characteristics as the AWGN. This result also indicates that in the face of strong clutter the weaker or far-off targets may be concealed under the correlation noise. Advanced signal processing techniques that adaptively remove the clutter energy from the processing output can be utilized to unmask the weak target responses.

4.3 Summary and Novelties

The OFDM pulse compression technique developed in Chapter 3 is analyzed to demonstrate its performance under the presence of AWGN and for a multiple target case. The random modulation symbols on the OFDM communication signal obliged the analysis to focus on the statistical properties. Analytical derivations of the expected value and the variance of the pulse compression output are supplemented with the Monte Carlo simulations to show that the delay - Doppler plane obtained through the OFDM pulse

compression method has favorable sidelobe characteristics.

While the analysis can be compared to similar studies on other noise waveforms [3], the complete coverage of both the delay and the Doppler response of the OFDM signal and pulse compression method using both analytical formulations and Monte Carlo simulations is a novel and rigorous approach. Moreover, the derivations and simulations based on the mathematical model of the OFDM signal echo are verified by the experiment results. The crucial validation of the mathematical model through experiments opens up the possibility to reliably predict the performance of the different OFDM implementations through Monte Carlo simulations.

The complete processing chain including the coherent integration of the compressed pulses is implemented in Monte Carlo simulations, which demonstrated the Doppler ambiguity solving capability of the OFDM pulse compression under the influence of AWGN. The multiple target scenario, which focuses on the effects of the correlation noise that is a result of the random signal content, points out the similarity between the effects of the correlation noise and the AWGN on the pulse compression output, a result also supplemented by the analytical derivations. The proven capability to solve Doppler ambiguity without resorting to transmitting multiple pulse bursts with different PRF and/or RF frees operation time of the radar which can be allocated to other tasks.

This chapter concludes the analysis and verification of the purported capabilities of the OFDM pulse compression for the OFDM signals with phase coded carriers. The analysis techniques and the verified OFDM signal echo models are expanded over more complex implementations of the OFDM signal in the next chapter.

Chapter 5

Generalization of the OFDM Radar Signal Processing

The OFDM pulse compression method was developed in Chapters 3 and 4 by considering the phase shift keying (PSK) modulation on the OFDM carriers. Since our methodology has as the starting point the analytical equations that model the echo signal and the processing method, the tractability of the PSK modulation expressions proved to be vital. The analytical equations, combined with the experimental results, validate the simulation tools, which opens up the possibility of assessing the performance of OFDM signals with different modulation techniques applied on their carriers. In this context, the performance of the OFDM pulse compression for the OFDM signal with 16-QAM modulation on its carriers is investigated by Monte Carlo simulations. The results are verified by analytical formulations and experimental results, proving once more the reliability of the OFDM signal echo model and the OFDM pulse compression implementation for the Monte Carlo simulations. It is also demonstrated that the variable power spectrum of the OFDM with 16-QAM modulation is compatible with the OFDM pulse compression method.

The high peak-to-average power ratio (PAPR) of the OFDM comes as a challenge in radar applications due to the requirement for high amplifier efficiency. As the same challenge is present for the communication systems, where mobility and battery life requirements push for higher power efficiency, many PAPR control techniques are proposed in the literature [19]. The OFDM pulse compression is tested for the PAPR-control methods that offer a significant reduction in the PAPR without seriously hampering the communication capability, namely the Golay complementary codes and the

single-carrier OFDM. The assessment of these PAPR-control methods for radar applications generated novel results, which were partially reported in [69]. One alternative to the PAPR-control methods is to clip the peaks of the OFDM signal; the effect of this method on the OFDM pulse compression performance is also assessed through the Monte Carlo simulations.

The final modification of the OFDM signal that is considered in this chapter aims at increasing the OFDM chip duration, so that the need for the coherent Doppler integration to achieve a high Doppler resolution is eliminated. The trade-off's involved in such modification are listed, and the possible violation of the narrowband assumption due to the increased OFDM chip duration is pointed out.

5.1 OFDM Modulation with Variable Power Spectrum

The OFDM pulse compression introduced in Chapter 3 is based on the compensation of the starting phases of the carriers, which is demonstrated to be equivalent to the ambiguity function. The flat power spectrum of the phase coded OFDM means that the phase components are the only modulation coefficients that must be compensated for. However, this approach is not completely true when the power spectrum of the OFDM is not flat, which is the case when the carriers have QAM modulation schemes. The QAM symbols consist of both phase and amplitude components, and the previous results on the statistical properties of the pulse compression output cannot be readily accepted as valid. Hence, the pulse compression has to be generalized for OFDM with fluctuating power spectrum.

The compensation proposed in Chapter 4 for the modulation coefficients on the carriers is based on the compensation of the starting phases by multiplication with their complex conjugates. Such compensation technique, coupled with uniformly distributed random phase coding, results into a Doppler sensitivity that is further exploited to solve the Doppler ambiguity. However, such compensation leaves a residual random component that is the amplitude of the modulation coefficient, when the modulation components belong to the QAM constellation. On one hand, this residual random component due to the fluctuating spectrum appears to be a drawback. On the other hand, the alternative approach based on the division of the received spectrum components by the transmitted ones [60] deviates from the matched filter implementation. The immediate implication of this deviation is the degradation of the signal to noise ratio (SNR), which is maximized by

the matched filter. Thus, investigations on QAM, and on some other modulation techniques also presented in this chapter, solely focus on the OFDM pulse compression technique developed in Chapter 3.

5.1.1 Analysis of the Pulse Compression Output for Quadrature Amplitude Modulation

The QAM symbol for communications can be assumed to have uniformly distributed random real and imaginary components that are independently determined. Thus, assumptions stated in Eq. (4.3) and Eq. (4.7), which determine the statistical properties of the OFDM pulse compression for the m-PSK modulated OFDM, have to be modified accordingly. The phase terms of the PSK modulated OFDM, namely the $\exp\{j\phi_m\}$ are replaced with the QAM symbol $a_m + jb_m$. The assumption of independent real and imaginary parts leads to the modification of Eq. (4.3):

$$E\left[(a_m + jb_m)(a_k - jb_k)\right] = \begin{cases} 0 & m \neq k \\ E[a_m^2] + E[b_m^2] & m = k \end{cases} . \tag{5.1}$$

The expected value for the real and imaginary components has to be evaluated by taking into account the possible modulation symbols for a selected QAM scheme. The expected value for OFDM with random QAM on its carriers turns out to be the same as that for the PSK modulated OFDM, except the scaling of the magnitude that is due to the amplitude modulation.

The expected value term that is part of the second moment expression, as given in Eq. (4.3), is also modified into:

$$E\left[(a_m + jb_m)(a_k - jb_k)(a_{\overline{m}} - jb_{\overline{m}})(a_{\overline{k}} + jb_{\overline{k}})\right] = \begin{cases} 4E[a_m^2 a_{\overline{m}}^2] & m = k, \overline{m} = \overline{k} \\ 4E[a_m^2 a_k^2] & m = \overline{m}, k = \overline{k} \\ 0 & otherwise \end{cases} . \tag{5.2}$$

It should be noted that the terms a_m, a_k and $a_{\overline{m}}$ are determined independently, and the expected values in Eq. (5.2) have to be evaluated by taking into account the possible modulation symbols for QAM.

With the expected value terms updated to reflect the QAM properties, the variance can be evaluated following the same steps as in Appendix A. The variance along the range cut for 16-QAM scheme is plotted in Figure 5.1 from both analytical calculations and Monte Carlo simulations. Results show that the pulse compression output along the zero-Doppler range cut

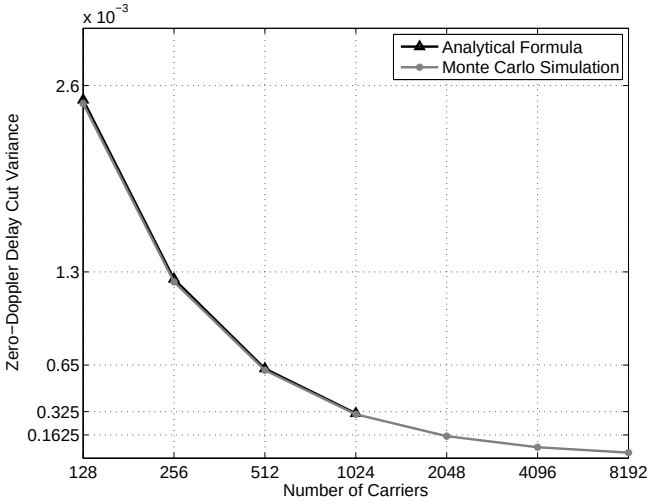

Figure 5.1: QAM modulation for OFDM carriers exhibit non-zero variance along the zero-Doppler delay cut due to the amplitudes that are not compensated for in the pulse compression.

for QPSK and QAM schemes has a different variance; the variance for the QAM scheme is non-zero (albeit lower than 1/N) along the zero-Doppler delay cut, whereas the variance is zero for the QPSK scheme. This is due to the residual random magnitude that is left over after the OFDM pulse compression. For the far-off sidelobes, however, the $\sigma^2 = 1/N$ rule is still valid.

5.1.2 Simulation and Experiment Results

Following the same methodology as in Paragraph 4.1.2, the analytically derived expected value and variance are compared to Monte Carlo simulations and validated through experiments. The Monte Carlo simulation script developed in Chapter 4 is used again; this time modulation coefficients over the OFDM carriers are changed to random QAM. The mean value of Monte Carlo simulation results still has the same Sinc-function profile in the zero-delay Doppler cut and the zero-Doppler delay cut. The variance that is plotted in Figure 5.2 does not fall to zero anymore along the zero-Doppler delay cut. This happens because the random amplitudes are not taken into account during the OFDM pulse compression due to the matched filter implementation. It means that the matched filtering operation takes just the complex conjugates of the modulating symbols, but leaves the random amplitudes untouched.

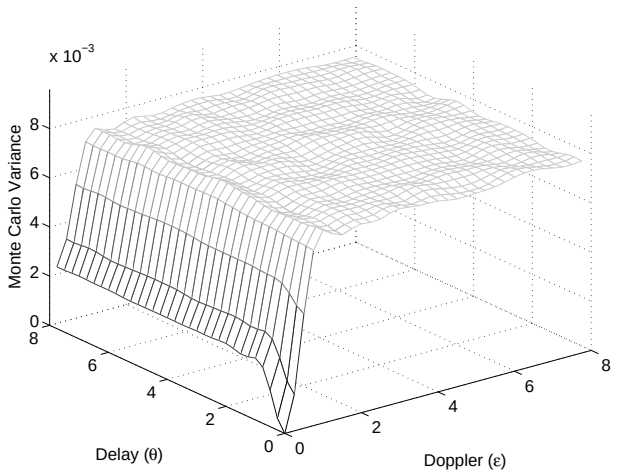

Figure 5.2: The variance of the OFDM pulse compression output for 16-QAM modulated OFDM is calculated from Monte Carlo simulations for N=128 carriers.

Experimental results obtained using the same waveform parameters presented in Table 4.1 are shown in Figure 5.3, where we observe a shallower trench along the zero-Doppler delay cut. The results were obtained by calculating the variance along the different range cuts for a section of the processing output that excludes the target. In this way the close-in sidelobes that follow the Sinc-shape function are excluded from the variance calculation. The variance along the trench is calculated as 1.36×10^{-6}, a value greater than the thermal noise level by an order of magnitude, whereas the variance along the delay cuts with non-zero Doppler value is calculated as 3.75×10^{-6}, which agrees with the $1/N$ rule revealed in Eq. (4.9).

The analytical derivations and simulation and experimental results show that the performance of the OFDM with QAM symbols is very similar to that of the PSK-modulated OFDM. Hence, it can be concluded that the OFDM pulse compression technique presented in this thesis is also applicable to QAM, which is frequently utilized in telecommunication systems.

5.2 OFDM Pulse Compression with PAPR Control Techniques

The OFDM signal is the sum of harmonics with different starting phases and amplitudes, and as explained in Chapter 2, has a variable envelope as a

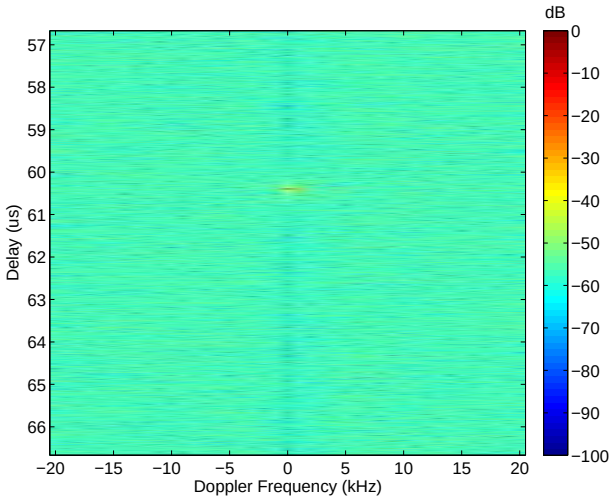

Figure 5.3: Experimental results for OFDM signal with 16-QAM modulation confirms the lower but non-zero variance along the zero-Doppler delay cut.

result. The extent of the envelope variation is assessed through the PAPR value, which relates the peak instantaneous power level to the average signal power. The non-unity PAPR has important implications for the amplifiers. The class-C amplifiers, which are preferred for their efficiency but operate in the saturation regime, cannot be used when the signal envelope is not constant [57]. The strong linearity requirements to guarantee an un-distorted signal imposes a significant power back-off in the amplifiers, which further deteriorates the amplifier efficiency. These concerns on the PAPR pose an important challenge, however the interest in mobile communication systems utilizing OFDM modulation creates a strong synergy between the communication and radar domains towards finding methods to limit the PAPR. The limited battery life in mobile communication systems also imposes strict efficiency criteria on the linear amplifiers, thus, such need for high efficiency also fuels the research for techniques to reduce the PAPR [19].

PAPR lowering techniques have the common aim of limiting the amplitude fluctuations in the time domain signal. There is a rich literature on such techniques; among the different methods two are chosen here, namely the Golay phase codes and the *single carrier*-OFDM (SC-OFDM). The Golay codes enable communications as the coding technique can be implemented for a useful number of carriers, and the remarkable reduction of the PAPR makes it a good candidate for radar applications [8, 45, 46]. The SC-OFDM is adopted for up-link communications in long-time evolution (LTE) communication systems [2].

5.2.1 Effects of Limiting the PAPR on the Pulse Compression Sidelobes

The investigation of pulse compression sidelobes in Chapter 4 and paragraph 5.1.1 revealed a distinct sidelobe behavior in the expected value and the variance of the ambiguity function. Both of these distinct sidelobe behaviors are the result of an OFDM radar signal carrying random phase coding; the sidelobes of the expected value are dominant in the vicinity of the target along the zero-delay Doppler cut and the zero-Doppler delay cut; the sidelobes of the variance behave as a noise floor, which is more important for the remaining parts of the delay-Doppler plane off the zero-delay and zero-Doppler cuts.

The ambiguity function, which is the principal method for determining the performance of a radar signal, can be too complicated to relate the various modifications on the radar signal to their immediate effects on its performance. However, the zero-delay Doppler cut and the zero-Doppler delay cut of the ambiguity function are related to the signal in a straightforward manner. The periodic ambiguity function (PAF) that was described in the Eq. (3.34) under Paragraph 3.2.3 equals:

$$\chi(\tau, f_d) = \frac{1}{T} \int_{-\infty}^{\infty} p(t) p^*(t+\tau) \exp\{j2\pi f_d t\} dt, \tag{5.3}$$

with the limits of the integration changed as, by definition, the signal $p(t)$ is equal to zero outside the interval $[0, T)$ that constitute the limits of the actual PAF expression in Eq. (3.34). The zero-delay Doppler cut is obtained from

$$\chi(0, f_d) = \frac{1}{T} \int_{-\infty}^{\infty} p(t) p^*(t) \exp\{j2\pi f_d t\} dt, \tag{5.4}$$

which implies that the zero-delay Doppler cut is determined solely by the instantaneous power of the transmitted radar signal. On the other hand, the zero-Doppler delay cut is given by:

$$\chi(\tau, 0) = \frac{1}{T} \int_{-\infty}^{\infty} p(t) p^*(t+\tau) dt, \tag{5.5}$$

which corresponds to the cyclic convolution of the transmitted radar signal

with itself. The cyclic convolution of two signals is equivalent to the inverse Fourier transform of the point-wise multiplication of their spectrum [11]; hence, Eq. (5.5) can be written as the inverse Fourier transform of the power spectrum of the radar signal, i.e.

$$\chi(\tau, 0) = \frac{1}{T} \int_{-\infty}^{\infty} P(f)P^*(f) \exp\{j2\pi f\tau\} df. \tag{5.6}$$

The reduction in PAPR of an OFDM signal can be considered as a modification of the zero-delay Doppler cut, independent on the means by which such reduction has been achieved. The time-domain behavior of the OFDM signal can be modified by simply changing the phases of the spectrum components. Such phase changes have no effect on the power spectrum.

The implication of this result is that it is possible to modify the zero-delay Doppler cut without changing the zero-Doppler delay cut by simply re-arranging the phases of the OFDM carriers. In this way any PAPR reduction method that relies solely on the re-arrangement of the phases will result in the modification of the zero-delay Doppler cut. It can be deduced that the nature of this modification will be a reduction in the variance of the ambiguity function, as the random fluctuations in the instantaneous power are reduced with the PAPR limitation. However, the exact manner of the change in the ambiguity function, and hence, in the radar signal performance, has to be analyzed for any PAPR reduction method of interest.

The effect of reducing the PAPR can be observed in the mean value and variance of the ambiguity function for OFDM signals that have an upper limit to their peak-to-mean envelope power ratio (PMEPR). Such PMEPR limit can be imposed by randomly generating phase codes and selecting only those codes that yield a PMEPR below the chosen limit. This way, the effect of limiting the PAPR can be assessed by observing the mean value and the variance for different PMEPR thresholds. For this purpose Monte Carlo simulations were run for the number of OFDM carriers $N = 128$ and PMEPR thresholds chosen as PMEPR ≤ 4 and PMEPR ≤ 3. The mean value of the ambiguity function is found to be unaffected by the PMEPR threshold. However, the variances of the ambiguity functions in Fig. 5.4 and Fig. 5.5, for PMEPR thresholds 4 and 3 respectively, exhibit lower values along the zero-delay Doppler cut, and the lower PMEPR threshold yields lower variance along the principal cut. These results confirm the previous assessment that the suppressed random fluctuations in the OFDM signal, which is due to the PMEPR limitation, translates into a lower variance along the zero-delay Doppler cut.

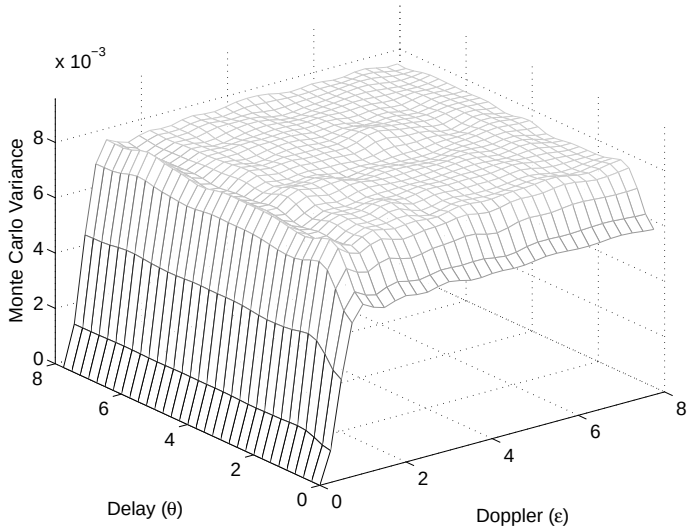

Figure 5.4: Variance of the Monte Carlo simulation result for QPSK-coded OFDM with N=128 carriers. Random phase codes that yield PMEPR ≤ 4 reduces the variance along the zero-delay Doppler axis.

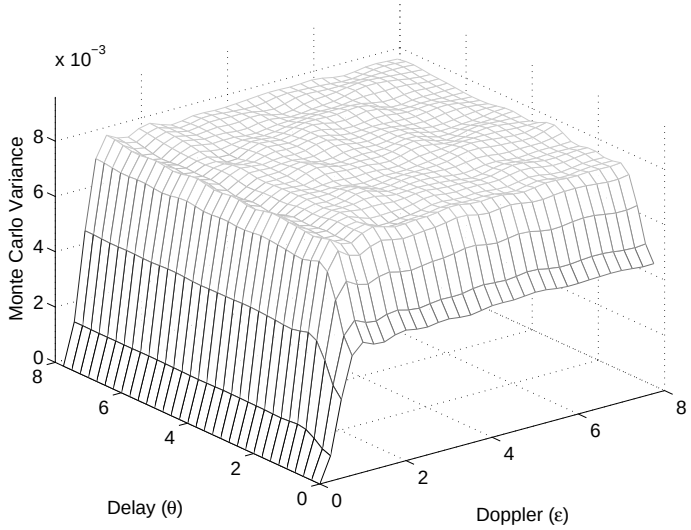

Figure 5.5: Variance of the Monte Carlo simulation result for QPSK-coded OFDM with N=128 carriers. The variance along the zero-delay Doppler axis is lower for random phase codes that yield PMEPR ≤ 3, compared with the case where PMEPR ≤ 4.

Such limitation of the PMEPR unfortunately is not compatible with the communications function, because the bits constituting the communication content cannot be mapped onto phase codes that yield low PMEPR in a structured manner. Coding techniques that are specifically aimed at OFDM radar signals are proposed in the literature [41]; those coding techniques do not offer any communication capability, as they were developed with the aim of optimizing the radar performance alone. Two other methods, namely the Golay codes and the single-carrier OFDM signals, that overcome this short-coming of no communications capability, are covered in the following paragraphs.

5.2.2 Golay Codes and their Effect on the Pulse Compression Sidelobes

Golay complementary series, as defined in [18], have the property that the sum of their respective autocorrelation series is zero everywhere except for the center term. In other words, the two complementary codes, when transmitted consecutively, yield sidelobes with opposite polarity that add up to zero when the range profiles from the two Golay complementary codes are summed up.

The Golay codes have another interesting property of limiting the PAPR for OFDM modulation due to their autocorrelation property that is described above [8, 45, 46]. When the starting phases for the carriers of the OFDM are arranged to constitute a Golay phase code, the PMEPR of the OFDM signal is strictly limited such that PMEPR $\leq$ 2. This property makes the Golay codes a candidate for limiting the PAPR of the radar signal. The peak power limiting property of Golay sequences can be exploited further by considering complementary sets consisting of 2^k Golay sequences. Sequences in such sets limit PMEPR values below 2^k [45]. For the remaining text of this section, Golay sequences will stand for sequences belonging to such complementary pair.

The Golay sequences are generated through the linear combination of *monomials* that spawn the *Boolean functions* of the desired length. A Boolean function is a function f from $\mathbf{Z}_2^m = \{(x_1, x_2, ..., x_m)|x_i \in \{0, 1\}\}$ to $\mathbf{Z}_2$ [8]. The Boolean variable x_i can attain only the values {0,1}, which may actually correspond to binary phase codes if the phase modulation technique is to be utilized in the implementation.

The Boolean function can be generalized onto $\mathbf{Z}_{2^h}$, which means that the Boolean variable can now attain the values $\{0, 1, ..., 2^h - 1\}$ [8]. Following from the previous example that associated the values $\{0, 1\}$ with the binary

phase coding, such generalization corresponds to utilizing larger phase constellations. In this case, linear combinations of monomials can generate all Boolean functions as long as the coefficients are chosen from the expanded set of values.

Instead of presenting their formal definition, the monomials are described as they are used in the generation of Golay sequences. If the numbers $\{1, 2, ..., 2^m\}$ are converted to binary representation, namely to base 2, and organized into a matrix $\mathbf{M}$ with rows corresponding to the numbers and columns corresponding to the binary digits, each column also corresponds to a monomial. As as example, if $m = 3$ is considered, then the matrix $\mathbf{M}$ would be

$$\mathbf{M} = \begin{bmatrix} 0 & 0 & 0 \\ 0 & 0 & 1 \\ 0 & 1 & 0 \\ 0 & 1 & 1 \\ 1 & 0 & 0 \\ 1 & 0 & 1 \\ 1 & 1 & 0 \\ 1 & 1 & 1 \end{bmatrix}. \tag{5.7}$$

where three monomials that generate the Golay sequences of length 8 constitute the columns of the matrix $\mathbf{M}$, i.e.

$$\begin{aligned} x_1 &= (00001111), \\ x_2 &= (00110011), \\ x_3 &= (01010101). \end{aligned} \tag{5.8}$$

Golay codes are generated through a specific combination of the monomials described above, which is formulated as a Boolean function:

$$f(x_1, x_2, ..., x_m) = \frac{q}{2} \sum_{i=0}^{m-2} x_{\pi(i)} x_{\pi(i+1)} + \sum_{i=0} m - 1 g_i x_i + g', \tag{5.9}$$

where $g_i \in \{0, 1, .., q-1\}$, $q = 2^h$ is the constellation size, π here is a permutation of $\{0, 1, .., m-1\}$, 2^m being the length of the Golay code, and x_i are the monomials [8, 66]. The number of Golay codes that can be generated using the function in Eq. (5.9) equals

$$\frac{m!}{2}q^{m+1}. \tag{5.10}$$

As explained in Paragraph 5.2.1, those randomly generated codes that yield a PMEPR lower than a certain threshold will result into a reduction of the noise floor along the zero-range Doppler cut of the ambiguity function. The utilization of Golay phase codes when generating the OFDM signal is expected to have a similar impact on the ambiguity function; however, it is also expected that the phase codes modulating the OFDM carriers carriers are not entirely independent of each other, due to the structure of the Golay sequences.

Monte Carlo simulation results for N=128 carriers confirm such reasoning; the results show no change in the mean value of the ambiguity functions, while the variance, depicted in Fig. 5.6, exhibits several high peaks that are spaced in a manner reflecting the structured nature of the Golay sequences. Such high peaks in the variance correspond to randomly occurring high peaks in the ambiguity function for any Golay coded OFDM radar signal. It should be noted that the occurrence of such high peaks does not conflict with the range sidelobe eliminating property of the complementary codes; the sidelobe elimination property is valid for the sum of autocorrelations for a complementary pair of Golay codes. The reduced variance along the zero-delay Doppler cut is also visible in Fig. 5.6.

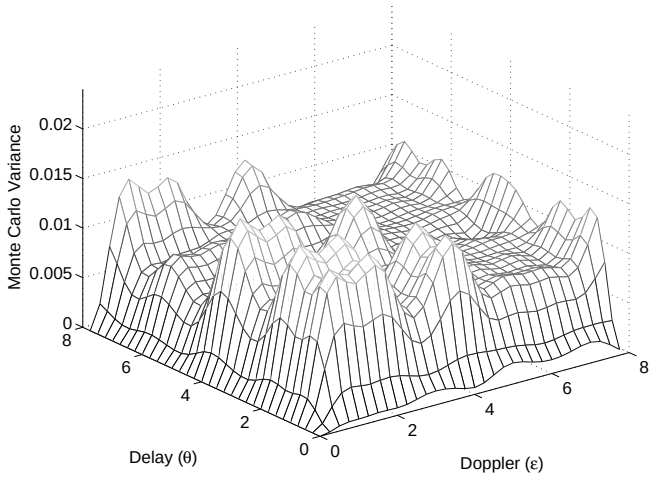

Figure 5.6: Monte Carlo simulation result for Golay-coded OFDM with N=128 carriers. Golay phase codes strictly limit PMEPR $\leq$ 2; however, in addition to the reduced variance along the zero-delay Doppler axis, there are several high variance peaks.

5.2.3 Single-Carrier OFDM

The OFDM signal consists of orthogonal carriers that can be independently modulated through an IFFT operation. It is possible to have a spreading matrix before the IFFT to pre-code the communication symbols; this may lead to effective spreading of the content of each carrier over the whole OFDM bandwidth. Such pre-coding matrices have to be orthogonal, i.e. consist of column vectors that form an orthogonal basis, to enable the recovery of the spread carrier contents. Examples of such spreading matrices are utilized in code-division multiple access (CDMA) to provide isolation between separate channels through coding, such as Walsh-Hadamard matrices [54].

As described in Chapter 3 the DFT is also a matrix operation with orthogonal column vectors, and the DFT matrix itself can come before the IFFT stage of the OFDM modulation as a spreading matrix. To the author's knowledge, such use of the DFT matrix was proposed first in [51]. The result is the cancellation of the DFT spreading matrix and the IDFT that modulated the OFDM signal, which results in a phase coded single carrier signal that is the CDMA modulation with a cyclic prefix. Such signal is called *DFT-spread* OFDM or *single carrier*-OFDM (SC-OFDM), which is adopted for the up-link communication in the long-term evolution (LTE) radio interface, where the power efficiency is very important due to the limited available transmission power [2, 22, 42, 43]. CDMA itself is a constant envelope signal, hence, the PAPR is of no concern for communication systems based on CDMA.

However, it is noted that the equivalence between the actual CDMA signal and the SC-OFDM holds only for the critical sampling in accordance with the Nyquist criterion, where the sampling frequency is twice the bandwidth of the baseband signal. The over-sampled SC-OFDM signal exhibits large spikes at phase transitions due to the strict limiting of the spectrum introduced by the combination of critically sampled DFT operation with a larger IDFT operation through zero-padding. In other words, simple zero-padding before the IDFT, which is also used to implement the up-conversion to IF digitally by modifying the arrangement of the zero-padding, does not work satisfactorily.

It is also noted that, the discrepancy between the critically sampled and the continuous versions of the same signal is a challenge when estimating the PMEPR of an OFDM signal. The discrepancy is alleviated, although not completely eliminated, when the PMEPR is calculated after over-sampling the signal [74].

In literature methods for reducing the phase transition spikes that involve raised cosine filters are proposed [22, 42, 43]. Since the emphasis throughout the thesis is on the digital processing of the signal in both the transmitter and the receiver, and since the spectrum components are handled directly during the OFDM modulation, the technique we have adopted is based on the frequency domain application of the raised cosine filtering on the SC-OFDM signal [22]. The frequency response of the raised cosine filter is given by

$$H(f) = \begin{cases} T & |f| \leq \frac{1-R}{2T} \\ \frac{T}{2}\left[1 + cos\left(\frac{\pi T}{R}\left[|f| - \frac{1-R}{2T}\right]\right)\right] & \frac{1-R}{2T} < |f| \leq \frac{1+R}{2T} \\ 0 & Otherwise \end{cases} . \quad (5.11)$$

where R is the roll-off factor and T is the sampling period.

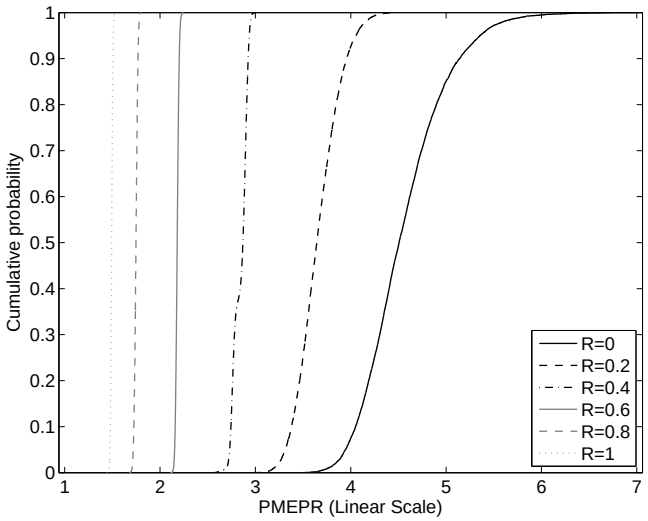

Figure 5.7: The cumulative distribution functions of PMEPR for different roll-off factors show that the PMEPR decreases with increasing roll-off.

The SC-OFDM signal with raised cosine filtering aims at reducing the time-domain fluctuations by trading off the favorable spectrum characteristics of the OFDM signal. In other words, the OFDM signal spectrum is broadened, without improving the range resolution or increasing the data content, by appending the OFDM spectrum with it's replica and applying a raised cosine filter by use of the Hadamard multiplication.

In the literature the raised cosine filter is shown to reduce the PMEPR of SC - OFDM, which is already lower than the PAPR of OFDM. The

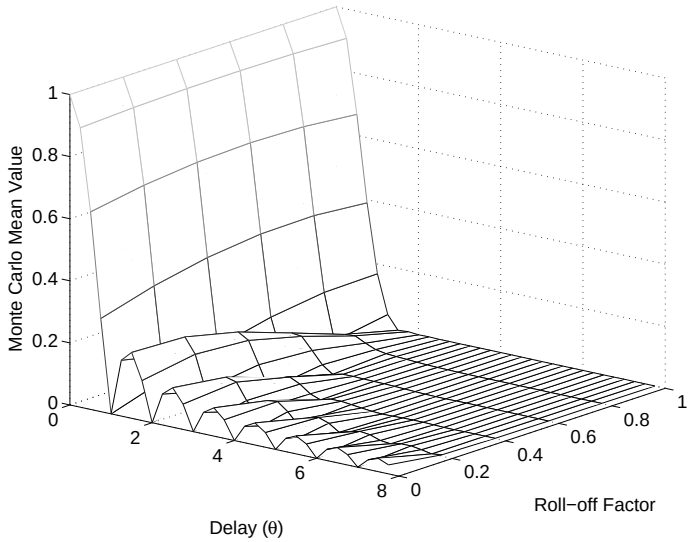

Figure 5.8: Mean value of the zero-Doppler delay cut for different roll-off factors, where the delay sidelobes decrease and the main lobe broadens as the roll-off increases.

cumulative distribution functions (CDF) for the PMEPR of SC-OFDM with different roll-off factors are plotted in Fig. 5.7. This result implies that the PMEPR is very close to one with QPSK modulation. It must be noted that this is not the case when QAM is chosen as modulation scheme of the SC-OFDM since QAM itself involves a non-constant envelope.

To evaluate the performance of the SC-OFDM, the mean and variance is calculated for Monte Carlo simulations with different roll-off factors for the raised cosine filter expression; thus, the effect of the roll-off factor R on the performance of SC-OFDM is also assessed. The results show that the mean value depends on the filter roll-off factor. The magnitude of the close-in sidelobes along the zero-Doppler delay cut decreases with increasing roll-off factor, eventually disappearing when the roll-off factor is 1. As the delay cut is the inverse Fourier transform of the power spectrum of the signal, the roll-off reduces the sidelobes associated with the rectangular power spectrum shape while the mainlobe broadens. Thus, the mean value of the Monte Carlo simulations is as expected. However, this decrease in the sidelobe levels is accompanied with the broadening of the main lobe for the delay cut. The variation of the delay cut with the filter roll-off factor is depicted in Fig. 5.8.

The variance, which is said to dominate the far-off sidelobes in the delay-Doppler plane, shows one major difference compared to the standard OFDM case. It can be immediately noticed in Fig. 5.9 that the variance

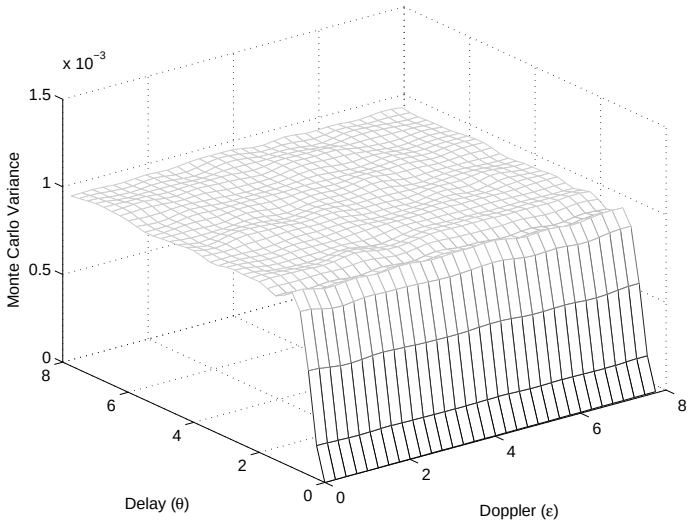

Figure 5.9: The variance, calculated from Monte Carlo simulations for N=1024 carriers and roll-off factor 0, shows zero variance along the zero-delay Doppler cut.

is zero along the zero-delay Doppler cut for SC-OFDM. For the standard OFDM the zero variance occurred along the zero-Doppler delay cut. The explanation to this phenomenon comes from the relation between the Doppler cut and the instantaneous power of the signal, which was explained in Paragraph 5.2.1.

The variance behavior in Fig. 5.9 is also verified by experimental results obtained using the same waveform parameters as presented in Table 4.1. The result is given in Fig. 5.10 in terms of the delay-Doppler plane generated by the OFDM pulse compression technique. The Doppler cut with the delay matched to that of the target has a variance equal to 2.2×10^{-7}, which is consistent with the thermal noise level, while the variance along a mismatched-delay Doppler cut is around 3.5×10^{-6}.

As explained previously, the zero-Doppler delay cut is purely determined by the power spectrum while the zero-delay Doppler cut depends on the envelope of the signal. The flat power spectrum of the PSK-modulated OFDM results in a delay cut having zero variance. Had the signal been actually a single carrier with PSK modulation, the time domain waveform would have a constant envelope which would yield zero variance in the Doppler cut. However, the SC-OFDM still has fluctuations in the time domain envelope in the form of spikes at phase transitions; thus, the zero-variance along the Doppler cut needs further verification.

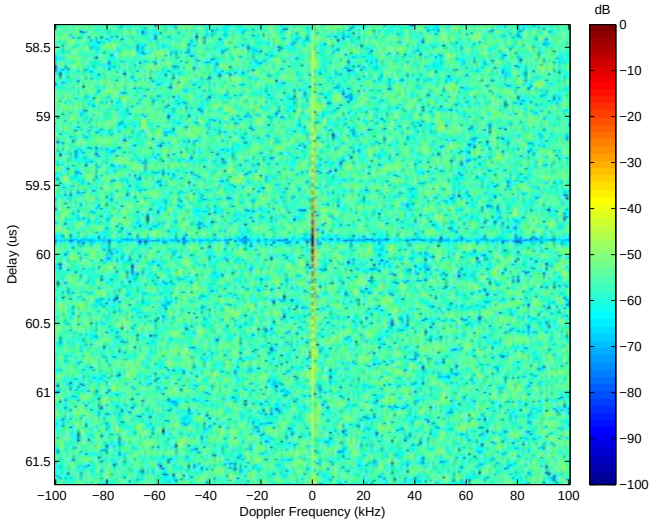

Figure 5.10: The experimental result exhibits a trench along the matched-delay Doppler cut in the correlation noise floor.

In order to verify that the variance along the zero-delay Doppler cut is equal to zero in spite of the fluctuations in the time domain envelope, analytical derivations were undertaken. Eq. (4.1) is the starting point, where the phase modulation terms have to be replaced with the modulation coefficients for the SC-OFDM. Again assuming m-PSK modulation as starting point, the DFT spreading matrix that precedes the IFFT in the SC-OFDM modulator modifies the modulation coefficients as

$$A_m \exp\{j\phi_m\} = \sum_{p=0}^{N-1} \exp\{j\phi_p\} \exp\{-j2\pi \frac{pm}{N}\}, \tag{5.12}$$

where the coefficient p and the second exponential term on the right-hand side are associated with the DFT spreading matrix.

The zero-delay Doppler cut is obtained by taking $\theta = 0$ and $R = 0$ in Eq. (4.1), and the equation is further simplified by considering a stationary target. Such approach is valid, since the non-zero velocity would already be compensated by the ϵ term in the formulation. Hence, the OFDM pulse compression for SC-OFDM signal is formulated as

$$\chi(0,\epsilon) = \frac{1}{N^2}\sum_{k=0}^{N-1}\sum_{n=0}^{N-1}\sum_{m=0}^{N-1}\Big[\exp\left\{j2\pi\frac{(m-k-\epsilon)n}{N}\right\} \sum_{p=0}^{N-1}\exp\{j\phi_p\}\exp\{-j2\pi\frac{pm}{N}\} \sum_{q=0}^{N-1}\exp\{j\phi_q\}\exp\{-j2\pi\frac{qk}{N}\}\Big], \tag{5.13}$$

where p and q are the indices for the discrete Fourier transform. The variance is calculated through

$$\sigma_\chi^2 = E\left[|\chi|^2\right] - |E[\chi]|^2, \tag{5.14}$$

which was introduced in Paragraph 4.1.2. It can be noticed that calculating the variance of Eq. (5.13) eventually boils down to calculating

$$E\left[\exp\{j(\phi_p - \phi_q - \phi_{\overline{p}} + \phi_{\overline{q}})\}\right] - E\left[\exp\{j(\phi_p - \phi_q\}\right] E\left[\exp\{j(-\phi_{\overline{p}} + \phi_{\overline{q}})\}\right]. \tag{5.15}$$

The individual expected values in Eq. (5.15)can be evaluated using the same assumptions as in Paragraph 4.1.2, which are

$$E\left[\exp\{j(\phi_p - \phi_q)\}\right] = \begin{cases} 0 & p \neq q \\ 1 & p = q \end{cases}. \tag{5.16}$$

and

$$E\left[\exp\{j(\phi_p - \phi_q - \phi_{\overline{p}} + \phi_{\overline{q}})\}\right] = \begin{cases} 1 & p = q, \overline{p} = \overline{q} \\ 1 & p = \overline{p}, q = \overline{q} \\ 0 & otherwise \end{cases}. \tag{5.17}$$

The subtraction operation in Eq. (5.15) yields a non-zero result only for the case $p = \overline{p}, q = \overline{q}, p \neq q, \overline{p} \neq \overline{q}$, which produces a simplified variance formulation for the zero-delay Doppler cut,

$$\sigma^2 = \frac{1}{N^4}\sum_{k,n,m}\sum_{\overline{k},\overline{n},\overline{m}}\exp\left\{j2\pi\frac{(m-k-\epsilon)n-(\overline{m}-\overline{k}-\epsilon)\overline{n}}{N}\right\} \sum_{p,q,p\neq q}\exp\left\{-j2\pi\frac{p(m-\overline{m})-q(k-\overline{k})}{N}\right\}. \tag{5.18}$$

The numerical solution for Eq. (5.18) yields zero for all values of ϵ, thus, the variance $\sigma^2 = 0$ for the zero-delay Doppler cut.

5.2.4 Effect of Clipping the Peaks

A simple alternative to other PAPR control techniques is clipping the OFDM signal, such that the peaks are eliminated beforehand to prevent the amplifier from entering into saturation. The effect of clipping on the communications performance is well-covered in the literature. It is shown that the trade-off between low SNR due to high PAPR and distortion due to clipping creates the opportunity to optimize the clipping ratio for better communication performance [35]. The clipping operation lowers the bandwidth efficiency of the OFDM, and thus, it is followed by filtering to reduce out-of-band emission. However, such filtering causes some of the peaks to regrow as well [32]. Hence, the clip-and-filter scheme is implemented in an iterative manner to satisfy both the peak-power and out-of-band emission criteria [1].

In this paragraph the effect of clipping on the radar performance is investigated, when there is no filtering afterwards. Two cases are considered: In the first case the clipping is not taken into account in the pulse compression; in other words, reference phases are generated **before** the OFDM signal is clipped. In the second case, reference phases for the pulse compression are generated **after** the OFDM signal is clipped, which means that the pulse compression is matched to the clipped OFDM signal. OFDM pulse compression performances for both cases are compared. Clipping the signal can be considered as adding another signal which negates the clipped peaks; if the added signal is not taken into account in the pulse compression, it may contribute into the correlation noise.

Monte Carlo simulations are conducted for an OFDM signal with $N = 1024$ QPSK modulated-carriers. For the two cases described above, Fig. 5.11 shows the effect of clipping on the variance of far-off sidelobes, range cut and Doppler cut as a plot of the variance versus the clipping threshold. In the previous paragraphs the effect of reduced PMEPR is shown to give a reduced variance along the zero-delay Doppler cut, which is determined solely by the Fourier transform of the instantaneous power of the signal. The same phenomenon of reduced variance is observed also for the clipped OFDM signal; as the clipping threshold is lowered, the fluctuations of the OFDM signal is also reduced, yielding lower variance along the zero-delay Doppler cut.

The clipping threshold in Fig. 5.11 is obtained by dividing the maximum permissible signal voltage to the square root of the average power

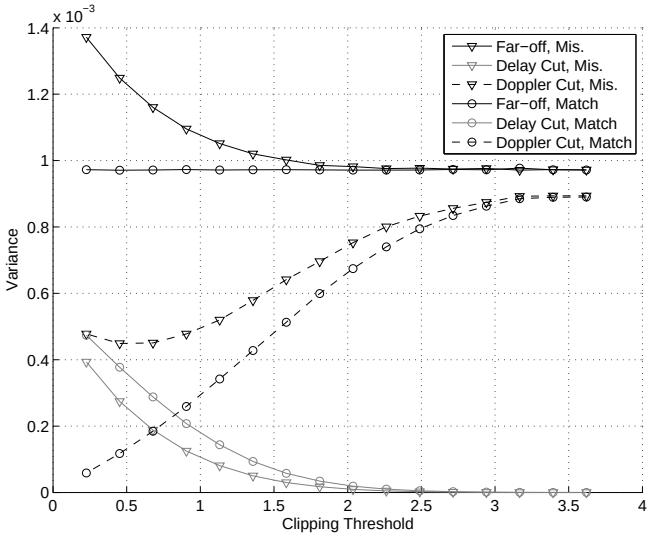

Figure 5.11: The effect of clipping the peaks of the OFDM with N=1024 carriers on the variances of far-off sidelobes, range cut and Doppler cut. 'Mis.' denotes the results for unclipped reference phases, while 'Match' denotes the results for reference phases generated after clipping.

before clipping. It is noted that the described threshold calculation does not correspond to the PMEPR after the clipping operation. Since the clipping also reduces the average power, the final PMEPR after clipping the signal is somewhat higher than what the clipping threshold indicates.

The response of OFDM pulse compression to the clipped OFDM signal, when the reference phases are taken after the clipping operation, compares favorably with the previous methods. However, the communication performance will obviously be affected by the clipping operation. A more comprehensive study of the communication fidelity for various PAPR control methods, which takes into account the rotating and directive radar beam and the associated communication channel properties, is proposed as future work.

5.3 Single Very Long OFDM Chip to Replace the Coherent Integration

Until this point in Chapter 5 the generalization of the OFDM pulse compression technique over different modulation techniques is discussed. For all

the investigated modulation techniques, the implicit assumption is that the coherent integration of the compressed pulses is the final step in the radar signal processing. However, it can be suggested that, extending the duration of the OFDM chip in order to increase the Doppler resolution is enough to eliminate the need for the coherent integration. Investigating such extension of the OFDM chip duration amounts to the generalization of the OFDM pulse compression technique over a larger set of waveform parameters.

The prime concern, when generalizing the OFDM pulse compression over different waveform parameters, is the validity of the fundamental assumptions that are declared at Paragraphs 3.1.4 and 3.1.2. Of these two assumptions, the range limit is of no concern as it is easily satisfied for increased OFDM chip duration. It can also be said that the increased chip duration permits the reduction of the relative duration of the guard interval; such reduction translates into higher data rate for telecommunications and better exploitation of the transmitted energy.

The narrowband assumption is independent of the chip duration, however it is tied to the number of carriers of the OFDM chip. For a fixed OFDM chip duration, which means for fixed carrier spacing, the number of carriers also determines the range resolution of the OFDM radar signal. Then, satisfying the narrowband assumption while increasing the OFDM chip duration necessitates limiting the range resolution. The narrowband condition given in Eq. (3.22) can be modified to incorporate the range resolution term R_{res}, which is

$$R_{res} = \frac{c}{2N\Delta f}. \tag{5.19}$$

The narrowband condition is

$$\frac{2v}{c} < \frac{1}{N}, \tag{5.20}$$

and by replacing the carrier number N into the range resolution term R_{res} gives the result

$$v < \Delta f R_{res}. \tag{5.21}$$

The narrowband condition in Eq. (5.21) effectively puts an upper-limit to the range resolution, which is determined not only by the carrier-spacing but also the velocities of the targets of interest. When the target velocity is faster than the limit imposed by Eq. (5.21), the change in the target

range during one OFDM chip is greater than the size of a resolution cell. In other words, the target migrates from one range cell to the next, or even further, during the OFDM chip duration. *Range migration* is a well-known challenge for high-range-resolution radars [21]. Since the aim in this chapter is to generalize the OFDM pulse compression as it is developed in Chapter 3, the violation of the range limit and the narrowband assumption are not investigated further in this chapter; they are covered in greater detail in Chapter 6, along with effects such as range migration and possible solutions.

To summarize, by reducing the carrier spacing the duration of the OFDM signal can be increased such that the higher Doppler resolution of the OFDM pulse compression eliminates the need for coherent Doppler integration. A shorter relative duration of the guard interval can correspond to longer ranges, thanks to greatly increased chip duration, which reduces the power spill. However, to keep the same range resolution the number of carriers has to be increased as well, which rapidly increases the computational burden of the processing and also increases the PAPR. Moreover, the range migration becomes significant even for lower target velocities. The trade-off between these aspects has to be analyzed based on the setting in which an OFDM radar signal is utilized.

5.4 Conclusions

In the earlier chapters the novel pulse compression technique was developed for the OFDM signal with the QPSK-modulation over its carriers. In this chapter, the constraint over the modulation scheme was removed and the OFDM pulse compression technique has been generalized over a wider array of modulation schemes. This generalization of the radar signal processing technique over the different implementations of OFDM demonstrates the power of pulse compression and the associated waveform properties of cyclic repetitiveness and carrier orthogonality. As long as these two properties are present and the relation between the spectrum components is well-defined, implementations of the OFDM waveform other than the ones investigated in this chapter can be utilized in radar systems. Moreover, these properties essentially describe the fundamental principles of the OFDM systems; the future proposals for OFDM communication signals are very likely to satisfy these conditions. For radar specific tasks, the relation between the spectrum components can be modified further to accommodate scenario-specific needs better.

As the final section demonstrates, fundamental assumptions regarding the relations between the target parameters and waveform parameters must

be considered carefully when designing the waveform parameters. It is possible that the narrowband assumption and the range limit that preserves the cyclic repetitiveness of the OFDM signal are violated for some targets, whether of interest or not. The generalization of the OFDM radar signal processing to encompass such situations necessitate an investigation that re-models the echo signal, which is undertaken in the next chapter.

Chapter 6

Beyond the Range and Velocity Limits

The OFDM pulse compression technique and the coherent integration of the OFDM chips, which was developed for phase coded OFDM carriers in Chapters 3 and 4, and later extended over other coding methods in Chapter 5, contains in its very foundation a set of assumptions regarding the upper limits for range and velocity of targets of interest. The upper limit for the range that was established in Paragraph 3.1.2 can be considered as specific for the OFDM signal, as the upper limit is determined by the duration of the cyclic prefix guard interval, which is a feature of the OFDM signal. However, the narrowband assumption that was defined in Paragraph 3.1.4 establishes a more fundamental constraint over the upper limit of the target radial velocity, which concerns the time-bandwidth product of the signal. For this reason, this chapter will first explore the implications of violation of the narrowband assumption.

The violation of the narrowband assumption gives rise to two closely related inaccuracies in the modeling of the signal echo. The first inaccuracy is the manner in which the Doppler effect is accounted for, namely the Doppler shift in the frequency of the signal. As the narrowband assumption fails, the actual Doppler effect that is the scaling on the signal cannot be accurately modeled as a frequency shift anymore, which is also the basis of the upper limit for the target radial velocity that was defined in Paragraph 3.1.4. The second inaccuracy is related to the target dynamics; with higher radial velocity, the point target does not occupy a single range bin during the extent of the radar signal but migrates from one range bin to the next. Such migration manifests in the signal echo model as a time-dependent phase

change, which is not taken into account in matched filtering that is developed for the narrowband echo model. The range migration occurs first at the level of coherent Doppler integration, where the OFDM pulse compression can still assume the Doppler effect to be a frequency shift. At higher velocities, the scaling becomes significant for the OFDM pulse compression. Compensation techniques for both effects are developed in this chapter and verified through simulations.

When a target is farther than the range limit, the received echo contains a portion of the preceding OFDM pulse as well as the current one. The resulting inter-symbol interference (ISI) will obviously cause a degradation of the radar performance. The OFDM pulse compression method is modified to take into account the preceding OFDM chip as well as the current one to reduce the interference. Hence, the OFDM signal that was proposed for short range surveillance tasks can now be utilized also for longer ranges.

6.1 Violation of the Narrowband Assumption for a Train of OFDM Chips

As the target velocity increases the narrowband assumption is violated first for the coherent Doppler integration, where the time duration of the whole train of OFDM chips means that the target can migrate from one range bin to the next even at moderate velocities, especially if the range resolution of the radar is high. The OFDM pulse compression method provides a novel and easy way of compensating for the range migration in such situations. The Doppler sensitivity of the OFDM pulse compression enables incorporating a phase correction operation that is in concert with the Doppler compensation, for the rate of phase migration is determined by the target velocity. The Doppler effect can still be modeled as a frequency shift at this stage. The technique was developed first in [71].

The train of OFDM chips is processed through coherent Doppler integration of pulses after pulse compression by the DFT operation that operates along the train of chips for the same range bin and the same cyclic shift, as explained in Eq. (3.46) in Paragraph 3.2.4. A more rigorous formulation, which incorporates the coherent integration DFT in the matrix notation adopted in Chapter 3, can be put forth in order to demonstrate the effect of violation of the narrowband assumption for the train of OFDM chips.

The OFDM radar signal echo presented in Eq. (3.24) has the content that changes with the OFDM chip index p. The concept of utilizing the radar signal for communication purposes calls for the starting phases and

amplitudes of OFDM carriers to change from chip to chip. Target parameters can also change from chip to chip, however, assuming only the target range to change from pulse to pulse is enough to demonstrate the effect of violating the narrowband assumption for the train of OFDM chips. In the light of this setting, components of the OFDM signal echo that change from chip to chip can be assigned chip index p:

$$\mathbf{s}_p = \psi_p \mathbf{\Gamma F}^{-1}(\mathbf{a}_p \otimes \boldsymbol{\phi}_p). \tag{6.1}$$

We can generalize the echo for a train of OFDM chips by defining an echo matrix $\mathbf{S} = [\mathbf{s}_0, \mathbf{s}_1, ...\mathbf{s}_{K-1}]$, where each column corresponds to the echo for one OFDM chip, as formulated in Eq. 6.1, and K is the total number of OFDM chips under consideration. To achieve such an echo matrix, components that depend on the chip index p have to be stacked to yield a suitable matrix operation structure. As each column of the echo matrix $\mathbf{S}$ has different ψ_p, these terms can be combined into a matrix $\boldsymbol{\psi} = diag\{\psi_p\}$. Also, column vectors $\mathbf{a}_p$ and $\boldsymbol{\phi}_p$ can be stacked as matrices $\mathbf{A} = [\mathbf{a}_0, \mathbf{a}_1, ...\mathbf{a}_{K-1}]$ and $\boldsymbol{\phi} = [\boldsymbol{\phi}_0, \boldsymbol{\phi}_1, ...\boldsymbol{\phi}_{K-1}]$ respectively. These matrices are structures such that each row corresponds to one carrier, or more generally one harmonic component, while each column corresponds to one OFDM chip, or more generally one pulse; the final echo matrix for the whole train of OFDM chips can be written as

$$\mathbf{S} = \mathbf{\Gamma F}^{-1}(\mathbf{A} \otimes \boldsymbol{\phi})\boldsymbol{\psi}. \tag{6.2}$$

As each column of the echo matrix in Eq. 6.2 is the echo for a single OFDM chip, matrix operations for the OFDM pulse compression are still valid once the compensation vector described in Eq. 3.26 is replaced by a compensation matrix $\mathbf{P} = [\mathrm{P}_0\mathrm{P}_1...\mathrm{P}_{K-1}]$. The resulting processing matrix for cyclic shift ϵ is of size N $\times$ K, where each column is the response for one OFDM chip and each row is for one sample on the range profile. With the final Doppler DFT, which is a K $\times$ K matrix, the coherent integration processing is formulated as

$$\mathbf{\Lambda}(\epsilon) = \mathbf{F}_{K\times K}(\mathbf{F^{-1}}\left[\mathbf{P} \otimes \left(\mathbf{C}_\epsilon^{-1}\mathbf{FS}\right)\right])^T, \tag{6.3}$$

where $(.)^T$ is the transpose operation.

6.1.1 Limits of the Narrowband Assumption

The change in the range of the target from chip to chip can be traced to the matrix $\mathbf{A}$, which contains the effects of the echo delay on the phases of the OFDM carriers, and the matrix $\boldsymbol{\phi}$. The ϕ_k term contains the phase term that is range-dependent; the change in phase from one pulse to the next manifests itself as the Doppler frequency shift which is measured in the coherent integration stage through utilizing the DFT in conventional pulse Doppler radars. Hence, the violation of the narrowband assumption for the train of OFDM chips occurs when the change in the target range modifies the matrix $\mathbf{A}$ significantly.

The change in the target range can be compared to the range resolution of the radar signal, which is determined by the bandwidth of the signal, to assess its significance. The signal processing gain from the coherent integration is reduced when the target range changes by more than the range resolution during the coherent integration duration; this phenomenon is called *the range migration*. Hence, the change in the matrix $\mathbf{A}$ is associated with the range migration, which is significant when

$$K \times \Delta R = KvT(1+\alpha) > \frac{c}{2N\Delta f}, \tag{6.4}$$

where ΔR is the change in the target range from chip to chip due to target velocity, and the term on the right hand side is the range resolution of the radar signal. The expression above can be re-arranged into

$$v > \frac{c}{2KN(1+\alpha)}. \tag{6.5}$$

In other words, the narrowband assumption for the train of OFDM chips is violated when the velocity is higher than the threshold derived in Eq. (6.5).

6.1.2 Range Migration Compensation

The range migration introduces extra phase terms in the entries of the matrix $\mathbf{A}$, which can be written as

$$a_{n,p} = \exp\left\{-j2\pi n\Delta f \frac{2(R_0 + p\Delta R)}{c}\right\}. \tag{6.6}$$

The signal processing scheme, which is formulated in Eq. (6.3), permits inserting another matrix $\mathbf{R}$, with entries

$$r_{n,p} = \exp\left\{ j2\pi n\Delta f \frac{2p\Delta R}{c} \right\}, \tag{6.7}$$

into the phase and Doppler compensation chain to also compensate for the range migration.

The crucial connection between the range migration and the target velocity, that is

$$\Delta R_\epsilon = v_\epsilon T(1+\alpha) = \frac{\epsilon c(1+\alpha)}{2f_c}, \tag{6.8}$$

is exploited at this stage to generate a range migration compensating matrix specifically for each cyclic shift ϵ. Hence, the coherent integration processing scheme is modified into

$$\mathbf{\Lambda}(\epsilon) = \mathbf{F}_{K\times K}(\mathbf{F^{-1}}\left[\mathbf{R}_\epsilon \otimes \mathbf{P} \otimes \left(\mathbf{C}_\epsilon^{-1}\mathbf{FS}\right)\right])^T, \tag{6.9}$$

where entries of the matrix $\mathbf{R}_\epsilon$ are

$$r_{n,p} = \exp\left\{ j2\pi n\Delta f \frac{\epsilon p(1+\alpha)}{f_c} \right\}. \tag{6.10}$$

Simulations are developed to demonstrate the effect of the range walk compensation operation on the coherent Doppler integration of a train of OFDM chips. Realizing the range walk effect requires the use of radar signals with high range and Doppler resolution. Moreover, it is important to determine the target velocity above which the range migration is significant. The radial velocity resolution is determined by the dwell time through the equation

$$T_{dwell} = \frac{c}{2f_c v_{res}}, \tag{6.11}$$

and the range resolution is determined by the signal bandwidth through the equation

$$R_{res} = \frac{c}{2N\Delta f}. \tag{6.12}$$

The significant range walk is assumed to be at least one range bin during the dwell time, which translates into a target radial velocity of

$$v = \frac{R_{res}}{T_{dwell}} = \frac{f_c v_{res}}{N\Delta f}. \tag{6.13}$$

The signal parameters, which are listed in Table 6.1, are chosen to imitate a case that is as realistic as possible, with the effects of range migration becoming significant even at moderate velocities. The target velocity that causes significant range walk is calculated as $v = 69.4m/s$. However, to demonstrate the range migration compensation effect more clearly, the target velocity is chosen twice the significant target velocity, which is $v = 138.8m/s$. In addition, the simulations over-sample the range profiles by a factor of two to better show the effects of the range walk. Finally, it must be noted that the velocity resolution term provided in Table 6.1 is based on the coherent integration time.

Table 6.1: Parameters for range migration simulations.

Parameter Name	**Parameter Value**
Carrier Spacing Δf	1 kHz
Number of Carriers N	10^5
Guard Interval Duration α	0.2
Number of Pulses K	18
RF Carrier Frequency f_c	10 GHz
Coherent Integration Time	21.6 ms
Range Resolution	1.5 m
Velocity Resolution	0.6944 m/s
Target Range R	15 m
Target Velocity v	138.8 m/s

Figure 6.1 is a composite plot of the range profiles for each OFDM chip, obtained from simulations, where the Doppler effect is compensated during the OFDM pulse compression. In other words, Figure 6.1 depicts the range profiles for cyclic shift $\epsilon = 9$, since ϵ is the integer that is closest to the division of the Doppler frequency shift by the OFDM carrier spacing:

$$\frac{f_d}{\Delta f} = \frac{2v}{c}\frac{f_c}{\Delta f} = \frac{2 \times 138.8 \times 10^{10}}{1000 \times 3 \times 10^8} = 9.253. \tag{6.14}$$

As it was explored previously, the range profiles only focus on targets with velocities matched to the Doppler compensation. The range migration of the target from pulse to pulse is clearly visible as the slanted line that depicts the target range versus the pulse number, where the peak of the target response is normalized and the scaling of the magnitude is linear. The range migration compensation fixes the target range to its initial value during the first OFDM chip for all pulses, which is shown in Figure 6.2.

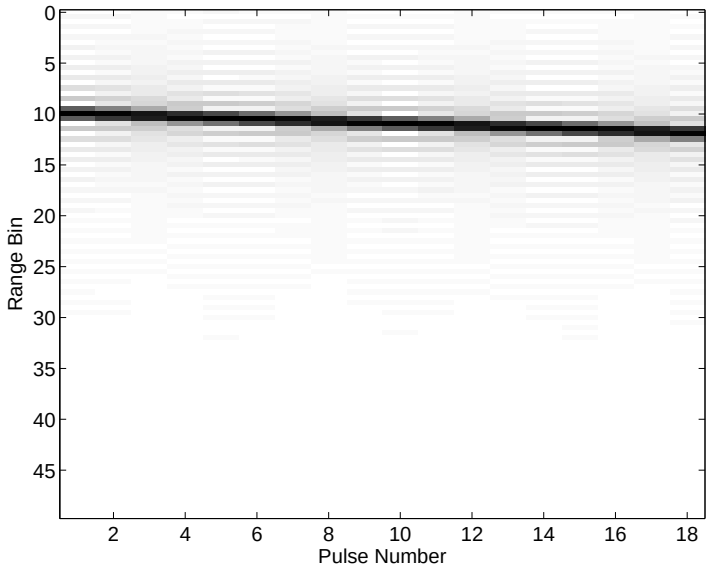

Figure 6.1: Doppler compensated pulse compression results for a train of 18 pulses shows the range walk of the target through the pulse train.

The results of the pulse compression with coherent Doppler integration for the range-walk-uncompensated and compensated cases are plotted in Fig. 6.3 and Fig. 6.4 respectively. Without the range migration compensation, the target appears to cover a number of range bins larger than its physical dimensions correspond to. Moreover, the velocity of the target is determined less accurately when there is range walk, which is evident from the target response appearing in the wrong Doppler bin and smeared over the neighboring bins in Figure 6.3. On the other hand, the coherent Doppler integration after the range migration compensation exhibits a focused target response in Figure 6.4.

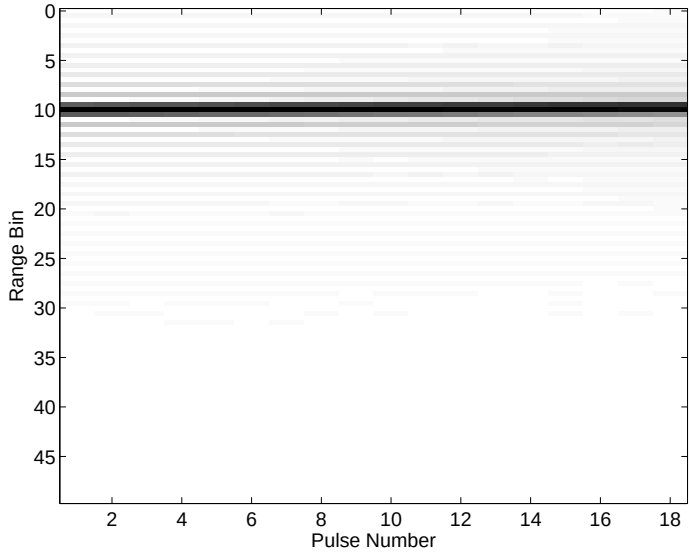

Figure 6.2: Doppler compensated pulse compression results for a train of 18 pulses, where the range walk is also compensated. It shows that the motion of the target is reduced to below one range bin.

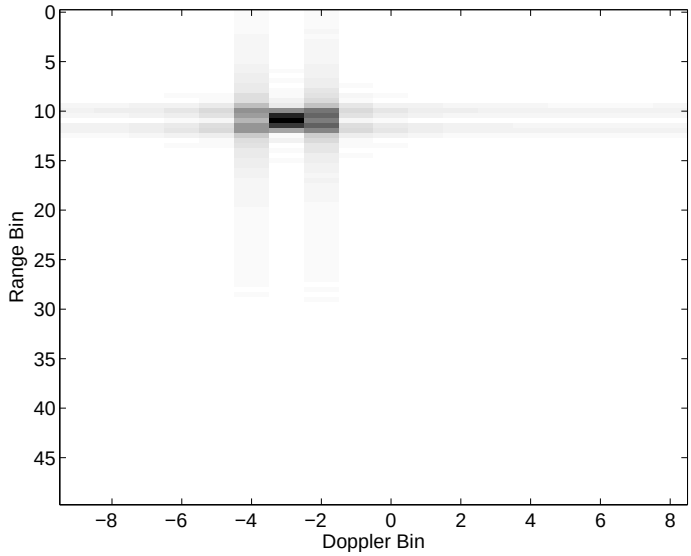

Figure 6.3: Doppler compensated coherent Doppler integration, without range walk compensation. It suffers from dispersed range response, and by consequence also the Doppler response.

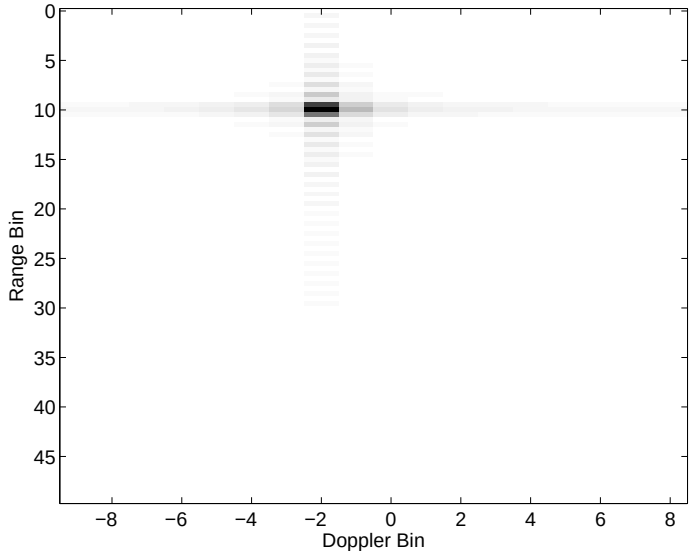

Figure 6.4: Doppler compensated coherent Doppler integration with range walk compensation eliminates the dispersing of the range and the Doppler responses.

The technique developed in this thesis extends the usability of wide bandwidth signals with narrow band processing techniques for higher target velocities, by eliminating the degradation of the performance due to range walk. It can also be compared to the Keystone transform [33, 34, 47], which scales the time axis for each spectrum component of the radar signal, provided that the pulse compression loss due to Doppler effect is negligible or absent. It is possible that other Doppler sensitive waveforms such as phase-coded pulse compression signals [27] can also benefit from the range migration compensation method that is developed in this thesis.

6.2 Violation of the Narrowband Assumption for the Single OFDM Chip

The narrowband assumption, as adopted for the formulation of the OFDM signal echo in Chapter 3, is

$$T\frac{2v}{c} < \frac{1}{N\Delta f}, \tag{6.15}$$

which resulted in the simplification of the $\boldsymbol{\beta}$ matrix to the IDFT matrix.

This condition was related to the amount of scaling the signal can undergo without significantly changing the phases of the $\boldsymbol{\beta}$ matrix elements from those of the IDFT matrix.

Another explanation for this condition is the limit on the range migration that may occur within the duration of a single OFDM chip. Similar to the range migration effect on the coherent Doppler integration, the result is the dispersion of the pulse compression peak and a loss in the pulse compression.

The echo model in Paragraph 3.1.1 has to be adopted in the OFDM pulse compression formula to see the effect of the narrowband assumption failure. The received wideband echo formulation in Eq. (3.18) is

$$\mathbf{s} = \psi \boldsymbol{\Gamma} \boldsymbol{\beta} (\mathbf{A} \otimes \boldsymbol{\phi}), \tag{6.16}$$

which is repeated here for convenience. The meaning of the $\boldsymbol{\beta}$ matrix needs greater attention at this stage, since it is no longer assumed as a mere inconvenience that is eliminated by the narrowband approximation. On the contrary, the $\boldsymbol{\beta}$ matrix now holds the center of the stage, as it embodies the actual Doppler effect that is the scaling of the signal, along with the $\boldsymbol{\Gamma}$ vector that holds the Doppler shift of the RF carrier frequency.

The matrix multiplication between the IDFT matrix and the spectrum components can be interpreted as the multiplication of each column, which corresponds to a harmonic component, by the associated spectral coefficient that sets the phase and amplitude of that harmonic component. When the IDFT matrix is replaced by the $\boldsymbol{\beta}$ matrix, the scaling along any single harmonic component translates into a frequency shift that depends on the harmonic frequency. Thus, the actual Doppler effect is not a uniform shift in the signal frequency but a scaling in the frequency domain as well as in the time domain.

The discrete processing formulation also provides another insight: If we consider a signal that is scaled due to the Doppler effect, the samples we obtain after the analog-to-digital (A/D) conversion will appear as if there is a sampling frequency offset in the system. We can visualize this phenomenon by marking each sampling instance on the original waveform and also on the waveform that underwent the Doppler effect. If the original waveform is scaled to match the waveform with the Doppler effect, we can observe that the sampling instances appear with a different period than the actual sampling period. In literature the sampling frequency offset for OFDM is formulated in a manner quite similar to ours, and modifying the twiddle factors in the FFT algorithm is proposed for its compensation [58].

6.2.1 Compensation of the Doppler Scaling

The echo signal in the OFDM pulse compression formula in Eq. (3.33) is replaced by the wideband OFDM echo expression in Eq. (6.16),

$$\boldsymbol{\chi}_{\epsilon} = \psi \mathbf{F}^{-\mathbf{1}} \left[\mathbf{P} \otimes \left(\mathbf{C}_{\epsilon}^{-1} \mathbf{F} \boldsymbol{\Gamma} \boldsymbol{\beta} \boldsymbol{A} \otimes \boldsymbol{\phi} \right) \right], \tag{6.17}$$

where the scalar ψ term is moved to the beginning of the equation. In Paragraph 3.2.2 it was demonstrated that the effect of the $\boldsymbol{\Gamma}$ matrix on the DFT matrix, which is to its left, is a cyclical shift of the rows downwards that is compensated by the $\mathbf{C}_{\epsilon}^{-1}$ matrix. The result of this cancellation is

$$\boldsymbol{\chi}_{\epsilon} = \psi \mathbf{F}^{-\mathbf{1}} \left[\mathbf{P} \otimes \left(\mathbf{F} \boldsymbol{\beta} (\boldsymbol{A} \otimes \boldsymbol{\phi}) \right) \right], \tag{6.18}$$

where it can immediately be observed that the DFT matrix and the $\boldsymbol{\beta}$ matrix do not cancel each other even when the cyclic shift $\mathbf{C}_{\epsilon}^{-1}$ compensates for the Doppler shift effect in the $\boldsymbol{\Gamma}$ matrix.

To compensate for the sampling frequency offset in communication systems, modifying the elements of the DFT matrix, which is multiplied by the received echo to recover the spectrum coefficients, is proposed in [58]. However, the cyclic shift operation cannot compensate for the Doppler shift in the carrier frequency when the DFT matrix $\mathbf{F}$ in between the $\mathbf{C}_{\epsilon}^{-1}$ and the $\boldsymbol{\Gamma}$ vector is modified. Thus, the OFDM pulse compression fails when the DFT matrix is modified. In other words, the expression in Eq. (6.17) cannot be simplified into Eq. (6.18) when the DFT matrix between the $\mathbf{C}_{\epsilon}^{-1}$ and the $\boldsymbol{\Gamma}$ is modified as proposed in [58].

The alternative operation is to interpolate the reference phases, thus, replacing the compensation vector $\mathbf{P}$ in Eq. (6.18) to obtain

$$\boldsymbol{\chi}_{\epsilon} = \psi \mathbf{F}^{-\mathbf{1}} \left[(\mathbf{F} \boldsymbol{\beta} \boldsymbol{\phi})^{*} \otimes \left(\mathbf{F} \boldsymbol{\beta} (\mathbf{A} \otimes \boldsymbol{\phi}) \right) \right]. \tag{6.19}$$

The proposed modification matches the reference phase vector ϕ to the OFDM echo that is under the influence of a scaling effect.

The failure of the narrowband assumption has been observed in Monte Carlo simulations, where a set of target velocities is chosen such that the phase of the coefficient of the $\boldsymbol{\beta}$ matrix in the lower right corner, which is $\beta^{(N-1)^2}$, changes approximately by $\pi/8$ with each increment in the target velocity. It is noted that the narrowband condition that was established in Eq. (3.23) limits this phase change by 2π. However, to generate a clearer

observation of the deterioration of the pulse compression, the phase change has to occur with smaller increments. The optimal result for the clarity of the simulation results were obtained when the phase of the $\boldsymbol{\beta}$ matrix element is incremented by $\pi/8$ with each increment in the target velocity. Thus, the target velocity is increased, starting from zero, with increments determined by

$$2\pi \frac{2\Delta v}{c} N = \frac{\pi}{8}, \tag{6.20}$$

where Δv is the increment step for the target velocity. There is another constraint, which is the maximum target velocity that the cyclic shift Doppler compensation can accommodate without an ambiguity in the velocity measurements. The OFDM pulse compression compensates for the Doppler shift by cyclically shifting the carrier coefficients, where each shift corresponds to a velocity step determined by the carrier spacing and the RF carrier frequency. The amount of cyclic shift also gives a measurement of the target velocity, albeit with a lower resolution. This extra Doppler measurement is used for solving the Doppler ambiguity in the coherent Doppler integration. In baseband processing, once the carriers are shifted by an amount greater than the number of carriers, an ambiguity in the Doppler measurements occurs. The maximum amount of cyclic shift, that is the number of carriers N, is related to the target velocity through

$$N = \frac{2v_{max}}{c} \frac{f_c}{\Delta f}. \tag{6.21}$$

Hence, the one-sided maximum velocity is given by

$$v_{max} = \frac{c}{2} \frac{\Delta f}{f_c} N. \tag{6.22}$$

Alternatively, the two-sided maximum velocity can be considered:

$$v_{max} = \pm \frac{1}{2} \frac{c}{2} \frac{\Delta f}{f_c} N. \tag{6.23}$$

The implication of Eq. (6.20) and Eq. (6.22) is that the higher the number of carriers, the easier it is to observe the effect of Doppler scaling on the OFDM pulse compression without suffering the Doppler ambiguity in the OFDM pulse compression. In other words, as the bandwidth-time product $BT = N$ increases, the Doppler scaling becomes more significant. While

the FFT and IFFT algorithms allow considerably large number of carriers to be used, the $\boldsymbol{\beta}$ matrix depletes the computer memory rapidly. As a result, the Doppler ambiguity had to be allowed in the simulations. The simulation parameters are listed in Table 6.2, where the velocity increment Δv is calculated as

$$\Delta v = \frac{c}{32N} = \frac{3 \times 10^8}{32 \times 4096} = 2289 m/s. \tag{6.24}$$

Table 6.2: Parameters for the Doppler scaling simulations.

Parameter Name	**Parameter Value**
Carrier Spacing Δf	1 kHz
Number of Carriers N	4096
RF Carrier Frequency f_c	10 GHz
Range Resolution	36.62 m
Velocity Resolution	15 m/s
Target Range R	366.2 m
Target Velocity Increment Δv	2289 m/s

To demonstrate the effect of the Doppler scaling, a composite range-velocity plot that shows the range cut at the cyclic shift that matches each target velocity is generated. Figure 6.5 shows the composite range cut plot for standard OFDM pulse compression, where the dispersion of the main lobe along with the range migration can be observed. Note that the peak of the main lobe is normalized and the the scaling of the magnitude is linear. In addition, the mean value of the target range-Doppler response for the target velocity of $14 \times \Delta v = 32043 m/s$ is plotted in Figure 6.6, which exhibits two features that require better explanation, namely the dislocation of the peak responses from the matched cyclic shift value and the cleaving of the target along the range cut.

The scaling of the OFDM signal echo, as described earlier, is not only a time - domain phenomenon; the harmonic components constituting the OFDM signal are also scaled, which can be considered as each carrier undergoing a Doppler shift in proportion to its own frequency. Thus, carriers

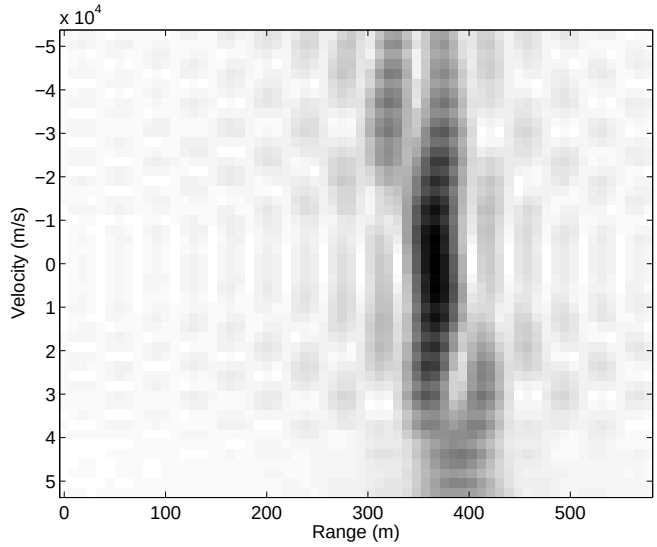

Figure 6.5: The composite range-velocity plane generated from combining the range cuts at the matched Doppler compensation for each velocity, reveals range migration associated with Doppler scaling.

with higher frequency have undergone a larger Doppler shift than those with lower frequency. Note that this scaling is usually assumed to be insignificant compared to the Doppler shift associated with the RF carrier frequency, however, the failure of the narrowband assumption also manifests as a frequency-domain scaling that cannot be ignored anymore. This frequency-domain scaling changes the outcome of the Doppler compensation that is cyclically shifting the carrier locations.

The immediate effect of the frequency-domain scaling is the gain of the OFDM pulse compression with respect to the amount of cyclic shift ϵ. With the narrowband assumption, the ϵ_v that is matched to the target velocity would yield the highest response. After the scaling, however, the ϵ_v that matches the Doppler shift for carriers with low frequencies cannot match the Doppler shift of carriers with high frequencies. Increasing the ϵ value, on the other hand, yields a match for the high-frequency carriers while missing the low-frequency ones. For this reason, at those velocities that create a Doppler scaling which dislocates the highest-frequency carrier by Δf, the ϵ value which yields the greatest pulse compression gain is $\epsilon_v + 0.5$.

The presence of high pulse compression gain for mismatched Doppler compensation is the reason for the second feature of the delay-Doppler response, which is the cleaving of the target into two. Numerical experiments

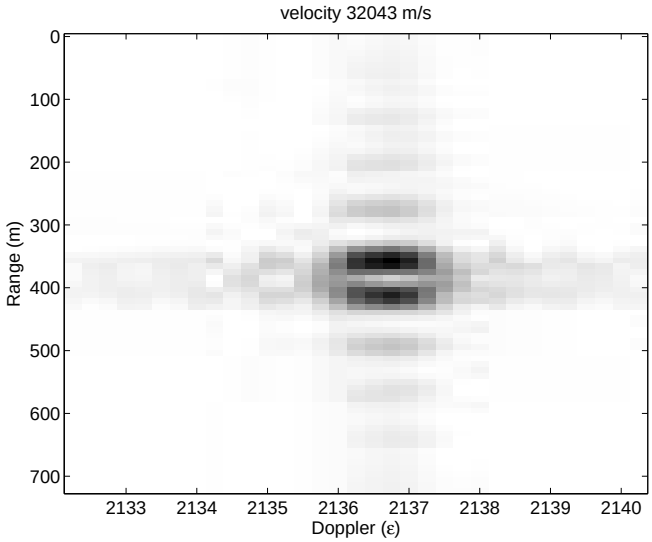

Figure 6.6: The mean value of the range-Doppler response for a target velocity of 32043 m/s demonstrates the dislocation of the peak response from the cyclic shift value that matches the target velocity and the cleaving of the target along the range cut.

that consider the cross-correlation of an OFDM signal with random phase coded carriers by its scaled version show that, scaling by itself accounts only for the spreading of the target response along the range cut. However, multiplying the scaled signal by a harmonic that has frequency equal to half the carrier spacing Δf cleaves the target response.

In the light of the fact that the peak response of the OFDM pulse compression is dislocated from the ϵ_v that is matched to the target velocity, a new composite range cut plot for standard OFDM pulse compression that incorporates range cuts with the peak response is generated, as depicted in figure 6.7, where the cleaving of the target is much more evident.

The effect of the Doppler scaling compensation through interpolation of the reference phases, as formulated in Eq. (6.19), is demonstrated through interpolating the reference phases by multiplication with a β matrix that is matched exactly to the target velocity. While this approach is unrealistic, because the target velocity cannot be known beforehand in a surveillance radar, it demonstrates the successful compensation of the range migration in the composite range-velocity plot in Figure 6.8. Moreover, the mean value of the target range-Doppler response for $v = 32043m/s$ clearly shows that the pulse compression focuses on the target with no cleaving and dislocation

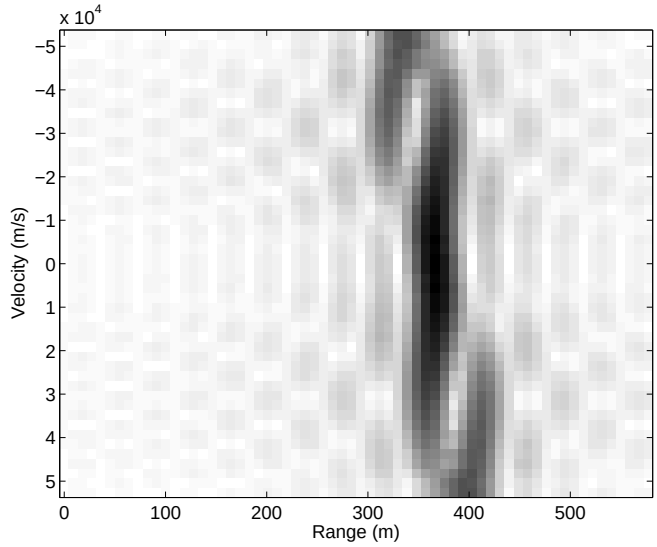

Figure 6.7: The composite range-velocity plane generated from combining the range cuts at the Doppler compensation that yields the peak pulse compression gain for each velocity, displays the range migration associated with the Doppler scaling with lesser pulse compression loss and stronger cleaving.

of the peak response from the cyclic shift value that matches the target velocity.

The compensation of the Doppler scaling, although it is demonstrated here for unrealistic target velocities due to memory constraints, can be necessary for targets with achievable velocities as soon as the range resolution is in the order of tens of centimeters and the Doppler resolution is in the order of a few meters per second.

6.3 Violation of the Range Limit

The range limit established in Paragraph 3.1.2 aims at preventing the interference from the preceding OFDM chip when the OFDM pulse compression is focused on the current chip, that is, the inter-symbol interference (ISI). Echoes from targets beyond the range limit include a portion of the preceding OFDM chip as well as the current chip, which necessitates a reassessment of the validity of the echo formulation in Chapter 3 as well as the OFDM pulse compression scheme that stems from it. An initial investigation of the effects of violating the range limit was presented in [68].

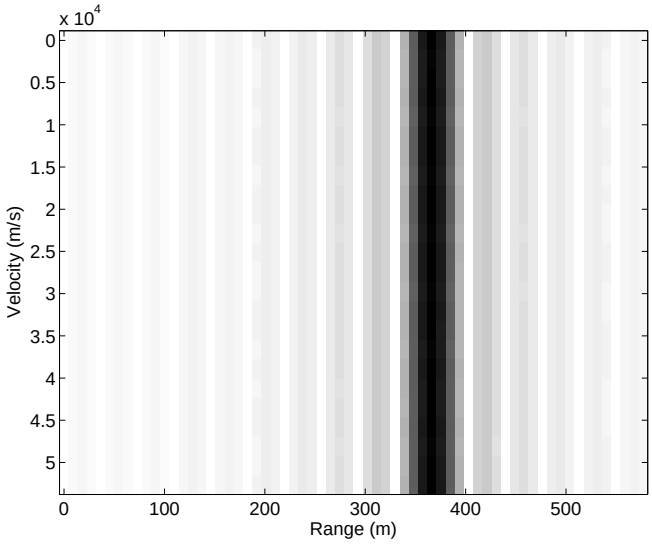

Figure 6.8: The composite range-velocity plane generated from combining the range cuts at the matched Doppler compensation for each velocity, displays the target response that exhibits no range migration after the reference phases are interpolated by the β matrix.

The echo from a distant target can be partitioned, as depicted in Fig. 6.10 as the part belonging to the current OFDM chip and the part belonging to the preceding OFDM chip. What we have in the receiver is effectively the sum of the echo of the current OFDM chip with shorter duration, which is the useful part for the pulse compression, and the echo of the previous OFDM chip, which is independent of the current OFDM chip, again with shorter duration. For convenience, the cyclic prefix guard interval duration is given in terms of its ratio to the OFDM chip duration, denoted by α, and the ratio of the duration of the received echo that belongs to the preceding chip to the OFDM chip duration is denoted by ξ.

6.3.1 Range Limit Violation for Single OFDM Chip

To understand the effect of the range limit violation, we can first investigate the echo of a single OFDM chip which is **not** preceded by another OFDM chip. In such setting only part of the OFDM signal echo coincides with the time frame of reception, effectively truncating the echo from its beginning and reducing the time duration of the received echo. However, different from the frequency modulated continuous wave (FMCW) radar signal, such reduction of the time duration is not coupled to the frequency band covered

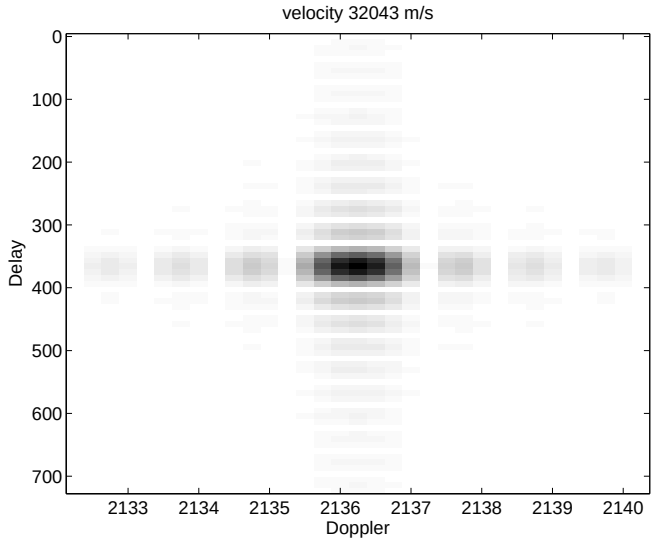

Figure 6.9: The mean value of the range-Doppler response for a target velocity of 32043 m/s focuses on the target clearly, with no cleaving along the range cut and dislocation of the peak response from the cyclic shift value that matches the target velocity.

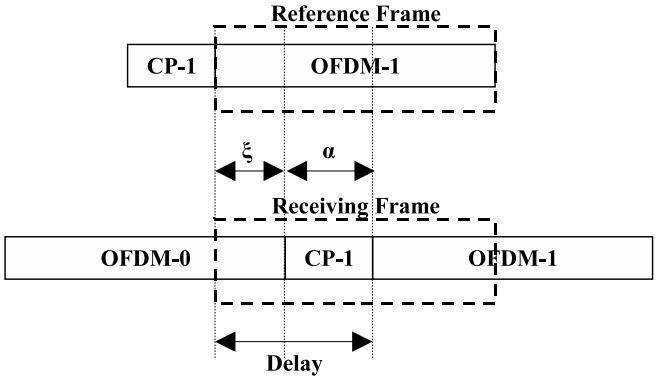

Figure 6.10: The OFDM signal echo from a distant target can be partitioned into two, as the part belonging to the current OFDM chip and the part belonging to the preceding OFDM chip. The part of the delay that is in excess of the guard interval duration $T\alpha$ is denoted as $T\xi$.

by the echo. Thus, the Doppler resolution, which is determined by the time duration of the received signal, is reduced, while the range resolution is not affected. The mean value calculated through Monte Carlo simulation affirms this observation; the zero Doppler range cut still exhibits the Sinc-function

profile with the same main lobe width as before, while the Doppler cut for the target range deviates from the Sinc-profile and has a wider main lobe. Moreover, due to the reduced signal energy received by the processor, the peak of the OFDM pulse compression output is reduced as well.

Apart from the effect on the Doppler resolution, there are two important consequences of the range limit violation. The first one, namely the inter-carrier interference (ICI) is due to the violation of the condition $T = 1/\Delta f$ that keeps the carriers orthogonal. The other consequence is the failure of the modeling of the matched filter as a cyclic convolution. The effect of the target range on the echo is not only in terms of carrier phases anymore, the echo is also truncated beyond the guard interval. This truncation eliminates the cyclical repetitiveness property of the echo, which disrupts the equivalence between the ambiguity function and the OFDM pulse compression.

Sidelobes of the Doppler cut in this setting are affected by the ICI, the mechanism of which can be demonstrated by considering the echo signal model introduced in Paragraph 3.1.4. The echo model in Eq. (3.24) is modified to include the truncation operation $\mathbf{\Xi}$, which is described as

$$\mathbf{\Xi} = diag\{\overbrace{00\ldots0}^{\xi N}\underbrace{11\ldots1}_{(1-\xi)N}\}, \tag{6.25}$$

and the echo model with the truncation operation is

$$\mathbf{s} = \psi\mathbf{\Xi\Gamma F}^{-1}(\mathbf{A}\otimes\boldsymbol{\phi}). \tag{6.26}$$

The echo model modifies the OFDM pulse compression as

$$\boldsymbol{\chi}_\epsilon = \psi\mathbf{F^{-1}}\left[\mathbf{P}\otimes\left(\mathbf{C}_\epsilon^{-1}\mathbf{F\Xi\Gamma F}^{-1}(\mathbf{A}\otimes\boldsymbol{\phi})\right)\right]. \tag{6.27}$$

The crucial step of the processing, which involves the truncation operation and creates the ICI, can be isolated for analysis as

$$\mathbf{F\Xi\Gamma F}^{-1}. \tag{6.28}$$

If we consider the expression above without the Doppler shift operation $\mathbf{\Gamma}$, its outcome is another matrix operation where the diagonal elements are equal to unity, while the immediate off-diagonal elements are also of significant magnitude. Figure 6.11 depicts, as an example, magnitudes of the

matrix elements for $N = 16$ carriers and $\xi = 0.5$. The magnitudes are reduced, but non-zero, for the more distant elements. Without the truncation operation those off-diagonal elements would be reduced to zero, yielding an identity matrix. The off-diagonal elements mathematically demonstrate the ICI, which can be observed from the fact that the multiplication of this matrix operation in Eq. (6.28) with the echo phase vector $(\mathbf{A} \otimes \boldsymbol{\phi})$ corresponds to multiplying the off-diagonals with the cyclically shifted versions of the echo phase vector. The presence of the Doppler shift $\boldsymbol{\Gamma}$ in this case also cyclically shifts the matrix operation.

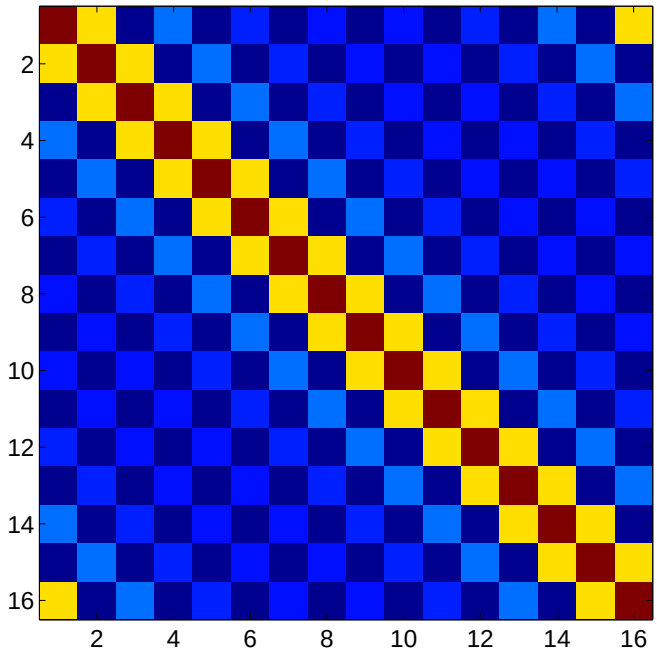

Figure 6.11: Matrix coefficients for the operation described in Eq. (6.28) are mapped for $N = 16$ carriers and a truncation of relative duration $\xi = 0.5$. The main diagonal has the highest magnitude and the two off-diagonals are at half the magnitude of the main diagonal.

The result of this analysis tells us that the Doppler cut for the target is modified as if there are separate targets corresponding to each significant off-diagonal with the matching Doppler shift. This observation explains the relation between the Doppler cut and the guard interval duration, which is depicted in the composite plot in Fig. 6.12 obtained from Monte Carlo simulations for single OFDM chips with $N = 128$ carriers. The target delay of $T/2$ is chosen as an example, which means that $\alpha + \xi = 0.5$. In other words, as the guard interval duration is shorter than $\alpha = 0.5$, the echo signal

is truncated and the ICI disrupts the Doppler cut. However, the Doppler cut follows again a Sinc-profile, albeit one with a wider main lobe, once the guard interval is eliminated. It is noted that the plot in Fig. 6.12 is not energy-normalized for all instances of α; the composite plot is generated such that the transmitted signal energy is fixed for all instances of α, which is energy-normalized only for $\alpha = 0.5$ where the received echo is not truncated. The variance of the OFDM pulse compression, which is again calculated through Monte Carlo simulations, also decreases with increasing target range, again due to the reduced signal energy received by the processor.

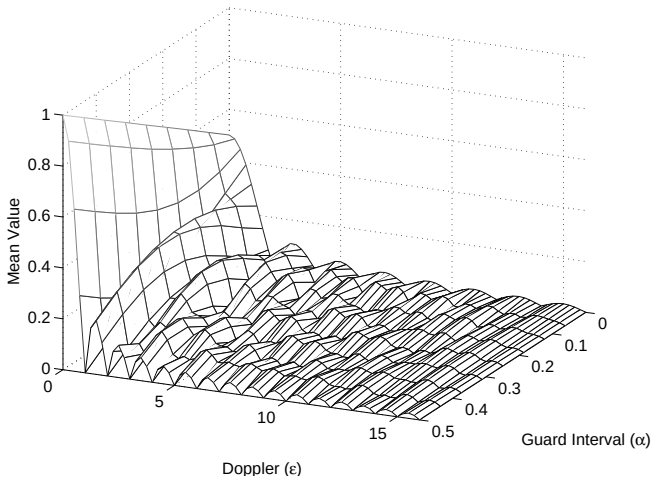

Figure 6.12: The composite plot of the mean values for the Doppler cuts, which are obtained from the OFDM pulse compression output for different guard interval durations α, is generated through Monte Carlo simulations for single OFDM chips with $N = 128$ carriers, where the target delay is fixed at $T/2$.

6.3.2 Interference from the Preceding OFDM Chip

For a train of OFDM chips the case of an isolated OFDM chip may only correspond to the first chip of the train. The more general case has to consider the effect of the preceding OFDM chip, which interferes with the current chip when it is present in the time frame of reception. The inter-symbol interference (ISI) was covered in Paragraph 2.2.1; here its effect on the OFDM pulse compression is investigated.

The mean value of the Monte Carlo simulations for an OFDM signal echo that includes a portion of the preceding OFDM chip is the same as that for the case of an isolated OFDM chip considered above (i.e. without

a preceding OFDM chip). The preceding OFDM chip, as it is independent of the current one, does not contribute to the mean value of the pulse compression output. The variance of the far-off sidelobes as demonstrated by the Monte Carlo simulations, however, does not decrease with the increasing target range anymore, which is due to the ISI. To understand this result, we can formulate the variance for an OFDM signal echo as described in Fig. 6.10. The echo itself can be written as the sum of two zero-padded echoes, one of the preceding OFDM chip that is zero-padded from the end, and the other of the current OFDM chip that is zero-padded from the beginning. The variance of the far-off sidelobes of the pulse compression output for the summation of two such uncorrelated signals can be simplified into the summation of the variances for the pulse compression of the individual signals. In summary, the pulse compression output sidelobes with interference from the preceding OFDM chip has the same expected value as the sidelobes for the isolated OFDM chip with zero-padding, as plotted in Figure 6.12, while the variance of the far-off sidelobes follows the 1/N rule due to the contribution from both the current OFDM chip and the ISI from the preceding OFDM chip.

The most important result of this behavior of OFDM pulse compression, when there is ISI in the echo, is the increase in the rate of the ambiguous velocity measurements, which is partly due to the lower Doppler resolution. It was demonstrated in Paragraph 4.2.2 that, the rate of the ambiguous Doppler measurements after the coherent Doppler integration increases as the guard interval duration α increases. The zero-padding or the ISI also contributes to the increase in the rate of ambiguous Doppler measurements, for they effectively reduce the duty cycle of the OFDM signal, which counts towards increased guard interval duration.

The other factor that determines the rate of the ambiguous velocity measurements is the ICI, the effect of which is described in Paragraph 6.3.1 as the apparent presence of multiple targets at the same range bin with different Doppler shifts. As a result of the ICI, the Doppler response of the OFDM pulse compression may exhibit higher sidelobes, depending on the relation between the guard interval duration α and truncation duration ξ. It is those higher sidelobes that render the over-sampling ineffective in reducing the number of ambiguous velocity measurements. To clearly demonstrate this effect, the processing result for a random train of OFDM chips is plotted in Figure 6.13, which shows the Doppler FFT response for different number of cyclic shifts ϵ. The guard interval is chosen as $\alpha = 0.2$, with the number of pulses equal to 18, and the same simulation parameters as those listed in Table 4.2 are used. The target range is $R = 75km$, which corresponds to $\xi = 0.3$ when $\alpha = 0.2$, and the velocity $v = 22.5m/s$ is especially chosen

such that it lies at the intersection of two cyclic shift Doppler bins and the effect of the high sidelobes is the most visible. Figure 6.13 depicts two peaks that are in the same FFT Doppler bin, which are actually the sidelobes of the responses from the two cyclic shift Doppler bins, $\epsilon = 1$ and $\epsilon = 2$, reinforcing each other. Such Doppler response for those velocities in the vicinity of the intersection of two Doppler bins makes solving the Doppler ambiguity impossible, in the presence of truncation of the received OFDM echoes when the target delay is larger than the guard interval duration.

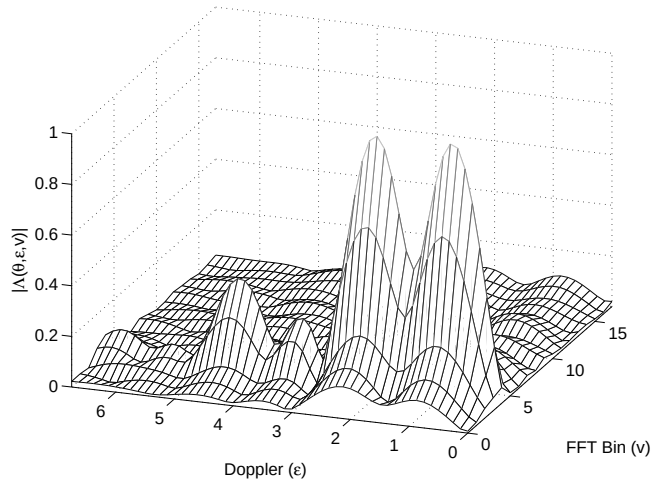

Figure 6.13: The processing result for a random train of OFDM chips, which shows the Doppler FFT response for different number of cyclic shifts ϵ, demonstrates the Doppler response for the target velocity $v = 22.5m/s$, which lies at the intersection of two cyclic shift Doppler bins.

6.3.3 OFDM Pulse Compression Method for Distant Targets

We have demonstrated that the reduced time span for the part of the OFDM signal echo, to which the OFDM pulse compression is matched, translates into reduced Doppler resolution and increased rate of ambiguous Doppler measurements. To eliminate the range dependence of the rate of ambiguous measurements, the Doppler resolution has to be restored regardless of the target range. For this purpose, the OFDM pulse compression has to be modified to include also the preceding OFDM chip as a reference in the pulse compression for the current OFDM chip.

To include the preceding OFDM chip in the reference of the pulse compression, two OFDM pulse compression stages can be used in parallel; one

OFDM pulse compression is focused on the current OFDM chip while the other is focused on the preceding OFDM chip. Their complex-valued outcomes are summed point-wise to combine the responses for the two OFDM chips, which restores the duty cycle of the OFDM chip. The composite plot in Fig. 6.14 that is obtained from Monte Carlo simulations for single OFDM chips with $N = 128$ carriers shows again the mean value of the Doppler cut for different guard interval durations. Different from the Fig. 6.12, the mean value of the Doppler cut always follows the Sinc-shaped profile regardless of the guard interval duration, which shows that including the preceding OFDM chip in the reference indeed compensates for the truncation of the current OFDM chip.

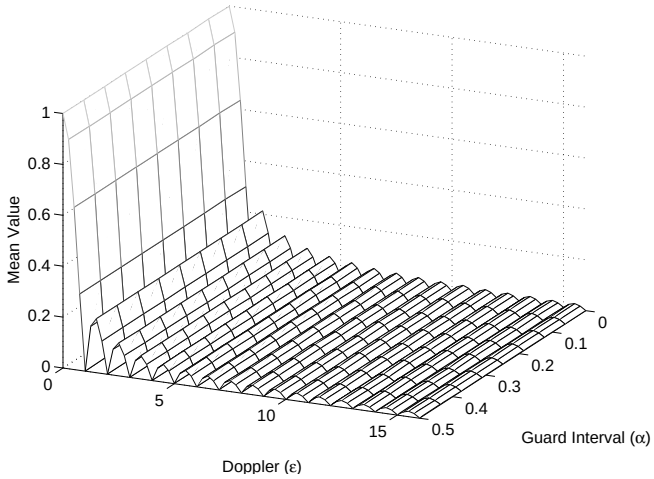

Figure 6.14: The composite plot of the mean values for the Doppler cuts, which are obtained from the OFDM pulse compression output for different guard interval durations α, is generated through Monte Carlo simulations for two OFDM chips with $N = 128$ carriers, where the target delay is fixed at $T/2$.

The mechanism of combining the pulse compression results with different references can be better understood by focusing on the truncation matrix, which was defined in Eq. (6.25). The truncation matrix was defined to isolate the part of the echo that belongs to the current OFDM chip. One can also define an *opposite truncation matrix* $\mathbf{\Xi}_o$ that isolates the part of the echo that belongs to the preceding OFDM chip:

$$\mathbf{\Xi}_o = diag\{\overbrace{11\ldots1}^{\xi N}\underbrace{00\ldots0}_{(1-\xi)N}\}. \tag{6.29}$$

This opposite truncation matrix can be utilized in the same manner as the truncation matrix in Eq. (6.27) to obtain the part of the echo that belongs to the preceding OFDM chip. As it was explained earlier in Eq. (6.28), it is possible to isolate the part of the pulse compression that involves the truncation operation and causes the ICI. This time the opposite truncation operation takes place, which is observed to yield the same banded-matrix structure that was depicted earlier in Fig. 6.11. The numerically generated matrices show that two off-diagonal elements each occupying the same positions in the two banded matrices respectively have the same magnitude but 180° phase difference.

We can consider now the combined echo, which is the sum of the parts belonging to the preceding and the current OFDM chips. The expected value for the OFDM pulse compression that is focused on the current chip was already described in Paragraph 6.3.2. When the focus is on the preceding chip the only difference is the utilization of the opposite truncation matrix. The same banded structure generates the same ICI effect, and when the results from the two OFDM pulse compression outputs are summed up, the ICI terms are also summed up. The 180° phase difference between the matching off-diagonal elements means that the ICI terms are eliminated if the random modulation coefficients have the same distribution for the two OFDM chips, and the Doppler-cut of the OFDM pulse compression output is restored.

The trade-off for restoring the Doppler cut is the doubling of the variance of the far-off sidelobes of the pulse compression output; in other words, the variance of the correlation noise floor is doubled for the far-off sidelobes. The far-off sidelobes are defined as those points in the delay-Doppler plane which are mismatched in both delay and Doppler. It is for those sidelobes that the correlation noise variance follows the $1/N$ rule, and it is for those sidelobes that the correlation noise variance is doubled when the preceding OFDM chip is included in the reference of the pulse compression. The variance calculation, which is described in detail in Appendix C, is simplified into the sum of four independent variance terms,

$$\sigma_{\chi}^2 = \sigma_{pp}^2 + \sigma_{pc}^2 + \sigma_{cp}^2 + \sigma_{cc}^2, \tag{6.30}$$

which is also given in C.10. The simplification is based on the zero covariance between the modulation components for the preceding and the current OFDM chips. The last two terms, which are $\sigma_{cp}^2 + \sigma_{cc}^2$, can be recognized as the variance for the pulse compression when only the current OFDM chip is included in the reference. The first two terms, which are $\sigma_{pp}^2 + \sigma_{pc}^2$, give the variance for the pulse compression when only the preceding OFDM chip is

included. Thus, the variance is doubled for the far-off sidelobes due to the addition of the two pulse compression outputs.

A feature that deserves attention is the possible elimination of the guard interval from the OFDM signal. The simulation results depicted in Fig. 6.12 and Fig. 6.14 also include the Doppler cut for the case of zero guard interval duration, that is, $\alpha = 0$. The standard OFDM pulse compression yields a Doppler cut that follows the Sinc-shaped profile with a wider main lobe, while including the preceding OFDM chip in the reference restores the original main lobe width, which can be observed in Fig. 6.12 and Fig. 6.14 respectively. However, it must be kept in mind that removal of the guard interval prohibits the use of the OFDM signal for communication purposes, while it completely eliminates the ambiguous velocity measurements.

6.4 Summary and Discussion

The OFDM pulse compression technique and the coherent integration of the OFDM chips were developed and formulated under certain assumptions regarding the velocity and range of the targets of interest. These assumptions are in agreement with the intended application of the OFDM radar signal, which is the surveillance of slow-moving small targets, such as persons and ground vehicles. However, the proposed OFDM pulse compression method can be applicable to a wider set of scenarios, which may involve other types of targets with greater velocities and other frequency bands at which the long-range performance is of interest. For this reason, the assumptions regarding the target dynamics are investigated, with the aim of discovering the consequences of their failure and, if possible, developing remedies for those consequences.

While the range limit for the targets of interest is introduced by the cyclic prefix guard interval, which is a feature of the OFDM signal and usually not applicable to other radar signals, the narrowband assumption is generally adopted for the investigation of all radar signals; this is especially true for those investigations that adopt the ambiguity function as the primary tool of performance evaluation for radar signals [78]. As greater bandwidths and higher range resolution is gradually introduced in a wide area of radar applications, investigations over the failure of the narrowband assumption may become a common feature of future radar signal performance analysis.

We have demonstrated in this chapter the two stages at which the narrowband assumption fails for the OFDM radar signal processing, namely the coherent integration stage at lower velocities and the pulse compression

stage itself at higher velocities. Both investigations not only reveal the behavior of the standard OFDM pulse compression for high target velocities, but also offer novel remedies for the failure of the narrowband assumption at both stages.

One novelty is the demonstration of the wideband Doppler effect on the OFDM signal echo by capitalizing over the easily accessible matrix formulations developed earlier in Chapter 3, which revealed two mechanisms of failure for the narrowband assumption. First, the target may migrate between range cells throughout the coherent Doppler integration duration. This range migration may occur even at relatively moderate velocities when the dwell time is kept long to obtain high Doppler resolution. The second failure of the narrowband assumption occurs when the target is fast enough, which, coupled with long pulse compression signal duration and large bandwidth, may lead to the actual Doppler effect revealing itself as the scaling of the signal. Both of these effects are isolated in the matrix formulation of the OFDM signal echo, which provides a unique wideband radar signal echo model.

The isolation of the wideband effects in the matrix formulation of the signal echo leads to improvements in the signal processing. By exploiting the Doppler sensitive nature of the OFDM radar signal, a novel range migration compensation operation has been developed for the coherent Doppler integration that corrects the phases of each OFDM chip in parallel with the Doppler compensation. The Doppler scaling is also isolated in the OFDM pulse compression stage, and another novel method to generate a reference signal for the pulse compression has been proposed. Both methods have been demonstrated to work through Monte Carlo simulations, and the results have been validated by further analysis. It is possible to extend these techniques to cover other Doppler sensitive pulse compression waveforms, such as the phase coded signals.

The range limit imposed by the duration of the cyclic prefix guard interval has been investigated by utilizing the Monte Carlo simulation tools developed in Chapter 4. The two mechanisms that affect the result of the OFDM pulse compression, namely the ICI and the ISI, have been explained and formulated to develop a remedy that is basically incorporating the reference modulation coefficients for the interfering OFDM chip, which is the preceding OFDM chip, in the pulse compression as well as the reference modulation coefficients for the current OFDM chip. The improvement in the OFDM pulse compression results have been demonstrated again through Monte Carlo simulations. The analysis of the effects of ISI and ICI on the OFDM radar signal performance produced a novel method of using the

OFDM radar signal for targets with delays longer than the cyclic prefix guard interval duration, which creates the possibility of utilizing the OFDM radar signal in a larger variety of applications.

Chapter 7

Conclusions, Novelties and Recommendations

7.1 General conclusions and discussions

The main focus of this thesis is the development of a wide-band radar signal with the dual-use as communication signal, and design of the associated radar signal processing technique.

The rationale behind the goal of combining the radar and communication functions in a single signal is to build a network of radars that is not dependent on the commercially available communication infrastructure. Moreover, using the same signal for both functions relaxes the time-frequency budget that would be very tight for combined high-resolution radar and communication operation with distinct signals for each function. However, the processing techniques explored in this thesis exclusively address the application in radar.

The orthogonal frequency division multiplexing (OFDM) is a multi-carrier spread-spectrum technique which finds wide-spread use in communications [49]. The flexible allocation of carriers and carrier contents is the prime motivation for choosing OFDM as a candidate for the multi-carrier radar signal. The bandwidth efficiency of the OFDM signal is much better, compared to the phase coded signals [29], and the Doppler sensitivity of the OFDM signal can be exploited in the radar signal processing to solve the Doppler ambiguity. With these factors as motivation, and since there are also examples of OFDM communication signals used for radar applications in the literature, primarily in the context of passive bistatic radars, OFDM is

adopted for the radar signal. The first step of the development of the OFDM radar signal processing was exploring the OFDM communication signal. The mathematical definition of the OFDM signal was given and its features that provide the orthogonality between the carriers were explored, namely the cyclic prefix guard interval and the chip duration that is the reciprocal of the carrier spacing.

The second step of the development of the OFDM radar signal processing was formulating the OFDM signal that is echoed from a point target. Matrix formulations were developed that explicitly feature the components of an OFDM radar signal echo, which are the carrier amplitudes and phases, the effect of the echo delay on the carriers, and the Doppler effect. Each pulse compression stage was formulated as another matrix operation. The OFDM pulse compression starts with the discrete Fourier transform to recover the carrier phases. The correlation operation in time domain is equivalent to a point-wise multiplication in the frequency domain, and in agreement with the matched filter implementation in the frequency domain, each received carrier phase is multiplied by the complex conjugate of the corresponding transmitted phases. The Doppler effect is compensated by cyclically shifting the received carrier phases before the point-wise multiplication. The result of this operation, when repeated for a number of cyclical shifts to cover all velocities of interest, produces the delay-Doppler plane, which was demonstrated to be equivalent to the ambiguity function. The conditions for this equivalence are that the delay of the echo is shorter than the cyclic prefix guard interval and that the Doppler effect can be modeled as a frequency shift.

Establishing the performance evaluation tools was the third step of the development of the OFDM radar signal processing. The equivalence between the ambiguity function and the OFDM pulse compression output enabled the utilization of the latter as a performance evaluation tool for the OFDM radar signal. The OFDM signal was assumed to be composed of carriers with random starting phases to emulate the random nature of the communications signal, and the random OFDM radar signal necessitated employing statistical methods next to the ambiguity function for performance assessment. The expected value and variance of the PSK-modulated OFDM radar signal after the OFDM pulse compression were calculated analytically. The mean value and the variance for the Monte Carlo simulation results were in excellent agreement with the analytically calculated results. It was revealed that the randomness of the OFDM radar signal generates a *correlation noise floor*, whose variance for far-off sidelobes of the delay-Doppler plane is inversely proportional to the number of carriers in the OFDM signal.

Experiments were conducted to test the validity of these results, where the radar transmitter and receiver chains were implemented using commercially available hardware and measurement instruments. An OFDM radar signal with random starting phases over its carriers was transmitted and the target was implemented by a transponder and a delay line, and the properties of the delay-Doppler plane that is obtained experimentally were in excellent agreement with the one obtained from analytical formulations and simulations. Obtaining the same results from analytical calculations, Monte Carlo simulations and experiments demonstrated the reliability of the Monte Carlo simulation setup, which was used in the later stages of the research as an experiment platform in its own right. Thus, establishing a reliable software experiment platform was the fourth step, which enabled demonstrating the Doppler ambiguity solving capability of the OFDM radar signal and helped to generalize the OFDM pulse compression method over the other OFDM signal implementations.

The capability of the OFDM radar signal to solve the Doppler ambiguity was first conjectured from the expected value of the periodic ambiguity function for a train of OFDM chips. The OFDM pulse compression provides a Doppler measurement with coarse resolution, and the high resolution but ambiguous Doppler measurement from the coherent Doppler integration of a train of OFDM chips is compared with this coarse Doppler measurement to eliminate the ambiguity. It was first predicted from the analytical formulations of the periodic ambiguity function, and later demonstrated by Monte Carlo simulations, that the ambiguity in the Doppler measurements decreases with decreasing cyclic prefix guard interval duration.

After demonstrating the reliability of the Monte Carlo simulation setup, performances of several different OFDM radar signal implementations were explored. An OFDM signal with 16-QAM was introduced, and the Monte Carlo simulation results were verified again through analytical calculations and experimental results. An important challenge of the OFDM radar is the high peak-power, which translates into strict linearity requirements for the power amplifiers. Two different peak-power control methods, namely the use of the Golay complementary codes for modulating the OFDM carriers and the single-carrier OFDM method, were explored and their performances were assessed through Monte Carlo simulations. The effect of clipping the peaks of the OFDM signal was also considered to provide a reference for the comparison of the performances of the peak-power control methods. Peak-power reduction techniques were shown to reduce the correlation noise along the zero-range Doppler cut, while the Golay complementary codes introduced regions of high correlation noise in the far-off sidelobes of the delay-Doppler plane.

The final step of the OFDM pulse compression development focused on the results of the OFDM pulse compression when the delay and velocity limits that were established earlier are violated. The narrowband condition, which permits modeling of the Doppler effect as a frequency shift and which assumes there is no range migration, was investigated first. The range migration was identified as the primary mechanism of the failure of the narrowband condition for the coherent Doppler integration, and a range migration compensation operation that runs in parallel with the Doppler compensation was developed. The Doppler scaling was identified as the mechanism of failure of the narrowband condition for the OFDM pulse compression when the high target velocity is coupled with the long chip duration. In such cases, the scaling effect becomes significant and the effect of motion can no longer be modeled by a simple frequency shift. The OFDM pulse compression was modified by interpolating the reference modulation coefficients, so that they match the scaled version of the originally transmitted OFDM signal. Both techniques are deemed applicable to other pulse compression waveforms that are sensitive to Doppler effects, where Doppler-sensitive means that the pulse compression is rapidly de-focused due to the Doppler effect.

Exceeding the delay limit was demonstrated to affect the Doppler response of the OFDM pulse compression adversely, which is a result of the truncation of the OFDM signal echo due to the delay exceeding the cyclic prefix guard interval duration. Lower Doppler resolution and higher Doppler sidelobes were observed in the Monte Carlo simulation results. These effects were explained by investigating the matrix formulations modified to reflect the truncation of the OFDM signal echo. The Doppler response was restored by including the OFDM chip that precedes the current OFDM chip in the pulse compression reference, which effectively freed the OFDM radar signal from the range limitation at the expense of more complicated signal processing and higher correlation noise.

7.2 Elements of novelty

The primary novelties presented in this dissertation are listed as follows:

- The matrix formulation of the OFDM radar signal echo and the OFDM pulse compression method. Each component of the OFDM signal and the effects of target delay and Doppler are described explicitly in the matrix formulation.

- A method to compensate for the losses due to the Doppler effect, which

recovers the pulse compression gain for the Doppler sensitive waveforms.

- A method to solve the Doppler ambiguity. The OFDM pulse compression of the Doppler sensitive OFDM signal provides a coarse Doppler measurement, which is used to solve the ambiguity in the high resolution Doppler measurement obtained from the coherent Doppler integration.

- A description of the effects of peak-power control techniques on the OFDM radar signal performance. The results show a performance comparable to the standard OFDM signal even when the peak power is limited to very modest values.

- A method to solve the range migration for pulse Doppler radars, where each pulse is an OFDM chip. The range migration is corrected by a compensation operation that is integrated with the Doppler compensation for the OFDM radar signal echo.

- A method to compensate for the Doppler scaling in the OFDM pulse compression. The reference phases are interpolated to match the Doppler scaling in the OFDM radar signal echo, which eliminates the pulse compression loss and the errors in the range and velocity measurements.

- A method to remove the maximum delay limit for the OFDM radar signal. The preceding OFDM chip is also added to the reference phases in the OFDM pulse compression to prevent its interference with the current OFDM chip.

7.3 Future research

In this dissertation the OFDM pulse compression method that utilizes an OFDM communication signal for radar tasks has been studied in detail. Using the ambiguity function tool, the feasibility of the OFDM pulse compression method is demonstrated from a performance perspective. Further investigation aimed at demonstrating the practical applicability of the OFDM pulse compression and improving its performance remains for future research. A list of suggestions for such future research is provided hereafter:

- Methods to enhance the performance of the radar by eliminating the strong stationary clutter. The correlation noise level is determined

by the strongest echoes, which may come from stationary clutter and mask the small, slow-moving targets. Space-time adaptive processing (STAP) techniques may be utilized to remove the stationary clutter.

- The effect of the complex radar cross section and Swerling target models on the OFDM pulse compression.
- Matched illumination methods to enhance target classification, when utilizing the OFDM signal in tracking radars.
- Coding methods to tailor the ambiguity function.
- More advanced interpolation and estimation methods for delay and Doppler measurements.
- Hardware implementation of the signal processing techniques using the state-of-the-art processors. The PARSAX system of the Delft University of Technology can accomodate the OFDM radar signal and the OFDM pulse compression technique.

The ultimate goal that lies behind the adoption of the OFDM communication signal as the radar waveform is to build a network of radars that can utilize their directive beams for the communications uplink. The future research direction that covers the communication related aspects of such a network of radars deserves special attention; a non-exhaustive list of suggestions for this particular topic is as follows:

- The characterization of the channel, which may be line-of-sight (LOS) or non-LOS.
- Filters that can cope with varying channel characteristics.
- Determining the time-dependent bit-error-rate (BER) due to the rotating antenna.
- A more comprehensive study of the communication fidelity for various OFDM peak-power control methods.
- Network protocols that can cope with the time-dependent BER.
- Determining the link budget to enable the sharing of useful data between the radars.
- Methods for accurate time/frequency alignment.

Presence of multiple radars in the same geographical region necessitates considering the possible interference between the individual radar systems, which may affect both the communications and the radar performances adversely. As the proposed radar network is intended for detecting and classifying small targets, each radar system already occupies a frequency band of significant size. Thus, separating the different radar stations in frequency may consume the available spectrum very rapidly as the number of radar stations increase. Other interference mitigation techniques, such as low cross-correlation coding, may also be researched in the future.

Appendices

Appendix A

Variance of the OFDM Pulse Compression Output

The variance of the OFDM pulse compression, as described in Section 4.1.2, is calculated from the equation

$$\sigma^2_{\chi(\theta,\epsilon)} = E\left[|\chi(\theta,\epsilon)|^2\right] - |E\left[\chi(\theta,\epsilon)\right]|^2, \tag{A.1}$$

where $\chi(\theta,\epsilon)$ is the pulse compression output. Finding an analytical expression for the variance involves the derivation of the second moment of the OFDM pulse compression output; namely, the $E\left[|\chi(\theta,\epsilon)|^2\right]$ term has to be evaluated. The square of the pulse compression output, since it is complex, is obtained through multiplying the Eq. (4.1) by its complex conjugate, which yields

$$\begin{aligned} E\left[|\chi(\theta,\epsilon)|^2\right] = \quad & \tfrac{1}{N^4} \sum_{k=0}^{N-1}\sum_{n=0}^{N-1}\sum_{m=0}^{N-1}\sum_{\overline{k}=0}^{N-1}\sum_{\overline{n}=0}^{N-1}\sum_{\overline{m}=0}^{N-1} \\ & \Big[\exp\left\{j2\pi(k-\overline{k})\left(\tfrac{\theta}{N} - \tfrac{2R\Delta f}{c}\right)\right\} \\ & \exp\left\{j2\pi\tfrac{(m-k-\epsilon)n-(\overline{m}-\overline{k}-\epsilon)\overline{n}}{N}\right\}\exp\left\{-j2\pi f_c\tfrac{2v}{c}\tfrac{(n-\overline{n})}{N\Delta f}\right\} \\ & E[\exp\{j(\phi_m - \phi_k - \phi_{\overline{m}} + \phi_{\overline{k}})\}]\Big]. \end{aligned} \tag{A.2}$$

The expected value for the phase expression in Eq. (A.2) can be simplified in a similar fashion to the expected value expression in Eq. (4.4), due to the uniform random distribution of the phases:

$$E\left[\exp\{j(\phi_m - \phi_k - \phi_{\overline{m}} + \phi_{\overline{k}})\}\right] = \begin{cases} 1 & m = k, \overline{m} = \overline{k} \\ 1 & m = \overline{m}, k = \overline{k} \\ 0 & m,\ otherwise \end{cases}. \tag{A.3}$$

This simplification reflects onto the second moment expression in Eq. (A.2) as

$$\begin{aligned} E\left[|\chi(\theta,\epsilon)|^2\right] = \quad & \tfrac{1}{N^4}\sum_{k=0}^{N-1}\sum_{n=0}^{N-1}\sum_{m=0}^{N-1}\sum_{\overline{n}=0}^{N-1}\Big[\exp\left\{j2\pi\tfrac{(m-k-\epsilon)(n-\overline{n})}{N}\right\} \\ & \exp\left\{-j2\pi f_c\tfrac{2v}{c}\tfrac{(n-\overline{n})}{N\Delta f}\right\}\Big] \\ & +\tfrac{1}{N^4}\sum_{k=0}^{N-1}\sum_{n=0}^{N-1}\sum_{\overline{k}=0}^{N-1}\sum_{\overline{n}=0}^{N-1}\Big[\exp\left\{j2\pi(k-\overline{k})\left(\tfrac{\theta}{N}-\tfrac{2R\Delta f}{c}\right)\right\} \\ & \exp\left\{j2\pi\tfrac{\epsilon(n-\overline{n})}{N}\right\}\exp\left\{-j2\pi f_c\tfrac{2v}{c}\tfrac{(n-\overline{n})}{N\Delta f}\right\}\Big]. \end{aligned} \tag{A.4}$$

The second set of summations in Eq. (A.4) is the same as the square of the expected value in Eq. (4.4). Thus, combining the Eq. (A.4) and the square of the Eq. (4.4) in Eq. (A.1) yields the variance as

$$\begin{aligned} \sigma^2_{\chi(\theta,\epsilon)} = \quad & \tfrac{1}{N^4}\sum_{k=0}^{N-1}\sum_{n=0}^{N-1}\sum_{m=0}^{N-1}\sum_{\overline{n}=0}^{N-1}\Big[\exp\left\{j2\pi\tfrac{(m-k-\epsilon)(n-\overline{n})}{N}\right\} \\ & \exp\left\{-j2\pi f_c\tfrac{2v}{c}\tfrac{n-\overline{n}}{N\Delta f}\right\}. \end{aligned} \tag{A.5}$$

It is interesting to note that the variance expression has no θ dependence.

Appendix B

Experiment Setup for OFDM Radar Signals

The experiment setup is designed to implement all the steps in an actual radar transceiver chain using commercially available equipment. The waveform generation and measurement equipment, epecially, is chosen from the commercially available measurement equipments. While the detailed description of the experiment setup is provided in [10], several points crucial for the OFDM radar signal generation and processing are explained here.

The OFDM signal is generated at the IF frequency digitally. The digital IF generation is based on the use of IFFT with size larger than the required number of carriers. In other words, the IF signal is generated by zero-padding the frequency coefficients from both the low frequency side and the high frequency side, as depicted in Fig. B.1.

The sampling frequency of the arbitrary waveform generator (Agilent N8241A) is 1.25Gs/s, which translates into an IFFT size of 125×10^6 for generating an OFDM signal with the carrier spacing $\Delta f = 1$kHz and the corresponding chip duration of $T = 1$ms. The IF is chosen to be 250MHz to obtain the optimum performance from the system components.

The real and imaginary parts of the comple OFDM signal at IF frequency are uploaded to the arbitrary waveform generator as the in-phase and quadrature signal components (I/Q), which are converted into analog and fed into the I/Q channels of the vector signal generator (E8267D). The vector signal generator upconverts the OFDM signal by mixing it with the local oscillator (LO) running at 9.8GHz. The image frequency, which arises due to the imbalance between the I and Q channels, is rejected through a filter at RF, which supresses the LO leakage by 10dB and the image

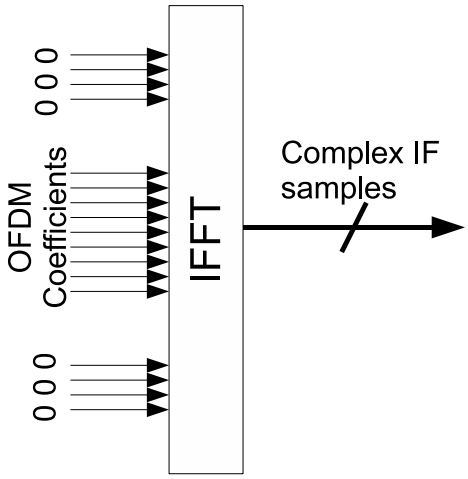

Figure B.1: The zero-padding method to generate the OFDM signal at IF.

components are suppressed by another 20dB on top of the reduction due to the I/Q modulation.

The RF signal is delayed through an optical delay line to emulate the actual delay a radar signal echo would undergo, and the output of the delay line is connected to an antenna, after the necessary amplification to compensate for the losses in the delay line. The antennas transmitting and receiving the radar signal echo is essetial to incorporate the effect of the environment, which may not be possible in software simulations.

The down-mixing is accomplished by using the reference LO signal from the vector signal generator, and the resulting down-mixed OFDM signal is again at IF. This arrangement, while necessitating higher sampling rate at the digital receiver, permits simpler implementation of the receiver hardware. It can be said that while the complete system can be considered as heterodyne, the analog hardware alone is homodyne.

The final component that completes the implementation of the transceiver chain is the digital oscilloscope (DSA91304A), which samples the IF signal at 5Gs/s. The recovered samples are recorded and transferred to a computer for offline processing. The high sampling rate is reduced to 1.25Gs/s by decimation, and the OFDM spectrum coefficients are recovered from the digital IF signal by an FFT, in the same fashion as the IF OFDM signal is generated.

Appendix C

Formulation of the Long-Range Pulse Compression Output

It was explained in Paragraph 6.3.3 that the variance of the correlation noise floor is doubled for the far-off sidelobes, when the pulse compression operation includes the preceding OFDM chip as well as the current one as the reference. The variance of the correlation noise floor in the far-off sidelobes is calculated by considering a point in the delay-Doppler plane, where ϵ is mismatched to the target velocity by a margin of at least 2. The combined pulse compression consists of four main components:

$$\begin{aligned}\boldsymbol{\chi}_{\epsilon,LR} = \quad & \psi\mathbf{F^{-1}}\left[\mathbf{P}_p \otimes \left(\mathbf{Q}_{p,\epsilon} \otimes (\mathbf{a} \otimes \boldsymbol{\phi}_p)\right)\right] \\ & +\psi\mathbf{F^{-1}}\left[\mathbf{P}_p \otimes (\mathbf{Q}_{c,\epsilon} \otimes (\mathbf{a} \otimes \boldsymbol{\phi}_c))\right] \\ & +\psi\mathbf{F^{-1}}\left[\mathbf{P}_c \otimes \left(\mathbf{Q}_{p,\epsilon} \otimes (\mathbf{a} \otimes \boldsymbol{\phi}_p)\right)\right] \\ & +\psi\mathbf{F^{-1}}\left[\mathbf{P}_c \otimes (\mathbf{Q}_{c,\epsilon} \otimes (\mathbf{a} \otimes \boldsymbol{\phi}_c))\right] \\ & = \boldsymbol{\chi}_{\epsilon,pp} + \boldsymbol{\chi}_{\epsilon,pc} + \boldsymbol{\chi}_{\epsilon,cp} + \boldsymbol{\chi}_{\epsilon,cc}, \end{aligned} \tag{C.1}$$

where $\mathbf{P}_p$ and $\mathbf{P}_c$ are the reference phases, while the $\boldsymbol{\phi}_p$ and $\boldsymbol{\phi}_c$ are the received phases that belong to the preceding and the current ODM chips, respectively. The expressions are groupped such that:

- $\boldsymbol{\chi}_{\epsilon,pp}$ replaces the expressions relating the reference from the preceding OFDM chip to the echo from the preceding OFDM chip,

- $\boldsymbol{\chi}_{\epsilon,pc}$ replaces the expressions relating the reference from the preceding OFDM chip to the echo from the current OFDM chip,
- $\boldsymbol{\chi}_{\epsilon,cp}$ replaces the expressions relating the reference from the current OFDM chip to the echo from the preceding OFDM chip,
- $\boldsymbol{\chi}_{\epsilon,cc}$ replaces the expressions relating the reference from the current OFDM chip to the echo from the current OFDM chip.

The terms

$$\mathbf{Q}_{c,\epsilon} = \mathbf{F}\boldsymbol{\Xi}\boldsymbol{\Gamma}_{\epsilon}\mathbf{F}^{-1}, \tag{C.2}$$

and

$$\mathbf{Q}_{p,\epsilon} = \mathbf{F}\boldsymbol{\Xi}_{\circ}\boldsymbol{\Gamma}_{\epsilon}\mathbf{F}^{-1}, \tag{C.3}$$

correspond to the banded matrices described in Eq. (6.28) for the current and the preceding OFDM chips respectively, and $\boldsymbol{\Gamma}_{\epsilon}$ indicates the residual Doppler effect after the cyclic shift operation compensates for a Doppler shift that is mismatched to the target velocity. Thus, the cyclic shift operation is eliminated from the expression for simpler treatment. It is noted that the effect of the residual Doppler shift $\boldsymbol{\Gamma}_{\epsilon}$ is still a cyclic shift of the banded matrices $\mathbf{Q}_{c,\epsilon}$ and $\mathbf{Q}_{p,\epsilon}$, which was explained also in Paragraph 6.3.1.

Each $\mathbf{Q}$ matrix can be decomposed into a sum of diagonal and off-diagonal matrices. By the distributive property of the Hadamard and ordinary matrix multiplication operations, each component of the combined pulse compression term can be decomposed further. An example is given for the component $\boldsymbol{\chi}_{\epsilon,pp}$:

$$\begin{aligned}\boldsymbol{\chi}_{\epsilon,pp} = \quad & \psi\mathbf{F}^{-\mathbf{1}}\left[\mathbf{P}_p \otimes \left(\mathbf{q}_{p,\epsilon,0} \otimes (\mathbf{a} \otimes \boldsymbol{\phi}_p)\right)\right] \\ & + \psi\mathbf{F}^{-\mathbf{1}}\left[\mathbf{P}_p \otimes \left(\mathbf{q}_{p,\epsilon,1} \otimes (\mathbf{a} \otimes \boldsymbol{\phi}_p)\right)\right] \\ & + \dots \\ & + \psi\mathbf{F}^{-\mathbf{1}}\left[\mathbf{P}_p \otimes \left(\mathbf{q}_{p,\epsilon,N-1} \otimes (\mathbf{a} \otimes \boldsymbol{\phi}_p)\right)\right],\end{aligned} \tag{C.4}$$

where $\mathbf{q}_{p,\epsilon,x}$ indicates the $\mathbf{x}^{\mathbf{th}}$ diagonal of the matrix $\mathbf{Q}_{p,\epsilon}$. When the index $x = 0$ the term corresponds to the main diagonal, and as the index increases, the corresponding diagonal is further lower in the matrix $\mathbf{Q}_{p,\epsilon}$.

When ϵ matches the target Doppler, the expected value for the other bands is zero due to the cyclic shift the off-diagonal band creates. The expected values for the main diagonals are summed up, which is again zero for the $\boldsymbol{\chi}_{\epsilon,pc}$ and $\boldsymbol{\chi}_{\epsilon,cp}$ components, while the $\boldsymbol{\chi}_{\epsilon,pp}$ and $\boldsymbol{\chi}_{\epsilon,cc}$ components are non-zero and summed up. However, when there is a mismatch between the ϵ and the target Doppler, one of the off-diagonal bands will move into the position of the diagonal due to the residual cyclic shift from the mismatch. The relation that

$$\mathbf{q}_{p,x} = -\mathbf{q}_{c,x}, x \neq 0 \tag{C.5}$$

means that the non-zero components $\boldsymbol{\chi}_{\epsilon,pp}$ and $\boldsymbol{\chi}_{\epsilon,cc}$ cancel each other in the case of mismatched ϵ.

The variance involves calculating the term

$$\sigma_\chi^2 = E\left[(\chi - E[\chi])^2\right], \tag{C.6}$$

which can be decomposed into the variance of the four components

$$\sigma_\chi^2 = E\left[\left(\boldsymbol{\chi}_{\epsilon,pp} + \boldsymbol{\chi}_{\epsilon,pc} + \boldsymbol{\chi}_{\epsilon,cp} + \boldsymbol{\chi}_{\epsilon,cc} - E[\boldsymbol{\chi}_{\epsilon,pp} + \boldsymbol{\chi}_{\epsilon,pc} + \boldsymbol{\chi}_{\epsilon,cp} + \boldsymbol{\chi}_{\epsilon,cc}]\right)^2\right]. \tag{C.7}$$

The variance can be decomposed further into

$$\begin{aligned}\sigma_{\chi}^{2} = \quad & \sigma_{pp}^{2} + \sigma_{pc}^{2} + \sigma_{cp}^{2} + \sigma_{cc}^{2} + \\ & E\left[\boldsymbol{\chi}_{\epsilon,pp} \otimes \boldsymbol{\chi}_{\epsilon,pc}^{*}\right] - E\left[\boldsymbol{\chi}_{\epsilon,pp}\right] \otimes E\left[\boldsymbol{\chi}_{\epsilon,pc}^{*}\right] + \\ & E\left[\boldsymbol{\chi}_{\epsilon,pp} \otimes \boldsymbol{\chi}_{\epsilon,cc}^{*}\right] - E\left[\boldsymbol{\chi}_{\epsilon,pp}\right] \otimes E\left[\boldsymbol{\chi}_{\epsilon,cc}^{*}\right] + \\ & E\left[\boldsymbol{\chi}_{\epsilon,pp} \otimes \boldsymbol{\chi}_{\epsilon,cp}^{*}\right] - E\left[\boldsymbol{\chi}_{\epsilon,pp}\right] \otimes E\left[\boldsymbol{\chi}_{\epsilon,cp}^{*}\right] + \\ & E\left[\boldsymbol{\chi}_{\epsilon,pc} \otimes \boldsymbol{\chi}_{\epsilon,cp}^{*}\right] - E\left[\boldsymbol{\chi}_{\epsilon,pc}\right] \otimes E\left[\boldsymbol{\chi}_{\epsilon,cp}^{*}\right] + \\ & E\left[\boldsymbol{\chi}_{\epsilon,pc} \otimes \boldsymbol{\chi}_{\epsilon,cc}^{*}\right] - E\left[\boldsymbol{\chi}_{\epsilon,pc}\right] \otimes E\left[\boldsymbol{\chi}_{\epsilon,cc}^{*}\right] + \\ & E\left[\boldsymbol{\chi}_{\epsilon,cp} \otimes \boldsymbol{\chi}_{\epsilon,cc}^{*}\right] - E\left[\boldsymbol{\chi}_{\epsilon,cp}\right] \otimes E\left[\boldsymbol{\chi}_{\epsilon,cc}^{*}\right] + \\ & E\left[\boldsymbol{\chi}_{\epsilon,pp}^{*} \otimes \boldsymbol{\chi}_{\epsilon,pc}\right] - E\left[\boldsymbol{\chi}_{\epsilon,pp}^{*}\right] \otimes E\left[\boldsymbol{\chi}_{\epsilon,pc}\right] + \\ & E\left[\boldsymbol{\chi}_{\epsilon,pp}^{*} \otimes \boldsymbol{\chi}_{\epsilon,cc}\right] - E\left[\boldsymbol{\chi}_{\epsilon,pp}^{*}\right] \otimes E\left[\boldsymbol{\chi}_{\epsilon,cc}\right] + \\ & E\left[\boldsymbol{\chi}_{\epsilon,pp}^{*} \otimes \boldsymbol{\chi}_{\epsilon,cp}\right] - E\left[\boldsymbol{\chi}_{\epsilon,pp}^{*}\right] \otimes E\left[\boldsymbol{\chi}_{\epsilon,cp}\right] + \\ & E\left[\boldsymbol{\chi}_{\epsilon,pc}^{*} \otimes \boldsymbol{\chi}_{\epsilon,cp}\right] - E\left[\boldsymbol{\chi}_{\epsilon,pc}^{*}\right] \otimes E\left[\boldsymbol{\chi}_{\epsilon,cp}\right] + \\ & E\left[\boldsymbol{\chi}_{\epsilon,pc}^{*} \otimes \boldsymbol{\chi}_{\epsilon,cc}\right] - E\left[\boldsymbol{\chi}_{\epsilon,pc}^{*}\right] \otimes E\left[\boldsymbol{\chi}_{\epsilon,cc}\right] + \\ & E\left[\boldsymbol{\chi}_{\epsilon,cp}^{*} \otimes \boldsymbol{\chi}_{\epsilon,cc}\right] - E\left[\boldsymbol{\chi}_{\epsilon,cp}^{*}\right] \otimes E\left[\boldsymbol{\chi}_{\epsilon,cc}\right]. \end{aligned} \tag{C.8}$$

where σ_{pp}^{2} is the variance for the $\boldsymbol{\chi}_{\epsilon,pp}$ term, and the other σ^{2} are the variances for their respective counterparts. We have to consider the relation between the expected values of the pulse compression components to see if the explicit expected value terms can be eliminated. A further decomposition of each component, which was described in Eq. (C.4), sheds light on the possible combinations that need to be considered. For example, the expected value term $E\left[\boldsymbol{\chi}_{\epsilon,pp} \otimes \boldsymbol{\chi}_{\epsilon,cc}^{*}\right]$ can be decomposed such that it is the sum of the terms

$$E\Big[\left\{\psi\mathbf{F}^{-1}\left[\mathbf{P}_{p} \otimes \left(\mathbf{q}_{p,\epsilon,x} \otimes \left(\mathbf{a} \otimes \boldsymbol{\phi}_{p}\right)\right)\right]\right\} \otimes \left\{\psi\mathbf{F}^{-1}\left[\mathbf{P}_{c} \otimes \left(\mathbf{q}_{c,\epsilon,y} \otimes \left(\mathbf{a} \otimes \boldsymbol{\phi}_{c}\right)\right)\right]\right\}^{*}\Big], \tag{C.9}$$

for all index values x and y.

The first important observation concerns the relation of the indexes of $\mathbf{q}_{p,\epsilon,x}$ and $\mathbf{q}_{c,\epsilon,y}$: If the indexes x and y are not equal, the different amount of cyclic shift will yield independent random sequences. As the expected value of the multiplication of two random variables with zero covariance is equal to the multiplication of the individual expected values,any such expected value term is eliminated.

The second observation concerns the $E\left[\boldsymbol{\chi}_{\epsilon,pp} \otimes \boldsymbol{\chi}_{\epsilon,cc}^{*}\right]$ case: The phases

for the two OFDM chips are randomly generated and, thus, have zero covariance. The pulse compression results for the two phase sequences have also zero covariance as a result when $x \neq 0$. For the case when $x = y = 0$, the corresponding components of $\boldsymbol{\chi}_{\epsilon,pp}$ and $\boldsymbol{\chi}_{\epsilon,cc}$ are deterministic, since the phases are compensated in the pulse compression. In the end, the corresponding expected value terms are eliminated.

The third observation concerns the $E\left[\boldsymbol{\chi}_{\epsilon,pc} \otimes \boldsymbol{\chi}^*_{\epsilon,cp}\right]$ case: The two components in this case may have non-zero covariance, since the same phase sequences are multiplied for both components. However, the conjugation operation for the second component is actually canceled due to the reference phases swapping position with the received phases. The result of the multiplication is complex-valued and the expected value for the multiplication of the two components is zero. The expected values for the individual components are also zero due to the multiplication of independent phase sequences. Hence, this component is also eliminated.

The final observation concerns the remaining terms: The presence of an independent phase sequence in either of the components in the expected value translates into zero covariance between those components, hence the expected values for all such components are also eliminated. As the result of all these observations, the variance is simplified into

$$\sigma^2_\chi = \sigma^2_{pp} + \sigma^2_{pc} + \sigma^2_{cp} + \sigma^2_{cc}. \tag{C.10}$$

It can be noticed that the variance for the pulse compression output when only the current OFDM chip is included in the reference was found to be in agreement with the $1/N$ rule in the far-off sidelobes. The variance term in Eq (C.10) includes both the pulse compression with the current OFDM chip as the reference and the pulse compression with the preceding OFDM chip as the reference. As result of the summation in Eq (C.10), the far-off sidelobes now have doubled variance, that is, the far-off sidelobes have variance equal to $2/N$.

Bibliography

[1] J. Armstrong, "Peak-to-average power reduction for OFDM by repeated clipping and frequency domain filtering," *Electronics Letters,* Vol. 38, No. 5, Feb. 2002, pp. 246–247.

[2] D. Astely, E. Dahlman, A. Furuskar, Y. Jading, M. Lindstrm, and S. Parkvall "LTE: The Evolution of Mobile Broadband," *IEEE Communications Magazine,* Vol. 47, No. 4, April 2009, pp. 44–51.

[3] S. R. J. Axelsson, "Noise radar using random phase and frequency modulation," *IEEE Trans. Geosci. Remote Sensing,* Vol. 42, No. 11, November 2004, pp. 2370–2384.

[4] P. Barrenechea, F. Elferink and J. Janssen, "FMCW Radar with Broadband Communication Capability," in *Proceedings of the* 4^{th} *European Radar Conference, EuRAD'07,* Munich/Germany, Oct. 2007, pp. 130–133.

[5] J. J. van de Beek, M. Sandell, P. O. Borjesson, "ML estimation of time and frequency offset in OFDM systems," *IEEE Trans. on Signal Processing,* Vol. 45, No. 7, July 1997, pp. 1800–1805.

[6] B. Chen, "Maximum likelihood estimation of OFDM carrier frequency offset," *IEEE Signal Processing Letters,* Vol. 9, No. 4, Apr. 2002, pp. 123–126.

[7] J. P. Costas, "A Study of a class of detection waveforms having nearly ideal range-Doppler ambiguity properties," *Proceedings of IEEE,* Vol. 72, No. 8, Aug. 1984, pp. 996–1009.

[8] J. A. Davis and J. Jedwab, "Peak-to-mean power control in OFDM, Golay complementary sequences, and Reed-Muller codes," *IEEE Trans. Inform. Theory,* Vol. 45, Nov. 1999, pp. 2397–2417.

[9] J. Duan, Z. He, C. Inan, "A Novel Doppler Radar Using only Two Pulses," in Proc. CIE06, 16-19 Oct. 2006.

[10] E. Mendez Dominguez, R. F. Tigrek, M. Ruggiano, G. Lellouch, W. J. A. de Heij, D. Bockstal, P. van Genderen, "Experimental set-up demonstrating combined use of OFDM for radar and communications," *Microwave Journal,* Vol. 53, No. 8, August Supplement 2010, pp. 22–36.

[11] M. Engels, *Wireless OFDM Systems: How to Make Them Work?* Kluwer Academic Publishers, 2002, pp. 37.

[12] A. Fasoula, H. Driessen, P. van Genderen, "2D Spatial Model Matching Using HRR Multi-Radar Data," in 11$^{\text{th}}$ *International Conference on Information Fusion,* Cologne/Germany, 30 June-3 July 2008, pp. 1–8.

[13] R. A. M. Fens, M. Ruggiano, G. Leus, "Channel Characterization Using Radar for Transmission of Communication Signals," in *Proc.* 1$^{\text{st}}$*t European Wireless Technology Conf.,* 27-28 October 2008, pp. 127–130.

[14] G. E. A. Franken, H. Nikookar, P. van Genderen, "Doppler Tolerance of OFDM-coded Radar Signals," in *Proc.* 3$^{\text{rd}}$ *European Radar Conf.,* 2006, pp. 108–111.

[15] A. Freedman, N. Levanon, "Properties of the Periodic Ambiguity Function," *IEEE Trans. on Aerospace and Electronic Systems,* Vol. 30, No. 3, July 1994, pp. 938–941.

[16] D. Garmatyuk, J. Schuerger, T. Y. Morton, K. Binns, M. Durbin, J. Kimani, "Feasibility Study of a Multi-Carrier Dual-Use Imaging Radar and Communication System," in *Proc.* 4$^{\text{th}}$ *European Radar Conf.,* 2007, pp. 194-197.

[17] P. van Genderen, H. Nikookar, "Radar Network Communication," in *Proc. Communications 2006,* 8-10 June 2006, pp. 313-316.

[18] M. Golay, "Complementary series," *IRE Trans. on Information Theory,* Vol. 7, No. 2, April 1961, pp. 82–87.

[19] S. H. Han, J. H. Lee, "An overview of peak-to-average power ratio reduction techniques for multicarrier transmission," *IEEE Wireless Commun.,* Vol. 12, No. 2, April 2005, pp. 56–65.

[20] E. Insanic, P. Siqueira, "Velocity Unfolding in Networked Radar System," in *Proc. IGARSS 2008,* 7-11 July 2008, Vol. 3, pp. 1103–1106.

[21] L. Jing, G. Hong, S. Weimin, "High speed space objects detection using noise frequency modulated pulse radar," in *IET International Radar Conf.,* 2009, pp. 1–5.

[22] V. Jungnickel, T. Hindelag, T. Haustein, W. Zirwas, "SC-FDMA Waveform Design, Performance, Power Dynamics and Evolution to MIMO," in *IEEE International Conference on Portable Information Devices,* Orlando, Florida, 25-29 March 2007.

[23] T. Keller, L. Hanzo, "Adaptive multicarrier modulation: A convenient framework for time-frequency processing in wireless communications," *Proceedings of the IEEE,* Vol. 88, No. 5, May 2000, pp. 611–640.

[24] A. Laourine, A. Stephenne, S. Affes, "A new OFDM synchronization symbol for carrier frequency offset estimation," *IEEE Signal Processing Letters,* Vol. 14, No. 5, May 2007, pp. 321–324.

[25] G. Lellouch, H. Nikookar, "On the capability of a radar network to support communications," in *Proc.* 14^{th} *IEEE Symposium on Communications and Vehicular Technology in the Benelux,* Nov. 2007, pp. 1-5.

[26] N. Levanon, *Radar Principles,* J. Wiley & Sons New York, 1988.

[27] N. Levanon, E. Mozeson, *Radar Signals,* Hoboken, NJ: John Wiley & Sons, 2004, pp. 42–46.

[28] N. Levanon, E. Mozeson, *Radar Signals,* Hoboken, NJ: John Wiley & Sons, 2004, pp. 213.

[29] N. Levanon, "Multifrequency complementary phase-coded radar signal," *IEE Proc. Radar Sonar Navig.,* Vol. 147, No. 6, Dec. 2000, pp. 276–284.

[30] N. Levanon, "Multifrequency signal structure for radar systems," U.S. Patent 6 392 588, May 21, 2002.

[31] N. Levanon, E. Mozeson, "Multicarrier radar signal pulse train and CW," *IEEE Trans. Aerospace and Electronic Systems,* Vol. 38, No. 2, April 2002, pp. 707–720.

[32] X. Li, L. Cimini, "Effects of clipping and filtering on the performance of OFDM," *IEEE Communications Letters,* Vol. 2, No. 5, May 1998, pp. 131–133.

[33] Y. Li, T. Long, "A long-term coherent integration method of phase-coded pulse train," in *Proc. ICSP 2008,* 9^{th} *International Conference on Signal Processing,* Beijing/China, 26-29 Oct. 2008, pp. 2334–2337.

[34] Y. Li, T. Zeng, T. Long, Z. Wang, "Range migration compensation and Doppler ambiguity resolution by Keystone transform," in *Proc. CIE06 International Conference on Radar,* 16-19 Oct. 2006.

[35] W. Liu, J. Lau, R. Cheng, "Considerations on applying OFDM in a highly efficient power amplifier," *IEEE Transactions on Circuits and Systems-II: Analog and Digital Signal Processing,* Vol. 46, No. 11, Nov. 1999, pp. 1329–1335.

[36] S. V. Maric, E. L. Titlebaum, "A class of frequency hop codes with nearly ideal characteristics for use in multiple-access spread-spectrum communications and radar and sonar systems," *IEEE Transactions on Communications,* Vol. 40, No. 9, Sept. 1992, pp. 1442–1447.

[37] J. Martin, "Range and Doppler accuracy improvement for pulsed Doppler radar," in *Radar 97,* Edinburgh/United Kingdom, 14-16 Oct. 1997, pp. 439–443.

[38] D. Matic, T. M. Coenen, F. C. Schoute, R. Prasad. "OFDM timing synchronisation: Possibilities and limits to the usage of the cyclic prefix for maximum likelihood estimation," in *VTC 1999* Amsterdam/The Netherlands, 19-22 Sep. 1999, Vol. 2, pp. 668–672.

[39] M. Morelli, C.-C. J. Kuo, M.-O. Pun, "Synchronization techniques for orthogonal frequency division multiple access (OFDMA): A tutorial review," *Proceedings of the IEEE,* Vol. 95, No. 7, July 2007, pp. 1394–1427.

[40] Y. Mostofi, D. C. Cox, "Mathematical Analysis of the Impact of Timing Synchronization Errors on the Performance of an OFDM System," *IEEE Transactions on Communications,* Vol. 54, No. 2, Feb. 2006, pp. 226–230.

[41] E. Mozeson, N. Levanon, "Multicarrier radar signals with low peak-to-mean envelope power ratio," *IEE Proc. Radar Sonar Navig.,* Vol. 150, No. 2, Apr. 2003, pp. 71–77.

[42] H. G. Myung, J. Lim, and D. J. Goodman, "Single Carrier FDMA for Uplink Wireless Transmission," *IEEE Vehicular Technology Magazine,* Vol. 1, No. 3, September 2006, pp. 30–38.

[43] M. Noune and A. Nix, "Frequency-Domain Precoding for Single Carrier Frequency-Division Multiple Access," *IEEE Communications Magazine,* Vol. 47, No. 6, June 2009, pp. 68–74.

[44] Y. Paichard, "Orthogonal multicarrier phased coded signal for netted radar systems," in *Proc. 2009 International Waveform Diversity and Design Conf.,* Orlando, FL/USA, 8-13 Feb. 2009, pp. 234–236.

[45] K. G. Paterson, "Generalized Reed-Muller codes and power control in OFDM modulation," *IEEE Trans. Inform. Theory,* Vol. 46, No. 1, Jan. 2000, pp. 104–120.

[46] K. G. Paterson, "On the existence and construction of good codes with low peak-to-average power ratios," *IEEE Trans. Inform. Theory,* Vol. 46, No. 6, Jan. 2000, pp. 104–120.

[47] R. P. Perry, R. C. DiPietro, R. L. Fante, "Coherent integration with range migration using Keystone formatting," in *Proc. IEEE Radar Conference,* 17-20 April 2007.

[48] D. Poullin, "Passive Detection Using Digital Broadcasters (DAB, DVB) with COFDM Modulation," *IEE Proc. Radar Sonar Navig.,* Vol. 152, No. 3, June 2005, pp. 143152.

[49] R. Prasad, *OFDM for wireless communication systems,* Artech House, 2004, pp. 11-14.

[50] N. Prasad, V. Shameem, U. B. Desai, S. N. Merchant, "Improvement in target detection performance of pulse coded Doppler radar based on multicarrier modulation with fast Fourier transform (FFT)," *IEE Proc. Radar Sonar Navig.,* Vol. 151, No. 1, Feb. 2004, pp. 11–17.

[51] K. Bruninghaus, H. Rohling, "Multi-carrier spread spectrum and its relationship to single-carrier transmission," in 48$^{\text{th}}$ *IEEE Vehicular Technology Conference,* Vol. 3, 18-21 May 1998, pp. 2329–2332.

[52] R. Saini, M. Cherniakov, "DTV signal ambiguity function analysis for radar application," *IEE Proc. Radar Sonar Navig.,* Vol. 152, No. 3, June 2005, pp. 133142.

[53] M. R. Schroeder, "Synthesis of low-peak-factor signals and binary sequences with low autocorrelation," *IEEE Trans. Inform. Theory,* Vol. 16, No. 1, January 1970, pp. 85–89.

[54] H. Schulze, C. Luders, *Theory and Applications of OFDM and CDMA Wideband Wireless Communications,* Wiley, 2005, pp. 96.

[55] M. A. Sebt, Y. Norouzi, A. Sheikhi, M. M. Nayebi, "OFDM radar signal design with optimized ambiguity function," in *Proc. IEEE Radar Conference, RADAR'08,* Rome/Italy, 26-30 May 2008, pp. 448–452.

[56] S. Sen, M. Hurtado, A. Nehorai, "Adaptive OFDM radar for detecting a moving target in urban scenarios," in *Proc. 2009 International Waveform Diversity and Design Conf.,* Orlando, FL/USA, 8-13 Feb. 2009, pp. 268–272.

[57] M. Skolnik, *Radar Handbook, 3rd Edition* McGraw Hill, 2008, pp. 11.19, 11.20.

[58] M. Sliskovic, "Sampling frequency offset estimation and correction in OFDM systems," in *IEEE ICECS 2001,* Vol. 1, Sept. 2001, pp. 437–440.

[59] M. Sliskovic, "Carrier and sampling frequency offset estimation and correction in multicarrier systems," in *IEEE GLOBECOM 2001,* Vol. 5, 2001, pp. 437–440.

[60] C. Sturm, E. Pancera, T. Zwick, W. Wiesbeck, "A Novel Approach to OFDM Radar Processing," in *Proc. IEEE Radar Conference,* Pasadena, 4-8 May 2009.

[61] S. C. Surender, R. M. Narayanan, "Covert Netted Wireless Noise Radar Sensor: OFDMA-Based Communication Architecture," in *MILCOM2006,* Washington, DC/USA, 23-26 Oct. 2006.

[62] S. J. Symons, J. A. H. Miles, J. R. Moon, "Comparison of Plot and Track Fusion for Naval Sensor Integration," in *Proc.* 5^{th} *International Conference on Information Fusion,* Annapolis/USA, 8-10 July 2002, pp. 1361–1366.

[63] C. M. Thompson, "Table of percentage points of the χ^2 distribution," Biometrika, Vol. 32, 1941.

[64] S. C. Thompson, A. U. Ahmed, J. G. Proakis, J. R. Zeidler, "Constant envelope OFDM," *IEEE Trans. on Communications,* Vol. 56, No. 8, Aug. 2008, pp. 1300–1312.

[65] R. F. Tigrek, W. J. A. de Heij, P. van Genderen, "A method for measuring the radial velocity of a target with a Doppler radar," European Patent Filing No. EP 08162331.6.

[66] R. F. Tigrek, W. J. A. de Heij, P. van Genderen, "A Golay code based approach to reduction of the PAPR and its consequence for the data throughput," in *Proc.* 4^{th} *European Radar Conf.,* Munich/Germany, 10-12 October 2007, pp. 146–149.

[67] R. F. Tigrek, W. J. A. de Heij, P. van Genderen, "Solving Doppler ambiguity by Doppler sensitive pulse compression using multi-carrier waveform," in *Proc.* 5^{th} *European Radar Conf.,* Amsterdam/The Netherlands, 30-31 October 2008, pp. 72–75.

[68] R. F. Tigrek, W. J. A. de Heij, P. van Genderen, "Multi-Carrier Radar Waveform Schemes for Range and Doppler Processing," in *IEEE Radar Conf.,* Pasadena/CA 4-8 May 2009, pp. 1–5.

[69] R. F. Tigrek, W. J. A. de Heij, P. van Genderen, "Relation between the Peak to Average Power Ratio and Doppler Sidelobes of the Multi-Carrier Radar Signal," in *International Radar Conf.,* Bordeaux/France, 12-16 October 2009, pp. 1–6.

[70] P. van Genderen, R. F. Tigrek, "Radar Waveforms with Communication Ability," in *Proc.* 4th *World Congress Aviation in the XXI*th *century,* Vol. 2, Kiev/Ukraine, 21-23 September 2010, pp. 22.19–22.27.

[71] R. F. Tigrek, P. van Genderen, "Compensation of Range Migration for Cyclically Repetitive Doppler-Sensitive Waveform (OFDM)," *IEEE Trans. Aerospace and Electronic Systems,* Vol. 46, No. 4.

[72] R. F. Tigrek, W. J. A. de Heij, P. van Genderen, "OFDM Communication Signals as the Radar Waveform to Solve Doppler Ambiguity," accepted for publication in *IEEE Trans. Aerospace and Electronic Systems.*

[73] Z. Wang, O. A. Krasnov, L. P. Ligthart, F. van der Zwan, "FPGA Based IF Digital Receiver for the PARSAX Polarimetric Agile Radar," in 18th *International Conference on Microwave, Radar and Wireles Communications (MICON)*, Vilnus/Lithuania, 14-16 June 2010, pp. 1–4.

[74] C. Wang, S. Ku, C. Yang, "An Improved Peak-to-Average Power Ratio Estimation Scheme for OFDM Systems," in *Proc. VTC2007,* Dublin/Ireland, 22-25 April 2007, pp. 2827–2831.

[75] S. Wei, D. L. Goeckel, and P. E. Kelly, "A modern extreme value theory approach to calculating the distribution of the PAPR in OFDM systems," in *Proc. IEEE ICC,* New York/NY, May 2002, pp. 1686–1690.

[76] W. Wei, P. Yingning, "An interpolation algorithm to improve range estimation for the linear frequency modulated radar," *IEEE Aerospace and Electron. Syst. Magazine,* Vol. 14, No. 7, July 1999, pp. 45–47.

[77] S. B. Weinstein, P. M. Ebert, "Data transmission by frequency-division multiplexing using the discrete Fourier transform," *IEEE Trans. on Communication Technology,* Vol. 19, No. 5, Oct 1971, pp. 628–634.

[78] P. M. Woodward, *Probability and Information Theory with Application to Radar,* Pergamon Press Ltd., London, 1953.

[79] T. Wu, Q. Qu, S. Yuan, X. Wei, "Research on a Method of Unambiguous Velocity Measurement of the Space Surveillance Low PRF Radars," in *Proc. ISIP,* 23-25 May 2008, pp. 527–532.

[80] W. Y. Zou, Y. Wu, "COFDM: An overview," *IEEE Trans. on Broadcasting,* Vol. 41, No. 1, Mar. 1995, pp. 1–8.

[81] "Orthogonal Frequency Division Multiplexing," U.S. Patent 3,488,445, Jan. 6, 1970.

List of Abbreviations

A/DC	Analog-to-Digital Converter
AWGN	Additive White Gaussian Noise
BER	Bit Error Rate
CDF	Cumulative Distribution Function
CDMA	Code Division Multiple Access
DFT-IDFT	Discrete Fourier Transform - Inverse Discrete Fourier Transform
FFT-IFFT	Fast Fourier Transform - Inverse Fast Fourier Transform
FLOPS	Floating Point Operations Per Second
FMCW	Frequency Modulated Continuous Wave
ISI	Inter-Symbol Interference
ICI	Inter-Carrier Interference
LCM	Least Common Multiple
LFM	Linear Frequency Modulation
LOS	Line of Sight
OFDM	Orthogonal Frequency Division Multiplexing
PAF	Periodic Ambiguity Function
PAPR	Peak-to-Average Power Ratio
PDF	Probability Distribution Function
PMERP	Peak-to-Mean Envelope Power Ratio
PRI	Pulse Repetition Interval
PRF	Pulse Repetition Frequency
PSK	Phase Shift Keying
QAM	Quadrature Amplitude Modulation
QPSK	Quadrature Phase Shift Keying
RCS	Radar Cross Section
SNR	Signal-to-Noise Ratio
SC-OFDM	Single-Carrier Orthogonal Frequency Division Multiplexing
SCR	Signal-to-Clutter Ratio

Summary

The concept of combining the information from multiple monostatic radars requires establishing a network that connects the radar stations. A network of radars requires communication links between the radars and possibly to a centralized fusion and control center, which can be very susceptible to interference and disruptions if based on commercially available communication infrastructure, in particular in conditions of emergency. The rationale behind the goal of combining the radar and communication functions in a single signal is to build a network of radars that is not dependent on the commercially available communication infrastructure. Moreover, using the same signal for both functions relaxes the time-frequency budget that would be very tight for combined high-resolution radar and communication operation with a separate signal for each function. Thus, we can state that the main focus of this thesis is the development of a wide-band radar signal with the potential dual-use as the communication signal and the design of the associated radar signal processing technique. While the signal combines both radar and communication functions, the processing technique that was developed in this thesis exclusively addresses the radar function.

The orthogonal frequency division multiplexing (OFDM) is a multi-carrier spread-spectrum technique which finds wide-spread use in communications. The flexible allocation of carriers and carrier contents is the prime motivation for choosing OFDM as a candidate for the multi-carrier radar signal. The bandwidth efficiency of the OFDM signal is much better compared to the phase coded signals, and the Doppler sensitivity of the OFDM signal can be exploited in the radar signal processing to solve the Doppler ambiguity. With these factors as motivation, and since there are also examples of OFDM communication signals used for radar applications in the literature, primarily in the context of passive bistatic radars, OFDM is adopted for the radar signal. The two fundamental components of the OFDM communication signal, namely the cyclic prefix guard interval and the random message content, are incorporated in the OFDM radar signal and the

signal processing technique is developed to make use of these features rather than avoid them. Different from the other techniques proposed in the literature there is no sharing of the spectrum and time budgets and therefore no associated degradation of the radar performance.

The signal processing method developed for the OFDM radar signal consists of pulse compression for the individual OFDM chips followed by the coherent Doppler integration of the compressed chips. The multi-carrier structure of the OFDM signal is exploited when developing the pulse compression technique to measure the Doppler effect on the individual OFDM chips. The Doppler effect, which is considered as a cause of pulse compression loss, is compensated for in the frequency domain, and the additional information on the Doppler effect helps solve the Doppler ambiguity occurring in the coherent integration stage.

The Doppler ambiguity is an important challenge for pulse-Doppler radar, where the pulse repetition frequency (PRF) determines both the Doppler ambiguity and the range ambiguity. The structure of the multicarrier signal and the unique outcome of the novel processing technique offer a new solution to the ambiguity in the Doppler measurements. The processing can be regarded as combining the result of pulse-Doppler processing with the Doppler sensitive response of the OFDM pulse compression. The peak target response occurs at a certain cyclic shift of the codes modulating each of the carriers, which by itself gives a coarse Doppler measurement. The high-resolution but ambiguous Doppler information from the coherent Doppler integration is compared with this unambiguous but coarse Doppler measurement to solve the Doppler ambiguity.

A Monte Carlo simulation platform was developed that is able to generate the ambiguity function and calculate its statistical properties. Establishing a reliable software experiment platform enabled demonstrating the Doppler ambiguity solving capability of the OFDM radar signal, and it helped to generalize the OFDM pulse compression method over the other OFDM signal implementations. The validity of the simulation platform was assured by a measurement campaign using a laboratory scale real-life radar with the same OFDM waveform.

The OFDM signal is the sum of harmonics with different starting phases and amplitudes, and as a result has a variable envelope. Peak-power limiting techniques aim to limit the amplitude fluctuations in the time domain signal in order to relax the linearity requirements for the power amplifiers. Two methods were considered for peak-power reduction; one method modulates the OFDM carriers by Golay complementary codes while the other method applies pre - coding by the DFT matrix to obtain the

single-carrier OFDM (SC-OFDM). The assessment of these PAPR-control methods for radar applications generated novel results, and answers the valid concerns regarding the linearity of the power amplifiers.

The OFDM pulse compression technique and the coherent integration of the OFDM chips contains in its very foundation a set of assumptions regarding the upper limits for range and velocity of targets of interest. The narrowband assumption establishes a fundamental constraint over the upper limit of the target radial velocity, which concerns the time-bandwidth product of the signal. With higher radial velocity, the point target does not occupy a single range bin during the extent of the radar signal but migrates from one range bin to the next. The range migration occurs first at the level of coherent Doppler integration, where the OFDM pulse compression can still assume the Doppler effect to be a frequency shift. At higher velocities, the actual Doppler effect that is the scaling on the signal cannot be accurately modeled as a frequency shift anymore. Compensation techniques for both effects were developed in this thesis and verified through simulations.

When a target is farther than the range limit, the received echo contains a portion of the preceding OFDM pulse as well as the current one. The resulting inter-symbol interference (ISI) will obviously cause a degradation of the radar performance. The OFDM pulse compression method is modified to take into account the preceding OFDM chip as well as the current one to reduce the interference. With this modification, the OFDM signal that was initially proposed for short range surveillance tasks can also be utilized for longer ranges.

In summary, the OFDM pulse compression method that utilizes an OFDM communication signal for radar tasks has been developed and reported in this dissertation. Using the ambiguity function tool, the feasibility of the OFDM pulse compression method was demonstrated from a performance perspective. Further investigation aimed at demonstrating the practical applicability of the OFDM pulse compression and improving its performance remains for future research. The ultimate goal that lies behind the adoption of the OFDM communication signal as the radar waveform is to build a network of radars that communicate through their directive beams. The future research direction that covers the communication related aspects of such a network of radars also deserves special attention.

Samenvatting

Het concept van het combineren van informatie uit verscheidene monostatische radars vereist een netwerk dat de radar stations met elkaar of met een centrale post verbindt. Zon netwerk kan heel gevoelig zijn voor storing en onderbreking, indien het zou zijn gebaseerd op de commercieel beschikbare communicatie-infrastructuur, in het bijzonder in noodsituaties. De grondgedachte achter de doelstelling de radar en communicatie functies in een enkel signaal te combineren is het bouwen van een netwerk van radars dat niet afhankelijk is van de commercieel beschikbare communicatie-infrastructuur. Bovendien, door hetzelfde signaal voor beide functies te gebruiken verruimt het tijd-frequentie budget dat anders zeer krap zou zijn voor de gecombineerde functies van hoge-resolutie radar en communicatie met een apart signaal voor elke functie. Zo kunnen we stellen dat het belangrijkste oogmerk van dit proefschrift is de ontwikkeling van een breedband radar signaal met het potentieel het tevens als communicatiesignaal te gebruiken, en het ontwerp van de bijbehorende radar signaalverwerkingstechniek. Alhoewel het signaal de radar- en communicatie functies combineert, heeft de verwerkingstechniek die werd ontwikkeld in dit proefschrift uitsluitend betrekking op de radar functie.

De Orthogonal Frequency Division Multiplexing (OFDM) is een multicarrier spread-spectrum techniek die wijdverspreide toepassing in de communicatie vindt. De flexibele toewijzing van de draaggolven en de inhoud van elke draaggolf is de belangrijkste motivatie voor het kiezen van OFDM als kandidaat voor het multi-carrier radarsignaal. De bandbreedte-efficiency van het OFDM-signaal is veel beter in vergelijking met fase-gecodeerde signalen, en de Doppler-gevoeligheid van het OFDM signaal kan worden uitgebuit in de radar signaalverwerking om de Doppler dubbelzinnigheid op te lossen. Met deze factoren als motivatie, en aangezien er ook andere voorbeelden van het gebruik van OFDM communicatie signalen voor radar toepassingen in de literatuur te vinden zijn, in de eerste plaats in het kader van passieve bistatische radars, is OFDM geadopteerd als het radar-signaal. De twee

fundamentele aspecten van het OFDM communicatie signaal, namelijk het cyclische prefix guard interval en de willekeurige inhoud van berichten, zijn in beschouwing genomen in het OFDM radar signaal en de signaal verwerking techniek is ontwikkeld om gebruik van deze aspecten te maken in plaats van ze te vermijden. Anders dan bij de andere voorgestelde technieken in de literatuur is er geen conflicterend gezamenlijk gebruik van het spectrum en van de tijd budgetten en derhalve is er geen bijbehorende aantasting van de radar prestaties.

De signaalverwerkingsmethode ontwikkeld voor het radar OFDM signaal bestaat uit pulscompressie voor de individuele OFDM chips, gevolgd door Doppler coherente integratie van de gecomprimeerde chips. De multicarrier structuur van het OFDM signaal wordt benut bij de ontwikkeling van de pulscompressie techniek om het Doppler effect op basis van de individuele OFDM chips te meten. Het Doppler effect, dat wordt beschouwd als een oorzaak van pulscompressie verlies, wordt gecompenseerd in het frequentiedomein, en de extra informatie over het Doppler effect helpt bij het oplossen van de Doppler dubbelzinnigheid die zich zou uiten bij coherente integratie.

De Doppler dubbelzinnigheid is een belangrijke eigenschap van puls-Doppler radar, waar de pulsherhalingsfrequentie (PRF) zowel de maximale ondubbelzinnige Doppler verschuiving als de maximale ondubbelzinnige afstand bepaalt. De structuur van het multicarrier signaal en het unieke resultaat van de nieuwe verwerkingstechniek bieden een nieuwe methode voor het oplossen van de dubbelzinnigheid in de Doppler metingen. De techniek kan worden opgevat als het combineren van de puls-Doppler verwerking met het Doppler gevoelige gedrag van de OFDM pulscompressie. Het maximum van de doelsresponsie treedt op bij een bepaalde cyclische verschuiving van de codes die elk van de draaggolven moduleren, waarbij op zichzelf een grove Doppler meting ontstaat. De dubbelzinnige Doppler informatie die uit de Doppler coherente integratie met hoge resolutie verkregen wordt, is vergeleken met deze ondubbelzinnige maar grove Doppler-metingen verkregen na de cyclische verschuiving teneinde de Doppler dubbelzinnigheid op te lossen en de hoge resolutie te behouden.

Een Monte Carlo simulatie platform is ontwikkeld dat in staat is de zogenaamde ambiguity function te genereren en haar statistische eigenschappen te berekenen. Het tot stand komen van een betrouwbaar simulatie software-platform maakte het mogelijk het vermogen van het OFDM radarsignaal om de Doppler dubbelzinnigheid op te lossen aan te tonen, en het hielp om de OFDM pulscompressie methode te generaliseren voor de andere OFDM signaal implementaties. De geldigheid van het simulatie platform

werd gevalideerd door een meetcampagne met behulp van een real-life radar op laboratoriumschaal met dezelfde OFDM golfvorm.

Het OFDM-signaal bestaat uit de som van harmonische signalen met verschillende startfasen en amplitudes, en heeft als gevolg daarvan een variabele omhullende. Technieken die de verhouding tussen het piek vermogen en het gemiddelde vermogen (de PAPR) beperken, streven naar het beperken van de amplitude variaties in het tijddomein signaal om de eisen aan de lineariteit van de eindversterkers minder stringent te maken. Twee methodes werden in ogenschouw genomen voor de vermindering van de PAPR: een methode die de OFDM draaggolven moduleert met complementaire Golay codes, terwijl de andere methode een pre-codering via de DFT matrix toepast om de zogenaamde *Single-Carrier* OFDM (SC-OFDM) te verkrijgen. De beoordeling van deze PAPR beperkingsmethoden voor de radar toepassingen leidde tot nieuwe resultaten, die een antwoord geven op de geldige bezorgdheid over de lineariteit van de eindversterkers.

De OFDM pulscompressie techniek en de coherente integratie van de OFDM chips bevatten een aantal fundamentele aannames met betrekking tot de bovengrenzen aan de afstand en de snelheid van de doelen. De smalbandveronderstelling vormt een fundamentele beperking aan de bovengrens van de radiale snelheid van het doel, waar het het product van de tijdsduur en de bandbreedte van het signaal betreft. Bij hogere radiale snelheid blijft een punt doel niet binnen een enkele afstandsbin tijdens de duur van de radar signaal maar migreert het van een afstandsbin naar de volgende. De afstandsmigratie treedt eerst op op het niveau van de coherente Doppler integratie, waarbij de OFDM puls compressie die voorafgaat aan de integratie nog steeds het Doppler-effect als een frequentie verschuiving kan aannemen. Bij hogere snelheden uit het werkelijke Doppler-effect zich in een de schaling van het signaal die niet meer nauwkeurig kan worden gemodelleerd met een enkelvoudige frequentie verschuiving. Compensatie technieken voor beide effecten werden ontwikkeld in dit proefschrift en geverifieerd door middel van simulaties. Wanneer een doel zich op grotere afstand bevindt dan de maximale ondubbelzinnige (bepaald door de PRF), bevat de ontvangen echo zowel een gedeelte van de voorgaande OFDM puls als van de huidige. De resulterende inter-symbool interferentie (ISI) zal uiteraard leiden tot een verslechtering van de radar prestaties. De OFDM pulscompressie methode is aangepast om rekening te houden met zowel de voorgaande OFDM-chip als de huidige teneinde de interferentie te verminderen. Met deze wijziging kan het OFDM signaal dat oorspronkelijk was voorgesteld voor de korte afstand bewakingstaken ook worden gebruikt voor langere afstanden.

Samengevat is in dit proefschrift een OFDM pulscompressie methode

ontwikkeld voor radartaken, gebaseerd op een OFDM-signaal zoals dat voor communicatie gebruikt wordt. Met behulp van de ambiguity function tool, werd de haalbaarheid van de OFDM pulscompressie methode aangetoond vanuit een prestatie-perspectief. Nader toekomstig onderzoek gericht op het demonstreren van de praktische toepasbaarheid van de OFDM pulscompressie en de verbetering van haar prestaties blijft nodig. Het uiteindelijke doel van het gebruik van het OFDM signaal als radar golfvorm is het bouwen van een netwerk van radars die met elkaar of met een centrale post communiceren via hun richtingsgevoelige antennebundels. Toekomstig onderzoek dat de communicatie gerelateerde aspecten van een dergelijk netwerk van radars dekt verdient ook speciale aandacht.

Acknowledgements

A Ph.D. study is truly a garden of thorns, and only with the close guidance of Prof. Piet van Genderen was I able to get through it. He provided me the freedom to explore my field of research by myself, and he helped me to get through whenever I got stuck. I hope his many qualities as a scientist and mentor has rubbed off on me. I am grateful for his supervision and guidance.

Prof. Leonardus Ligthart has closely monitored the progress of my research. I thank him very much for his numerous reviews of the thesis, which contributed greatly to its content and clarity.

My Ph.D. research was in the context of the PLACE project in Thales Nederland, and I would like to thank our project manager, Eddy van Eeuwijk, for his efforts to provide us this opportunity to pursue our Ph.D. research in Thales Nederland. Eddy has organizing the meetings with our supervisors and colloquiums in Hengelo, which contributed greatly to our research.

I wish to thank Prof. Altunkan Hızal and Prof. Tuncay Birand for suggesting that Müge and I apply for Ph.D. positions at TU Delft.

I should like to express heartfelt gratitude to Wim de Heij for supervising my Ph.D. research. The experiments, results of which are presented in this dissertation, were made possible by his expertise; he brought together the radar transmitter and receiver chains.

During my time as Marie Curie Fellow in Thales Nederland, I had the privilege to work with four colleagues, each from a different country in Europe. Angie , Gabriel and Mayazzurra, it was good to be sharing the same office with you guys. I enjoyed our trips to Hengelo, and our occasional dinners together will also be remembered fondly. We have accomplished much together; we did a very nice job in organizing the First Student Challenge in European Microwave Week in 2008. Elias joined us later, and helped us greatly with the experiments. His positive attitude and personality made the experiments enjoyable despite the extremely tight schedule.

The experiments would not be possible without the contribution of Philips MiPlaza and Agilent. We have worked in close cooperation with Daniel Bockstal from Agilent and Mark de Haas from MiPlaza. I thank them both for their support during the experiments.

I wish to express my thanks to Huub Langeraar, Adriaan Smits and Amanda Kramer for their hospitality and help. I will fondly remember all my colleagues in Thales Nederland Delft: Denis, Erik, Evert, Frank, Gilles, Jan, Joris, Joris Janssen, Marten, Radmilla, Ronnie, Rogier, Rob...

During my time in IRCTR as a guest researcher, the PARSAX team kindly provided me with the facilities I needed for the completion of my research, for that I am grateful. I should also like to express my gratitude to Prof. Yarovoy, for offering me a post-doc researcher position in the STARS project.

The last couple of months before the Ph.D. defense are hard due to the tight schedule: Besides other tasks, there are a number of documents one has to fill. Special thanks go to Marjon for her help during this period.

One of the greatest things about my time in Delft is my new friends. We had many interesting discussions with Mahmut over many cups of tea. We enjoyed watching TV series with Anıl, Pervin, and also my little friend Ender. Thank you guys for making my life happier.

My dear family, your support during this past four and a half years was vital for us. Sevgi Tigrek was with us here in Delft, and she helped us countless times in many things during our Ph.D. study. It was also good to have someone who has been there and done that, that is, the Ph.D. study. We organized trips, watched numerous movies, and been through sad moments as well as the happy ones together. My mother came here to help us when I was lying with a broken ankle. My father's support gave me the much needed confidence. My brother, my uncles, aunts, my in-laws... I thank you all for your support.

And the other half of "we", my wife, Müge Tanyer-Tiğrek... I know that I am not an easy person, even capricious sometimes. I thank you for your patience and for your support, and I appreciate your prodding me into action when I procrastinate (that being said, I will still sulk and make a face when you interrupt my procrastination). Leaving the Ph.D. behind us, we continue our journey together. Who knows where our steps will take us?

R. Fırat Tiğrek

Delft, October 2010

About the author

Recep Fırat TİĞREK was born in Antalya, Turkey, on 7 February, 1981. He received his B.Sc. and M.Sc. degrees from Middle East Technical University in Ankara, Turkey in June 2002 and August 2005 respectively. During his M.Sc. research he investigated plasma antennas. From December 2002 to January 2006, he was also with ASELSAN Inc., Ankara, where he worked as electronic test design engineer and he developed instrument management, data acquisition and processing software for various antenna test ranges. Between March 2006 and March 2009, he joined Thales Nederland as *Marie Curie Fellow*, and became a Ph.D. candidate at the International Research Center for Telecommunications and Radar (IRCTR) at the Delft University of Technology in Delft, the Netherlands. From March 2009 till January 2010 he continued his Ph.D. as a guest researcher, in contribution to the PARSAX project in IRCTR. His research focused on radar waveform design and signal processing, results of which are reported in this dissertation. Since January 2010, he is a post-doc researcher at IRCTR, TU Delft. His current research involves sensor management, more specifically, resource management for radar.

Author's Publications

Patents

1. R. F. Tigrek, W. J. A. de Heij, "A method for measuring the radial velocity of a target with a Doppler radar," European Patent Filing No. EP 08162331.6.

Refereed Journal Papers

1. R. F. Tigrek, W. J. A. de Heij, P. van Genderen, "OFDM Communication Signals as the Radar Waveform to Solve Doppler Ambiguity," accepted for publication in *IEEE Trans. Aerospace and Electronic Systems.*

2. R. F. Tigrek, P. van Genderen, "Compensation of Range Migration for Cyclically Repetitive Doppler-Sensitive Waveform (OFDM)," *IEEE Trans. Aerospace and Electronic Systems,* Vol. 46, No. 4.

3. E. Mendez Dominguez, R. F. Tigrek, M. Ruggiano, G. Lellouch, W. J. A. de Heij, D. Bockstal, P. van Genderen, "Experimental set-up demonstrating combined use of OFDM for radar and communications," *Microwave Journal,* Vol. 53, No. 8, August Supplement 2010, pp. 22–36.

Refereed Conference Papers

1. P. van Genderen, R. F. Tigrek, "Radar Waveforms with Communication Ability," in *Proc.* 4$^{\text{th}}$ *World Congress Aviation in the XXI*$^{\text{th}}$ *century,* Vol. 2, Kiev/Ukraine, 21-23 September 2010, pp. 22.19–22.27.

2. R. F. Tigrek, W. J. A. de Heij, P. van Genderen, "Relation between the Peak to Average Power Ratio and Doppler Sidelobes of the Multi-

Carrier Radar Signal," in *International Radar Conf.,* Bordeaux/France, 12-16 October 2009, pp. 1–6.

3. R. F. Tigrek, W. J. A. de Heij, P. van Genderen, "Multi-Carrier Radar Waveform Schemes for Range and Doppler Processing," in *IEEE Radar Conf.,* Pasadena/CA 4-8 May 2009, pp. 1–5.

4. R. F. Tigrek, W. J. A. de Heij, P. van Genderen, "Solving Doppler ambiguity by Doppler sensitive pulse compression using multi-carrier waveform," in *Proc.* 5$^{\text{th}}$ *European Radar Conf.,* Amsterdam/The Netherlands, 30-31 October 2008, pp. 72–75 (Paper nominee for Young Engineer Prize).

5. R. F. Tigrek, W. J. A. de Heij, P. van Genderen, "A Golay code based approach to reduction of the PAPR and its consequence for the data throughput," in *Proc.* 4$^{\text{th}}$ *European Radar Conf.,* Munich/Germany, 10-12 October 2007, pp. 146–149.

M.Sc. Thesis

R. F. Tigrek, "An Investigation on the Plasma Antennas," *Masters Thesis,* Middle East Technical University, Ankara, August, 2005.